NATURAL ALTERATION OF BASE-METAL SULPHIDES IN BROKEN LIMESTONE

by

JOHN DAVID SALTER

A thesis submitted for the degree of Doctor of Philosophy of the University of London and the Diploma of Membership of Imperial College

Department of Mineral Resources Engineering
Imperial College of Science and Technology
London SW7

March 1984

Abstract

The alteration of galena, chalcopyrite, and sphalerite from an undisturbed 300 year old mine dump has been examined by a variety of techniques. The minerals were found to have altered to their stable oxidate mineral assemblage, cerussite; goethite plus malachite; and smithsonite. All the sulphides were altered, and the relative rates of alteration were found to be sphalerite >> chalcopyrite $\geqslant$ galena. All the sphalerite was altered to smithsonite, whilst more than 50% of the galena was altered to cerussite. The stable oxidate mineral assemblage and the relative rates of formation of the minerals were predicted from the literature.

Galena alters concentrically to cerussite; the overall amount of alteration was measured by chemical methods and by linear image analysis. The two methods produced very similar results. The ratio of cerussite to galena increased with decreasing particle size (and also with decreasing galena grain size). The galena-cerussite linear grade distribution data did not, in general, fit the ideal concentric cubes model because the particles showed a range of structural complexity and alteration states.

Detailed electron probe analysis of the galena-cerussite interface showed a previously unrecorded intermediate zone, some 10 μm thick, which was not detectable by optical methods unless (rarely) negative polishing relief caused a textural variation at the interface. This intermediate zone was detected around all galena grains and always showed the same chemical variations. These variations correspond with a zoning effect that was also shown by SEM.

The features of the intermediate region have been explained in terms of a new model of the alteration of galena to cerussite. The initial oxidation of galena leads to the formation of a basic lead thiosulphate at the galena 'surface'. This thiosulphate dissolves, releasing lead and thiosulphate species. The lead precipitates as lead carbonate when it encounters bicarbonate ions outside the thiosulphate zone, and the aqueous thiosulphate species diffuse to the bulk solution. The rate of formation of the thiosulphate is greater than the overall rate of formation of the carbonate, thus causing the formation of a detectable intermediate region.

Acknowledgements

I wish to thank the Trustees of the Stanley Elmore Fund of the Institution of Mining and Metallurgy for their generous support of this work.

Grateful thanks are also extended to my supervisor, Dr M.P. Jones, for his patient guidance during the course of this research, and for carefully reviewing this thesis.

Thanks are also expressed to the technical and academic staff of the Mineral Technology Section, RSM, for their assistance, especially Mrs E.Lewis for her help with microprobe techniques.

Contents

Page

Title

Abstract (ii)

Acknowledgements (iii)

Table of contents (iv)

List of figures (viii)

List of tables (x)

Chapter One INTRODUCTION

1.1 General 1
1.2 Scope of investigation 2
1.3 Aims 2
1.4 Presentation 2

Chapter Two MATERIAL INVESTIGATED

2.1 Source of material 4
2.2 Ecton Hill geology 4
2.3 Ecton Hill mining history 6
2.4 The Dutchman dump
  2.4.1 Historical 8
  2.4.2 Surface features 9
2.5 Sampling and sample preparation 9

Chapter Three BASE-METAL SULPHIDE ALTERATION

3.1 Background to the chemistry of sulphide minerals 10
3.2 Minerals considered 13
3.3 Chemical considerations in the aqueous oxidation of galena by oxygen
  3.3.1 Basic solutions 15
  3.3.2 Neutral solutions 18
  3.3.3 Acid solutions 20

Page

3.3.4 Carbonate solutions 21
3.3.5 Mechanism of oxidation by dissolved oxygen 30
3.3.6 Effect on the oxidation rate of different variables 35
3.4 Mineralogy of galena alteration 38
3.5 Chemical considerations in the aqueous oxidation of chalcopyrite by oxygen
3.5.1 Neutral solutions 39
3.5.2 Acidic solutions 40
3.5.3 Alkaline solutions 42
3.5.4 Carbonate solutions 43
3.5.5 Mechanism 55
3.6 Chemical considerations in the aqueous oxidation of sphalerite by oxygen 58
3.7 Conclusions 66

Chapter Four PRELIMINARY RESULTS

4.1 Size and chemical analyses
4.1.1 Mineral samples 67
4.1.2 Water samples 69
4.2 Heavy liquid separation 71
4.3 Optical mineralogy 72
4.4 Summary 77

Chapter Five QUANTIFICATION OF GALENA ALTERATION

5.1 Introduction 78
5.2 Image analysis 78
5.3 Area image analysis
5.3.1 Equipment and procedure 79
5.3.2 Results 79
5.4 Linear image analysis
5.4.1 The linear image analyser 81
5.4.2 Procedure 81
5.4.3 Results 83
5.4.4 Discussion 88
5.5 Chemical analysis
5.5.1 General 98
5.5.2 Procedure 98

Page

5.5.3 Results 99

5.5.4 Discussion of chemical results 99

5.6 Summary 104

Chapter Six STUDIES OF THE GALENA-CERUSSITE INTERFACE

6.1 Introduction 105

6.2 Microprobe studies of the galena-cerussite interface

6.2.1 Techniques 106

6.2.2 Results 106

6.2.3 Discussion 111

6.3 Interpretation of microprobe results

6.3.1 General 113

6.3.2 Lead and sulphur aqueous chemistry 115

6.3.3 Transport considerations 120

6.3.4 Reaction considerations 122

6.4 Mechanism for the natural alteration of galena to cerussite 128

6.5 Summary 131

Chapter Seven ALTERATION FEATURES OF SPHALERITE, CHALCOPYRITE, AND PYRITE

7.1 General 132

7.2 Microprobe studies

7.2.1 Zinc minerals 132

7.2.2 Chalcopyrite 132

7.2.3 Pyrite 135

7.3 Summary 138

Chapter Eight CONCLUSIONS 138

References 140

Appendices 1. Description of Woodward's (1729) Ecton samples 147

2. Climatic data 148

3. Size distributions of the Dutchman dump samples 152

4. Summary of size and chemical data for the Dutchman dump samples 153

Page

5. A linear analysis results print-out 158
6. Linear intercept data 167
7. Solid phases in the Pb-S-CO_3 system 174

List of Figures

Page

2.1 Plan of Ecton Hill showing the principal surface features 7

3.1 Eh-pH diagram for sulphur 16

3.2 Stability fields of galena, anglesite, and cerussite as functions of pH and Eh 26

3.3 Stability relations among lead compounds in water, $P_{CO_2} = 10^{-4}$ 27

3.4 Stability relations among lead compounds in water, $\Sigma CO_2 = 0.1$ 28

3.5 Stability fields of anglesite and leadhillite in terms of pH and a_{SO_4} relative to hydrocerussite at $a_{H_2CO_3}{}^{\circ} = 10^{-6.38}$, and to cerussite at $a_{H_2CO_3}{}^{\circ} = 10^{-4.4}$ 31

3.6 Diagrammatic representation of the processes taking place during the steady period of galena oxidation 34

3.7 Relationships between dissolved copper carbonate species as a function of $p^{[CO_3]}$ and pH at 25°C and 1 atm pressure 44

3.8 Relationships in the Cu-H_2O-O_2-CO_2 system as a function of pH, $p^{[CO_3]}$ and Eh at $p[Cu^{-}] =$ 25°C, and 1 atm pressure 44

3.9 Values of $p^{[Cu]}$ in equilibrium with tenorite, malachite, and azurite in terms of $p^{[CO_3]}$ and pH at 25°C 46

3.10 Values of $p^{[Cu]}$ in equilibrium with the major oxidised phases in the Cu-H_2O-O_2-S system at various $p^{[SO_4{}^{2-}]}$ values at 25°C and 1 atm pressure 46

3.11 Effect of sulphate activity on Cu solubility 47

3.12 Stability of hematite, magnetite, and siderite as functions of Eh, pH and p_{CO_2} at 25°C and 1 atm pressure 51

3.13 Stability of iron minerals at 25°C, $p_{CO_2} = 10^{-2.0}$ and 1 atm total pressure 52

3.14 Stability of hematite, magnetite, and siderite in aqueous solution containing total dissolved carbonate species of 10^{-2}M at 25°C and 1 atm total pressure 53

3.15 Element concentration profiles (measured by Auger electron spectroscopy) in the oxide layer formed on chalcopyrite after 30 minutes of wet oxidation 56

3.16 Element concentration profiles (determined by microprobe analysis) across a chalcopyrite oxidation rim 56

3.17 Stability fields of sphalerite and smithsonite as functions of pH and Eh, $\Sigma_{CO_2} = 0.03$ 62

3.18 Stability fields of sphalerite and smithsonite as functions of pH and Eh 63

Page

3.19 Stability fields of smithsonite, hydrozincite, and zinc hydroxide in solutions free from silica at 25°C 63

4.1 Typical altered cuboid galena grains 74
4.2 Typical altered chalcopyrite grains 75
4.3 A typical smithsonite grain 76

5.1 Cameca CAMEBAX-MICRO control system architecture 82
5.2 Baryte linear intercept distributions, -150 ÷ 104 µm, +2.96 SG material 89
5.3 Linear intercept distributions - concentric cubes model 91
5.4 Combined alteration distributions with superimposed concentric cubes data 92
5.5 A typical galena-cerussite particle which would give rise to multiple linear intercepts 95
5.6 3-intercept particle distributions showing concentric cube behaviour 96
5.7 Linear intercept distributions - concentric spheres model 97
5.8 Values of galena oxidation determined by chemical analyses 100

6.1 Typical BSE images of the galena-cerussite interface 107
6.2 Typical variations in the lead and sulphur content across galena-cerussite interfaces 108
6.3 Typical variations in the lead, sulphur and trace element contents across the galena-cerussite interface 110
6.4 Typical SEM images of the galena-cerussite interface 112
6.5 Generalised galena-cerussite alteration profile 114
6.6 Part of the Eh-pH diagram for the galena-water system 117
6.7 Part of the Eh-pH diagram for the galena-oxygen-water system 117
6.8 Distribution diagram of Pb(II) hydrolysis products 119
6.9 Variation of Pb^{2+} and $PbCO_3^{\circ}$ content of ground waters with pH 121
6.10 Steady-state diffusion boundary at the solid-liquid interface 123
6.11 Typical lead:sulphur mass ratios across the galena-cerussite interface 126

7.1 Element concentration profiles across a chalcopyrite-goethite-malachite particle 133
7.2 BSE image of an altered chalcopyrite grain 134
7.3 BSE and characteristic X-ray density images of an altered pyrite grain in baryte 136

List of Tables

		Page
3.1	Some physical properties of galena, chalcopyrite, and sphalerite	14
3.2	Principal inorganic forms of lead migration in the groundwaters of sulphide deposits	24
4.1	Results of the analyses of Ecton water samples	69
4.2	Heavy liquid separation results	71
5.1	Area analysis - summary	80
5.2	Cerussite linear distribution data	84
5.3	Galena linear distribution data	85
5.4	Smithsonite linear distribution data	86
5.5	Baryte linear distribution data	87
5.6	Volumetric ratio of cerussite to galena as determined by linear image analysis	88
5.7	Intercept distributions of galena and cerussite composite particles	93
5.8	Comparison of linear and chemical measurements of galena alteration	103

CHAPTER ONE

Introduction

1.1 General

The mining industry generates vast quantities of waste rock material. Much of this material is stored in waste dumps and is subjected to sub-aerial weathering. Since the material is seldom in equilibrium with its new surroundings it alters and may release harmful substances into the natural drainage system. In addition, potentially recoverable metals may be lost from dumps during the storage period.

There is a great deal of literature on the design, construction, operation, and mechanical stability of mineral waste storage facilities. In addition, the modelling of artificial leaching operations from mine dumps has also received attention. These models are mainly concerned with metal recoveries and little mineralogical detail is contained in this literature.

However, the chemical stability of dumps is directly linked with the mineralogical changes that take place within them. The nature of the changes, and of the mineralogical products of these changes, depend upon the prevailing geochemical environment. Commercial dump-leaching operations intentionally increase the chemical, and hence , the mineralogical instability of dumps in order to produce the desired product(s).

The physical stability of a dump is also closely related to the mineralogical changes that take place during storage. Thus, dump stability can be seriously reduced by the accelerated alteration which is caused by intentional acid leaching such as that used for the recovery of copper. On the other hand, the cementing action caused by the secondary iron-rich minerals formed during acid leaching can initially improve the mechanical stability of a dump. However, these clay and clay-like minerals may react further with the acidic leach solutions and accelerate the precipitation of jarosite and various hydrated iron hydroxides. This tertiary mineralisation can lead to additional instability in old dumps that have low surface and interior permeabilities.

A great deal of work has been carried out on the accelerated alteration of minerals in dumps at low pH to recover metal values by leaching, but little attention has been paid to the natural, short-term alteration of minerals at alkaline pH. The present work is a study of this neglected area.

The selected waste dump is known to have consisted originally of primary base-metal sulphides and common vein minerals in a limestone matrix. This dump has lain undisturbed since its formation: it has not been subjected to any artificial alteration processes, and, therefore, all the alteration seen in the dump is the effect of natural weathering.

1.2 Scope of investigation

This work is concerned with the nature and extent of the natural mineralogical alteration of a mine waste dump which was originally composed of primary base-metal sulphides and vein minerals in a limestone matrix.

1.3 Aims

The general aim of this work is to determine, in a quantitative manner, the nature of the changes that have taken place in the base-metal sulphide minerals within the dump.

1.4 Presentation

The findings of this investigation are presented as follows.

Chapter Two describes the source of the material studied, together with the sampling and sample preparation details.

Chapter Three is a literature review of the alteration of base-metal sulphide minerals.

Chapter Four describes the chemical and size analyses of the study material, together with its optical mineralogy.

Chapter Five describes the quantification of galena alteration by image analysis and chemical techniques.

The detailed analysis of the galena-cerussite interface by microprobe is described in Chapter Six. A new model of the alteration of galena to cerussite is developed in this chapter.

Chapter Seven describes the alteration features of chalcopyrite, sphalerite, and pyrite.

The conclusions of the investigation are presented in Chapter Eight.

CHAPTER TWO

Material Investigated

2.1 Source of material

The extensive metalliferous mining industry in Great Britain during the 17th, 18th and 19th centuries produced a large number of waste dumps that contained significant amounts of sulphide minerals. Many of these dumps have been removed or reworked (often many times over), and those that remain often lack documented histories. However, the Dutchman mine dump at Ecton Hill, north Staffordshire, still exists in an undisturbed form and the dates of its formation are known. Furthermore, the mineralogy of the original material can be established by comparison with the adjacent Ecton Hill deposits and also by the evidence afforded by Woodward (1729), a noted early geologist. He described specimens from the mine which he collected shortly after its closure in the late 17th century. His specimens have been preserved under museum conditions and are available for comparison with the current dump material.

The material studied during this investigation was obtained from the Dutchman mine dump at Ecton Hill. Some comparative studies were also carried out on material from other mine dumps on Ecton Hill.

2.2 Ecton Hill geology

Ecton Hill, in the eastern wall of the steep Manifold valley, consists of a complex anticline of variable reef-facies Carboniferous limestones and shales. The valuable base-metal mineralisation occurs as sulphide veins. Large deposits occur at some of the intersections of these veins and massive chalcopyrite pipes developed in zones with many closely spaced veins.

The common ore-vein minerals are chalcopyrite, galena, sphalerite, baryte and calcite. Sarjeant (1956), and Kirkham and Ford (1967) identified the following minerals at Ecton including those on the waste dumps and in the old underground workings:

'Common' minerals: chalcopyrite, malachite, galena, sphalerite, limonite and fluorite.

'Uncommon' minerals: bornite, pyrite, arsenopyrite, dolomite, smithsonite, baryte and manganese wad.

'Rare' minerals: azurite, chalcocite, tenorite, rosasite, chalcanthite, cuprite, cerussite, bitumen, celestite, native copper, and hydrozincite (stalactitic in old workings).

Ecton Hill was exposed in Recent geological time as the post-glacial drainage pattern carved out the Manifold river valley. Roby and Porter (1972) claim that following this period, some supergene enrichment of the copper sulphides took place producing malachite at higher levels, and chalcocite and bornite deeper in the hill. They produce no evidence to support this statement. On the other hand, Kirkham and Ford (1967) concluded that there was no firm evidence of supergene enrichment and cite the presence of copper carbonates in Vivian's lode in Clayton Mine at adit level, well below the natural water table, and the presence of unaltered chalcopyrite in the much higher Fly mine (above Dutchman).

It is a primary assumption of this work that the waste material from the Dutchman mine was composed of unaltered, base-metal sulphides, with the common vein minerals in a limestone matrix, when it was dumped on surface. There is little doubt that this assumption is valid with regard to vein minerals, such as baryte and fluorite, and to the limestone matrix, since the Dutchman workings are in massive limestone and are intersected by mineralised veins (Roby and Porter (1972)). The assumption regarding the sulphide minerals may need to be qualified because of the very slight possibility that these minerals had been altered, in situ, before the mining activity took place. However, the following points strongly suggest that no noticeable in situ alteration had occurred.

1. The ore mined from Dutchman was a copper sulphide (Roby and Porter (1972)). Neither primary base-metal oxides nor supergene sulphides are known to have occurred in Dutchman. Underground,

base-metal carbonates are restricted to superficial coatings on sulphide remnants (Cox (1981)) in old mine openings.

2. Kirkham and Ford (1967) found unaltered chalcopyrite in the Fly mine above Dutchman. They also recognise that both mines worked the same vein.

3. Kirkham and Ford (1967) note the presence of unaltered galena in the, now inaccessible, Dutchman workings.

In addition, the site was visited by John Woodward, the noted early geologist, during the early 18th century. He collected some specimens which now form part of the Woodwardian Collection, housed in the Sedgewick Museum at the University of Cambridge. These specimens, each of a few hundred grams, are described in Woodward (1729) under 'Second Additional English Native Fossils'. There is no precise information as to the date of collection of the Ecton specimens. Forbes (1982) states that Woodward started collecting minerals in 1688, but that his fair copy catalogue containing these minerals is dated 14 April 1725. The structure of his cataloging system implies a date of collection toward the latter part of the period 1688-1725. Woodward's descriptions of these specimens, presented in Appendix I, and the now slightly corroded specimens support the assumption that the ore minerals in the Dutchman mine were primary sulphides.

From the descriptions given in Appendix I of this thesis, it is seen that when Woodward collected his specimens, the galena was still unaltered but that some of the other sulphides had already undergone a slight degree of alteration. This alteration is not surprising since Woodward may have collected the material after it had been exposed for about 50 years. Thus, it is seen that the primary copper and zinc sulphides oxidised rapidly in the dump.

2.3 Ecton Hill mining history

The history of the extensive mining activity at Ecton Hill is documented by Roby and Porter (1972). The first dated record is from 1654 for a sale of 'ore' (Derbyshire Records Office). The copper, lead and zinc deposits have been worked at various times since then and some seventy workings are scattered over the hill.

Figure 2.1 Plan of Ecton Hill showing the principal surface features (from Roby and Porter (1972))

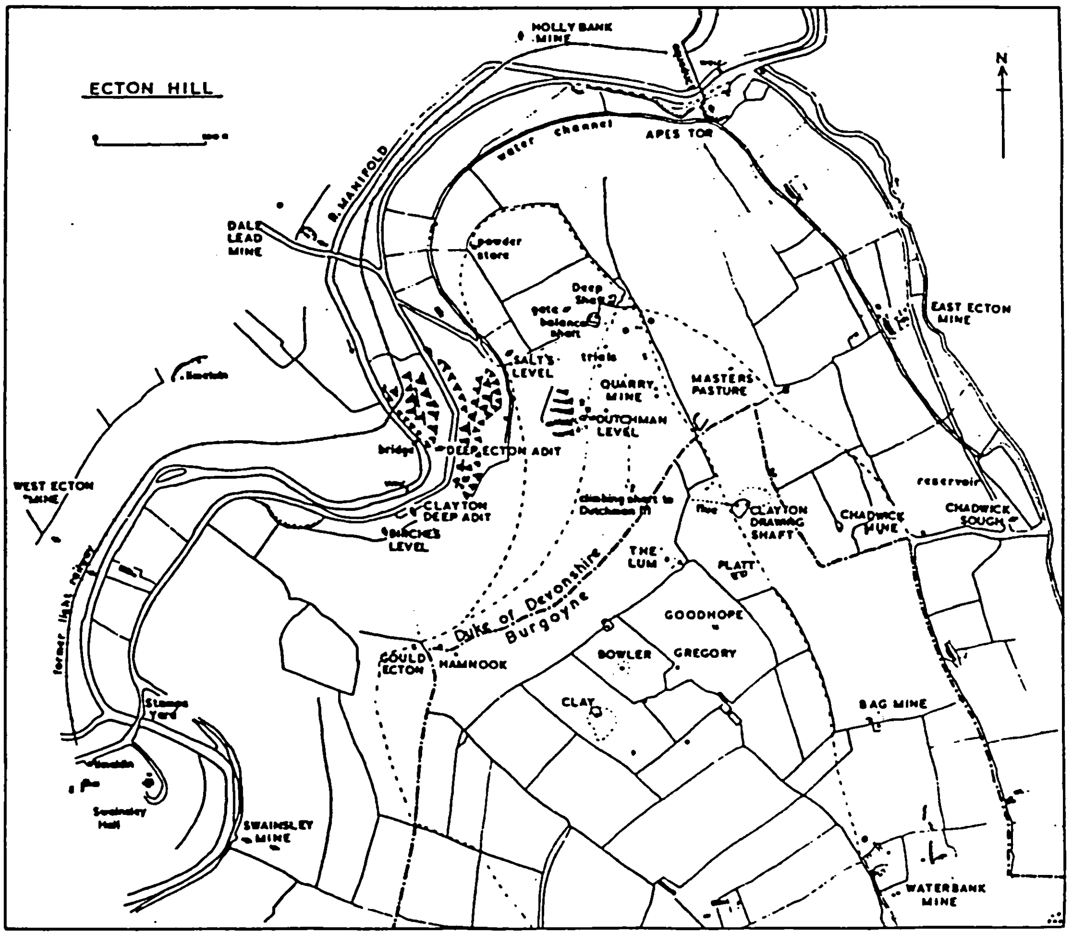
ECTON HILL
N
HOLLY BANK MINE
R. MANIFOLD
water channel
APES TOR
DALE LEAD MINE
powder store
Deep Shaft?
gate or balance shaft
SALT'S LEVEL
trials
QUARRY MINE
DUTCHMAN LEVEL
MASTERS PASTURE
EAST ECTON MINE
bridge
DEEP ECTON ADIT
WEST ECTON MINE
CLAYTON DEEP ADIT
BIRCHES LEVEL
climbing shaft to Dutchman (?)
flue
CLAYTON DRAWING SHAFT
CHADWICK MINE
reservoir
CHADWICK SOUGH
THE LUM
PLATT
former light railway
Duke of Devonshire
Burgoyne
GOODHOPE
BOWLER
GREGORY
GOULD ECTON
HAMNOOK
CLAY
BAG MINE
Stamps Yard
Swainsley Hall
SWAINSLEY MINE
WATERBANK MINE

Large profits were made from working the massive chalcopyrite pipes at Ecton Hill. However, the opening of the Parys Mountain deposits in Anglesey ended this profitability. Thus, production at the Duke of Devonshire's Ecton mines fell from a peak of 4000 tons of 'ore' (concentrates) raised in 1786, to zero at the final closure in 1825.

Between 1826 and 1857 many of the mines and the dumps on the hill were worked with varying degrees of success by cost-book companies of mine adventurers. Later, following company law reforms, these became limited liability companies and interest in mining at Ecton increased again. This was short-lived, however, and all the mines closed by 1891, leaving the accessible mine waste to be removed for railway ballast and road metal.

2.4 The Dutchman mine

2.4.1 Historical

The 3rd Earl of Devonshire 'reopened' the Ecton mines in 1660. His miners worked a level, now known as the Dutchman mine, continuously for the next five years, producing 587 kibbles of copper 'ore' (concentrates) which yielded five tons of copper metal (Roby and Porter (1972)). In 1665 the mine was let to Mr. Mumma, a Dutchman, who worked the mine for a short period; at least until 1668 for the Duke collected one sixth of the 'ore' mined as duty during that year. However, the mine could not have been worked for much longer for Plot (1686), who visited the area in 1680, wrote that the mines had been sufficiently long abandoned for the workforce to have dispersed.

Little activity took place at Dutchman after the 17th century. The last mention of Dutchman is in 1880 when a 'little work' was done there (Kirkham and Ford (1967)). Since then the site has remained ostensibly intact in its isolated position on the hill. Its position, and the relatively small amounts of waste material there compared with those from the major pipe workings, have deterred the removal and retreatment of the waste.

It is concluded that the base of the dump is composed of the remains of the mining activity in the 1660s but that the upper levels may contain a little development waste from later periods.

2.4.2 Surface features

All that now remains at the Dutchman site is the unvegetated, free draining, waste rock dump, and, above it some building foundations. The mouth of the adit was sealed in the 1970s and a dam in the level enables supplies of water to be stored for the houses nearby. A small stream issues from the base of the seal and flows into the dump.

It is possible to recognise two distinct zones in the waste dump. The northern half consists of coarse, blocky, barren limestone whilst the southern half contains much finer mineral material. The coarse material appears to be development rock, and the fine material is thought to have been discarded from ore dressing operations.

2.5 Sampling and sample preparation

Samples of the dump material were taken in March 1981. Four samples of between 5 and 10Kg were taken from the finer-sized zone just above soil level. Samples of the coarser rock were also taken. Mineral specimens that showed particular alteration features were handpicked from other dumps on the hillside for comparative work. The stream issuing from the Dutchman adit was sampled at various locations as was the River Manifold. The water sampling was repeated in February 1982.

The mineralogical samples were air-dried at room temperature. Each sample was riffled into halves. One half was set aside as a reserve, and the other was wet screened into size fractions and then air dried prior to further work. The water samples were analysed as soon as possible upon return to London.

CHAPTER THREE

Base-Metal Sulphide Alteration

3.1 Background to the chemistry of sulphide minerals

The sulphide minerals form an important group of ore minerals. Almost all metal sulphides are crystalline solids and thermochemical data for many of these are listed in standard works. These data show that the sulphide minerals, in general, are thermodynamically unstable in the presence of oxidising agents and that an oxidation reaction should proceed substantially to completion as long as sufficient oxidising agents and time are available (Woodcock (1961)). The kinetics of these reactions, however, dictate whether oxidation takes place at a measurable rate. The oxidation reactions are invariably exothermic, and the rates of these reactions increase when sulphides are mined, comminuted, and exposed to the atmosphere (Pearse (1980)).

Sulphides exhibit a remarkable diversity of structure types and unusual stereochemical behaviour of both the metal and the sulphur atoms. Sulphur-sulphur and metal-metal bonds play an important part in stabilising many sulphides and Pauling (1970) recognises 20 types of sulphur atoms in sulphides with formal charges ranging from S^{2+} to S^{3-} being formed by different electronic configurations. A review of chemical bonding in sulphide minerals reveals a confusing array of models of varying complexity (Vaughan and Craig (1978)). This is partly as a result of the localised and delocalised behaviour of electrons in sulphides and their consequent diversity of physical properties. No single model provides an adequate description of all these properties. Sulphides are most simply represented by ionic models in which the ions are considered to be charged spheres of a particular radius. This approach is useful when considering the geometrical relationships within sulphide structures and between structure types. However, it suffers from the inconsistencies of ionic radii found in the sulphide minerals, as opposed to the consistency seen in the oxides. Thus, ionic models and the use of ionic radii still persist in discussions of sulphide crystal chemistry despite the complications introduced by the contributions from covalent and metallic bonding.

The concept of simple sulphides and their derivative and composite structures (Vaughan and Craig (1978)) is important in the classification of sulphides and also in the clarification of the relationships between sulphides. For example, the relationships between chalcopyrite and its stuffed derivatives (e.g. talnakite ($Cu_9Fe_8S_{16}$), where additional metal atoms are located in the unoccupied set of tetrahedral sites of the cubic close packed sulphur lattice), or between troilite (FeS) and the pyrrhotites (Fe_7S_8), are a structural rationalisation of what would, until recently, have been vaguely described as non-stoichiometry.

All non-transition metal sulphides are diamagnetic insulators or semiconductors (Jellinek (1968)) because, in terms of a simple band structure model, the valence and conduction bands are filled and empty respectively and do not overlap. The valence band in such sulphides is generally made up of sulphur 3p and 3s type electron orbitals and the conduction band of metal s and p orbitals. In the transition metal sulphides, the electronic structures, and hence the electrical and magnetic properties, are complicated by the presence of the d electrons. The variety of possible arrangements of these electrons causes the diversity in electrical and magnetic properties seen in minerals. Jellinek (1968) divided the transition metal sulphides into four groups:

1. Semiconductors with paramagnetism or diamagnetism.
2. Metallic conduction of p-type with paramagnetism.
3. Metallic conduction of n-type with paramagnetism.
4. Metallic conduction with Pauli paramagnetism.

It is well known that the chemical behaviour of natural sulphides differs in degree for different specimens although the general type of behaviour is similar. The reason for these differences in behaviour can be explained by one or more of the following effects:

1. Variation from stoichiometric composition.

Many sulphide minerals can exist as homogeneous phases over a limited range of compositions. Variable compositions can arise in three ways - subtractive solid solution (as in pyrite and pyrrhotite); substitutional solid solution (as in sphalerite); and in interstitial compounds (as in the $CuS_{0.5}$-CuS system). As previously noted, many stoichiometric variations are now being recognised as structural variations.

2. Phase changes.

Many pairs of sulphides (e.g. sphalerite and chalcopyrite) form solid solutions with each other when heated. Other structural effects are caused by heating, e.g. pyrrhotite undergoes a reversible transformation to an orthorhombic form above 140°C, while chalcocite is in a state of cation disorder above 105°C.

3. Crystal defects.

Crystal defects are known to have pronounced effects on sulphide oxidation, e.g. in pyrite (Warren (1956)). Many types of defect are known. Macroscopic defects or textures such as zoning or banding can also be important.

4. Bacterial catalysis.

Certain bacteria enhance the rates of acid leaching of many sulphides. The bacterium Thiobacillus ferroxidans and others have been studied in great detail. Dave et al (1979) showed that T. ferroxidans uses sulphides as energy sources and that sulphide oxidation at acid pH is enhanced by the presence of iron.

5. Electrochemical effects.

Electrochemical, or galvanic, effects are important in composite particles containing two or more sulphides. Sulphides assume definite electrode potentials in aqueous solution and it is well known that when two sulphide minerals are in intimate contact, the mineral with the lower potential is oxidised much faster than when it is not in contact with a mineral of higher potential.

The rate of any chemical reaction between a solid and a liquid is affected by the nature of the solid surface and by the surface area. The classical theory of the dissolution of solids in liquids does not always apply to sulphides - the rate of dissolution is often not directly proportional to the surface area, probably because oxidation occurs at preferred sites (lattice defects). The oxidation of sulphide minerals in an aqueous system takes place in the sequence:

1. Transfer of oxidising species to the aqueous system.
2. Transport of reactants from the bulk solution to the liquid-solid interface.
3. Adsorption of reactants on the solid surface.
4. Reaction at, or on, the surface.
5. Desorption of products.
6. Transport of products from the liquid-solid interface to the bulk system.

However, Woodcock (1961) claims that neither adsorption nor desorption are rate controlling, while the transport of reactants occurs either across a diffusion layer or through an insoluble layer on the mineral surface. Sulphide minerals often give rise to insoluble oxidation products which exert transport control over the sulphide oxidation.

3.2 Minerals considered

The major minerals considered in this study are galena, chalcopyrite, and sphalerite. Table 3.1 lists some of their important physical properties.

Although the chemistry of these sulphide minerals has received much attention in the literature, most of the published work on the oxidation of the sulphide minerals is concerned with commercial leaching operations. Few reports are concerned with the oxidation of sulphides under ambient conditions. The classic work on sulphide oxidation is that of Eadington (1966), and later, Eadington and Prosser (1969), which report on extensive studies of the surface oxidation of synthetic galena.

Galena, chalcopyrite, and sphalerite are relatively insoluble in aqueous solution; their solubility products are:

Galena:	3.4×10^{-28} to 4.3×10^{-30} (Leja (1982)); 3.4×10^{-28} at 18°C (Weast (1981)).
Chalcopyrite:	1.2×10^{-22} at 110°C (Vukotic (1961)).
Sphalerite:	1.6×10^{-24} to 7.4×10^{-27} (Leja (1982)); 1.2×10^{-23} at 18°C (Weast (1981)).

Therefore, their rates of oxidation in aqueous solution should be commensurately slow. When a sulphide mineral undergoes oxidation in air or in aqueous solution, the possible products consist of a

Table 3.1 Some physical properties of galena, chalcopyrite and sphalerite

	Galena	Chalcopyrite	Sphalerite
Nominal composition	PbS	$CuFeS_2$	ZnS
Crystal system	Cubic	Tetragonal	Cubic
Space group	$F_{m\bar{3}m}$	$I_{\bar{4}2d}$	$F_{\bar{4}3m}$
Unit cell dimensions (Å)	a=5.936[1]	a=5.25[2] c=10.32	a=5.43[3]
Unit cell contents	4(PbS)	$4(CuFeS_2)$	4(ZnS)
Magnetic properties[3]	Diamagnetic	Antiferromagnetic	Diamagnetic
Electrical properties	Semiconductor(a)	Semiconductor(b)	Semiconductor(c)

(a) Galena shows a range of non-stoichiometry of 0.1 atomic % (Bloem and Kruger (1956)); metal-rich varieties are n-type, and sulphur-rich varieties are p-type semiconductors. Most natural galena samples exhibit n-type conductivity, although carrier concentrations are strongly influenced by the presence of silver, bismuth and antimony in the samples.[3] Shuey (1975) observes that galena exhibiting p-type conductivity occurs particularly from limestone-lead-zinc deposits.

(b) At room temperature most chalcopyrite shows n-type conduction.[3]

(c) Pure zinc sulphide is a semiconductor though the band gap is so large that it is sometimes described as an insulator.[3] Semiconduction in sphalerite may by p- or n-type depending on stoichiometry. Sphalerite and wurtzite are now known not to be true polymorphs; sphalerite is zinc-deficient, and wurtzite sulphur-deficient compared with the stoichiometric compound. Thus, sphalerite is expected to exhibit p-type conduction, which is the observed case.[3]

1 Mason and Berry (1968)

2 Habashi (1978)

3 Vaughan and Craig (1978)

variety of phases - elemental sulphur, metal hydroxides, metal thiosulphates, metal polythionates, metal sulphates, volatile sulphur dioxide, and residual metal oxides. The number of possible species increases rapidly with multiple valency of the metallic element(s). Despite such a wide range of possible species, few of them are thermodynamically stable.

It is often useful to define geochemical environments in terms of oxidation potential (Eh, or redox potential) and pH, because these quantities are the consequence of an overall chemical balance of the substances present and not vice versa (Sato (1966)). For example, the Eh-pH diagram of the sulphur-water system, Figure 3.1, shows that, at one atmosphere total pressure, the only valency states appearing on the diagram are S^{2-}, S° and S^{6+}, with only HSO_4^-, SO_4^{2+}, $H_2S_{(aq)}$, HS^- and S^{2-} being of significance in aqueous solutions under geologically likely conditions. However, it should be noted that these regions of stability indicate the dominant, but not the only, species present; the boundaries indicate equal activities* of the species in adjacent fields. The intermediate sulphur species, such as thiosulphate and polythionate, are absent from the diagram because they are thermodynamically unstable with respect to sulphur and sulphate. However, thermodynamic instability does not prevent their formation. It is therefore possible for them to exist in significant quantities if the rate of further reaction is slow relative to their rate of formation.

3.3 Chemical considerations in the aqueous oxidation of galena by oxygen

3.3.1 Basic solutions

The oxidation products of galena in basic solutions depend on the pH of the solution and on the base used.

Plante and Sutherland (1949) found that in solutions of pH 9 to 10 (Na_2CO_3 or NaOH) at room temperature, galena oxidises to give

---

* The activity, a_x, of a species x is the dimensionless, thermodynamic or effective concentration of species x. Activities are taken to be equal to concentrations unless otherwise stated.

Figure 3.1 Eh-pH diagram for sulphur (from Burkin (1966))

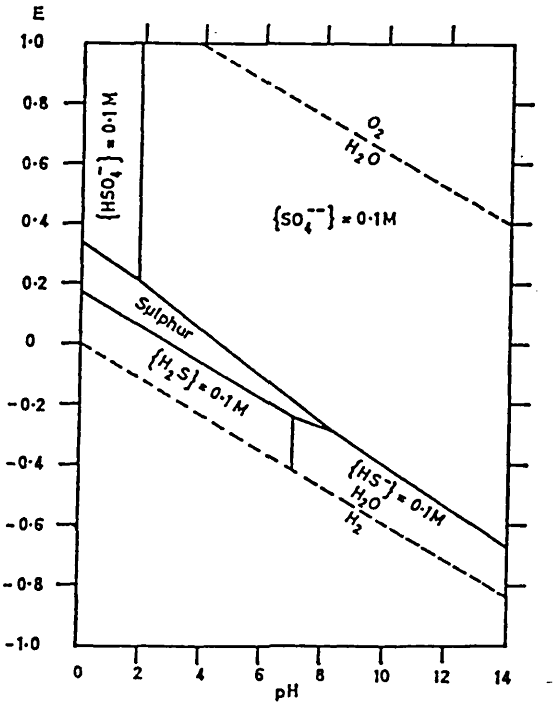

activities of sulphur-containing ions = 0.1

t = 25°C, 1 atm pressure

sulphate, lead, and thiosulphate ions. They also found that the ratio of thiosulphate to sulphate increases as oxidation proceeds.

Anderson et al (1953) found that galena oxidises according to

$$PbS + 2O_2 + 3OH^- = HPbO_2^- + SO_4^{2-} + H_2O \qquad (3.1)$$

in 1 Mdm^{-3} sodium hydroxide solution at 100°C. They detected no other oxidation products and, after an initial induction period attributed to the dissolution of a surface oxidation film, the oxidation rate was almost linear. The reaction rate was found to be proportional to the exposed surface area (indicating a heterogeneous reaction) and to the square root of the oxygen pressure. Increasing the concentration of the sodium hydroxide was found to decrease the reaction rate. This was attributed to the decrease in solubility of oxygen in concentrated sodium hydroxide solutions.

Seraphim and Samis (1956) found that galena oxidises in ammonium acetate solutions at about 100°C according to

$$PbS + \tfrac{1}{2}O_2 + 2NH_4COOCH_3 = Pb(COOCH_3)_2 + S + 2NH_S + H_2O \qquad (3.2)$$

Very little further oxidation was seen to occur. The rate controlling step was shown to be the diffusion of a lead species through the oxidised product layer (mainly sulphur) to the aqueous medium. An induction period of up to 60 minutes was evident in these tests.

Vizsolyi et al (1963) found that, in the presence of ammonia, galena oxidises almost completely to give sulphate ions and very little sulphur. The reactions were described by

$$2PbS + 4O_2 + 2NH_3 + 2H_2O = PbO.PbSO_4 + H_2O + (NH_4)_2SO_4 \qquad (3.3)$$

and the rate of oxidation was found to be proportional to the ammonia concentration. Oxidation in the presence of ammonium sulphate, however, was found to be slower than that in free ammonia.

Eadington (1966) found that at pH9 (NH_3 and $HClO_4$), galena oxidises to give thiosulphate as the predominant product, with sulphate only appearing after some hours and remaining at a constant, low level.

A small proportion of polythionate, determined as tetrathionate, $S_4O_6^{2-}$, was detected in the oxidation product together with a nearly constant amount of elemental sulphur. However, thermodynamically, from the Eh-pH diagram evaluated by Majima (1969), no elemental sulphur should exist at this pH. Eadington's work showed that under basic conditions oxidation proceeds via sulphur; under these conditions, thiosulphate is more stable with respect to disproportionation than in neutral solutions. The formation of the tetrathionate species is in agreement with the findings of Forward et al (1964), who showed that thiosulphate oxidises to give tetrathionate in basic solutions.

3.3.2 Neutral solutions

In the oxidising leach tests described in section 3.3.1, workers, other than Eadington (1966), found that galena oxidises relatively slowly to give lead sulphate, $PbSO_4$ (anglesite) in neutral solutions, without the addition of other reagents.

Reuter and Stein (1957) found that at near-room temperature, the initial reaction between galena, water and oxygen is

$$2PbS + 2H_2O + O_2 = 2Pb^{2+} + 4OH^- + 2S^\circ \qquad (3.4)$$

which is followed by

$$4Pb^{2+} + 8OH^- + 4S = 2PbS + PbO.PbS_2O_3.nH_2O + (4-n)H_2O \qquad (3.5)$$

They detected very little sulphate over the length of their experiments (usually 24 hours). However, at about 100°C, they found that reactions (3.4) and (3.5) are followed by

$$PbO.PbS_2O_3.nH_2O = PbS + PbSO_4 + nH_2O \qquad (3.6)$$

At higher temperatures, galena appeared to oxidise completely to lead sulphate without intermediate products.

Other authors have produced conflicting accounts of the nature of the oxidation products of galena at near-room temperature. Leja et al (1963), using infra-red spectroscopy, found lead thiosulphate to be the predominant oxidation product. Greenler (1962), also using infra-red spectroscopy, reported lead sulphate to be the predominant species. Previously, Hagihara (1952) used electron diffraction techniques to show that galena oxidises predominantly to lead sulphate with no thiosulphate. However, the possibility that the predominant species may change with time was not considered in any of these studies. More recently, Steger and Disjardins (1980), who investigated the oxidation of galena in air at 52°C and 68% relative humidity, found sulphate to be the only sulphur species formed in an oxidation which proceeded via a linear rate law.

Taylor et al (1934) found that after galena had been exposed to air for 'a long time' it reduced iodine solutions (indicating the presence of thiosulphate) and that barium sulphate was precipitated from an acid extract by the addition of barium chloride. They found that the ratio of reducing ions to sulphate decreased as oxidation proceeded. Although their oxidation and analytical procedures now appear a little crude, their results indicate that the relative proportions of the species change with time. This may account for the conflicting conclusions drawn by other authors.

In addition to the work described above, there are many reports in the literature of the qualitative observations of the displacement into solution of sulphate or thiosulphate ions on the addition of xanthates to partially oxidised galena (Eadington (1966)).

Eadington (1966) showed that in neutral solutions galena oxidises to give thiosulphate, sulphate and lead ions, together with a very small, constant amount of sulphur. The quantity of thiosulphate was found to increase for twelve hours and then to remain constant. No sulphate was detected until after six hours oxidation, but, thereafter, the quantity of sulphate was found to increase with time and exceeded the quantity of thiosulphate after about twelve hours. Two conclusions can be drawn from these observations:

1. The nature of the principal oxidation product depends on the time of oxidation.

2. The constant quantities of sulphur and thiosulphate (after twelve hours), together with the increasing amount of sulphate

formed with time, suggest that the oxidation reaction goes via sulphur and thiosulphate as intermediates in the formation of sulphate. This effect is in accordance with the suggestions of Reuter and Stein (1957):

$$2PbS + 2H_2O + O_2 = 2Pb^{2+} + 4OH^- + 2S^\circ \qquad (3.4)$$

$$4Pb^{2+} + 8OH^- + 4S^\circ = 2PbS + PbO.PbS_2O_3.nH_2O + (4-n)H_2O \qquad (3.5)$$

$$PbO.PbS_2O_3.nH_2O = PbS + PbSO_4 + nH_2O \qquad (3.6)$$

In neutral solutions it appears that reaction (3.4) occurs first and that this is followed by reaction (3.5), which is faster. The disproportionation of the basic thiosulphate into sulphate, reaction (3.6), is somewhat slower as shown by the relative quantities of sulphur and thiosulphate.

3.3.3 Acid solutions

Vizsolyi et al (1963) showed that in the presence of sulphuric acid (pH less than 2) at about 120°C and several atmospheres pressure of oxygen, galena oxidises thus:

$$PbS + H_2SO_4 + \tfrac{1}{2}O_2 = PbSO_4 + H_2O + S^\circ \qquad (3.7)$$

Above a pH of 2, the reaction was found to go at least partially to sulphate,

$$PbS + 2O_2 = PbSO_4 \qquad (3.8)$$

They found that the fastest reaction occurred in the presence of a considerable excess of sulphuric acid.

Forward and Peters (1965), in a study of the oxidation of thiosulphate in solution as a function of pH, suggested that thiosulphate is the first oxidation product of sulphides at low temperature and that it is further oxidation or decomposition of the thiosulphate that produces other sulphur species. They also showed that the formation of sulphur is favoured by low pH, and tetrathionate by high pH.

Eadington (1966) found that, at pH 2, galena oxidises to give almost exclusively sulphur and lead ions. After 20 hours, the formation of sulphate was detected. In more acid solutions (pH less than 1.5), sulphur is a thermodynamically stable oxidation product. Since the formation of sulphate is most likely to have occurred via sulphur under acidic conditions, the rate of oxidation of sulphur to sulphate is slow relative to the rate of oxidation of galena. No other oxidation products were detected, and thus, under acid conditions, they must be unstable.

3.3.4 Carbonate solutions

The aqueous chemistry of a limestone environment is governed by the carbonate system. The principles of carbonate aqueous chemistry are documented by Garrels and Christ (1965), and the finite equilibrium values are under constant review. The fundamental equilibria describing the carbonate system are as follows, where the numerical values of the equilibrium constants apply at 25°C.

$$[Ca^{2+}][CO_3^{2-}] = K_{CaCO_3} = 10^{-8.3} \qquad (3.9)$$

$$\frac{[H^+][HCO_3^-]}{[H_2CO_3]} = K_{H_2CO_3} = 10^{-6.4} \qquad (3.10)$$

$$\frac{[H^+][CO_3^{2-}]}{[HCO_3^-]} = K_{HCO_3^-} = 10^{-10.3} \qquad (3.11)$$

$$\frac{[H_2CO_3]}{P_{CO_2}} = K_{CO_2} = 10^{-1.47} \qquad (3.12)$$

$$[H^+][OH^-] = K_{H_2O} = 10^{-14.0} \qquad (3.13)$$

Aqueous solutions of carbon dioxide contain CO_2 molecules as well as carbonic acid molecules, H_2CO_3. However, the ratio CO_2:H_2CO_3 is approximately 386:1 (Garrels and Christ (1965)). Despite this, it is customary to represent all aqueous carbon dioxide as H_2CO_3 and to use equation (3.10) for the first dissociation constant. This incurs no loss of generality since the hydration state of a dissolved species does not need to be stated for thermodynamic purposes. Some authors use the notation $H_2CO_3^*$ to denote $CO_{2(aq)} + H_2CO_3$, the total dissolved carbon dioxide content.

To develop these equations it is necessary to define the limiting properties of the chemical system to which they apply. The Dutchman dump will be considered to be a body of calcite reacting with water in a system open to the atmosphere. The parameters of such a system have been calculated by Garrels and Christ (1965). They found that the equilibrium pH of such a system is 8.4, and the equilibrium activities of the various species present are:

$[Ca^{2+}] = 10^{-3.4}$ $[HCO_3^-] = 10^{-3.0}$

$[CO_3^{2-}] = 10^{-4.9}$ $[H_2CO_3] = 10^{-5.0}$

Thus, the dominant aqueous species resulting from the weathering of limestone under atmospheric conditions should be calcium and bicarbonate ions; that is observed experimentally (Bertenshaw (1979)). These equilibrium conditions should be established after a precipitation flow path of a few tens of centimetres in the dump (Dreybrodt (1980)).

Organic agents are known to have pronounced effects on carbonate equilibria. However, the barren nature of the Dutchman dump limits these effects. Aside from the small stream that issues from the adit and runs into the top of the dump, the only other water reaching the dump is direct precipitation which amounts, on average, to $1.24 m^3/m^2$ land/year (Appendix 2). This precipitation is of a neutral character and should cause no unusual effects.

From the preceding sections it is seen that the aqueous oxidation of galena leads to the formation of lead ions and various oxidised sulphur species in solution. Lead is usually bivalent in natural waters since quadrivalent (simple) lead ions can exist only at very high values of Eh, which are not found in natural waters (Goleva et al (1970)).

The solution geochemistry of lead is markedly influenced by the formation of complexes with the principal anions present in solution and by the formation of insoluble precipitates with these anions; the least soluble phase generally controls the solubility of lead. As previously stated, the principal anion in the carbonate regime considered is the bicarbonate ion, HCO_3^-.

Goleva et al (1970) state that lead exists as $PbHCO_3^+$, $PbOH^+$, $PbCO_3^\circ$, $Pb(CO_3)_2^{2-}$, and other complexes in carbonate solutions, whilst the content of lead in weakly alkaline waters is controlled by the formation of the poorly soluble hydroxide and carbonate. The authors produced thermodynamic calculations using the instability constants of lead complexes, experimentally measured concentrations of species in natural waters, and the equations of Garrels and Christ (1965) to determine the principal inorganic forms of lead in the groundwaters of sulphide deposits (Table 3.2).

The authors noted that a 'considerable' part of lead in natural waters is bound in organic complexes of unknown composition. Also, Thornber and Wildman (1979) pointed out that the adsorption of base metals onto clays and hydrous oxides of iron and manganese is a potentially important factor which is likely to influence solubilities particularly in neutral and alkaline solutions.

Goleva et al (1970) noted that in weakly acid, neutral, and alkaline media, the oxidation of galena is less intensive than in acid media and only small amounts of lead (<10 ppm) pass into solution and form the sparingly soluble carbonate, cerussite ($K_{sp} = 7.4 \times 10^{-14}$, Mann and Deutscher (1980)). Precipitation of cerussite begins when the ratio of the activities of the ions $CO_3^{2-}:SO_4^{2-}$ exceeds $10^{-4.9}$. However, in the presence of an excess of free carbon dioxide, the solubility of cerussite increases, probably as a result of the stable bicarbonate complex, $PbHCO_3^+$. No data on the stability of $PbHCO_3^+$ was available to Goleva et al (1970), but the fact that the solubility of lead sulphide increases in bicarbonate solutions suggests that the lead may exist as $PbHCO_3^+$. Further, by analogy with bicarbonate ions of other elements, log $K_{PbHCO_3^+}$ was estimated to be about 3. The sulphur released during oxidation was considered by Goleva et al (1970) to exist as the sulphate ion, SO_4^{2-}. Their field determinations of the forms of sulphur in cold (<10°C) waters around sulphide deposits showed that they seldom contain thiosulphate ions in significant amounts, except in the immediate vicinity of the oxidising sulphide ores. However, in non-equilibrium fumaroles, lead can migrate as very stable thiosulphate complexes, $PbS_2O_3^\circ$, $Pb(S_2O_3)_3^{4-}$, $Pb(S_2O_3)_2^{2-}$. For example, the weakly acid solfataras of Kamchatka, USSR, contain up to 41 ppm of lead thiosulphates (Goleva et al (1970)).

Table 3.2 Principal inorganic form of lead migration in the groundwaters of sulphide deposits (after Goleva et al (1970)).

	Principal chemical & geochemical parameters of aquifers	
Type	Weakly acid to weakly alkaline	alkaline
pH	4.5 to 7.5	7.5 to 9.5
Eh(v)	0.3 to 0.7	0.1 to 0.3
ionic strength	0.06 to 0.2	0.002 to 0.1
main anions (ppm)	SO_4^{2-} n.10-n.10^2	HCO_3^- n.10^2-n.10^3
	HCO_3^- n.10-n.10^2	CO_3^{2-} n.10-n.10^2
	Cl^- n.10-n.10^2	Cl^- n.10-n.10^2

Lead species	% of total lead occurring as species	
Pb^{2+}	10 - 47	8 - 20
$PbSO_4^{\circ}$	1.5 - 22	<1.5
$Pb(SO_4)_2^{2-}$	5 - 15	0
$PbCl^+$	0.1 - 9	<1
$PbCl_2^{\circ}$	5 - 93	<0.1
$PbHCO_3^+$	10 - 68	25 - 82
$PbCO_3^{\circ}$	5 - 35	30 - 90
$Pb(CO_3)_2^{2-}$	<0.5	36 - 85
$PbOH^+$	0.2 - 1.5	<2.5
$Pb(OH)_2^{\circ}$	0	3.5 - 6
$Pb(HS)_2^{\circ}$	0	0

Garrels (1954) constructed an Eh-pH diagram for the Pb-S-CO_2-H_2O system which shows cerussite to be the stable phase under the conditions under consideration (Figure 3.2). The quoted case, however, considers a high total sulphur activity, but, if the sulphur activity is reduced, it would move the anglesite-cerussite boundary toward the acid region. The boundary between anglesite and galena, and that between cerussite and galena, would be changed very little because their positions are insensitive to total sulphur. The maximum calculated lead activity for the assumed condition is of the order of 10^{-7}; from this it would be predicted that lead could not be transported in groundwaters (Garrels (1954)).

Takahashi (1960) recalculated Garrel's (1954) lead stability fields with the additional consideration of the $PbOH^+$ complex ion and the stability fields of the lead oxides. The cerussite-galena-anglesite fields are basically unchanged. Of the oxides, massicot, PbO, and minium, Pb_2PbO_4, are seen to be unstable in the presence of any aqueous carbon dioxide species, and plattnerite, PbO_2, is stable only in strongly oxidising conditions which cannot exist in nature.

Garrels and Christ (1965) further extended the work of Garrels (1954) in the calculation of Figures 3.3 and 3.4. Figure 3.3 illustrates a system resembling conditions of surface oxidation. Although the total sulphur activity is high (10^{-1}), the carbon dioxide partial pressure is nearly that of the atmosphere (10^{-4}). Under such conditions, the diagram indicates the insolubility of lead; the activity of the ions exceeds 10^{-6} only under very alkaline or very acid conditions. Also, the diagram simplifies to the major minerals usually observed in the field: galena, cerussite, and anglesite, with a small field of plattnerite under unusual conditions. Figure 3.4 is a variation of Figure 3.3 in that it shows conditions that might be expected in an oxidising galena deposit which is isolated from the atmosphere but has a fairly high dissolved carbonate, as well as a high dissolved sulphur content. Hydrocerussite appears on the diagram owing to the fact that the system has a fixed total carbon dioxide content, and at high pH values the hydrocerussite can compete with the normal carbonate. When the carbon dioxide partial pressure is constant, the total carbonate content rises with pH and cerussite persists as the stable phase.

Figure 3.2: Stability fields of galena, anglesite, and cerussite as functions of pH and Eh (from Garrels (1954))

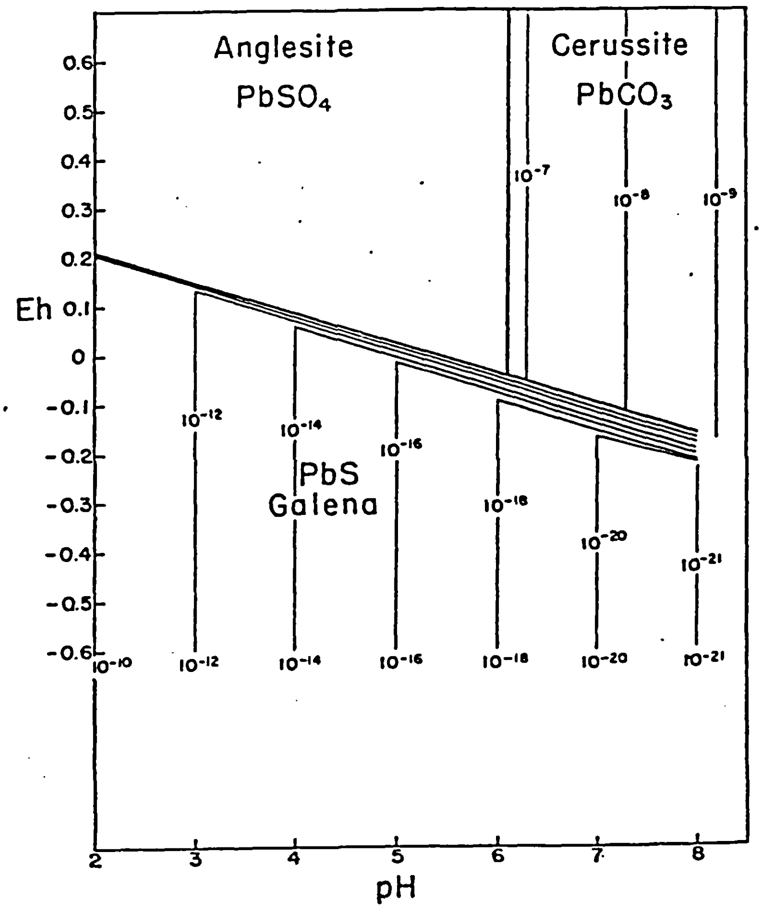

Contours are for activity of Pb^{2+}

$\Sigma CO_2 = 0.03$, $\Sigma S = 0.1$, $t = 25°C$

Figure 3.3 Stability relations among lead compounds in water, $P_{CO_2} = 10^{-4}$ (from Garrels and Christ (1965))

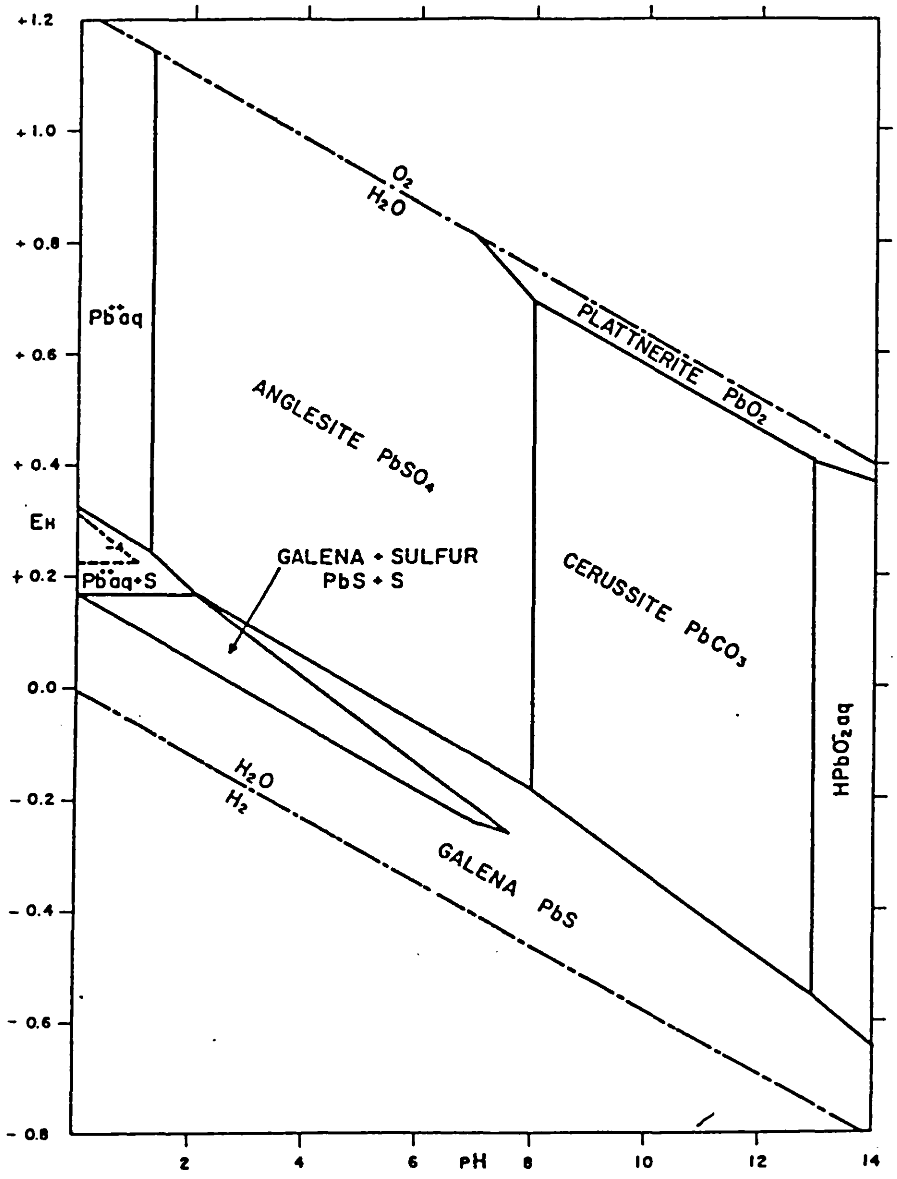

Boundaries of solids at total ionic activity of 10^{-6}

$P_{CO_2} = 10^{-4}$, $\Sigma S = 0.1$, t = 25°C, 1 atm pressure

Figure 3.4 Stability relations among lead compounds in water, ΣCO_2 = 0.1 (from Garells and Christ (1965))

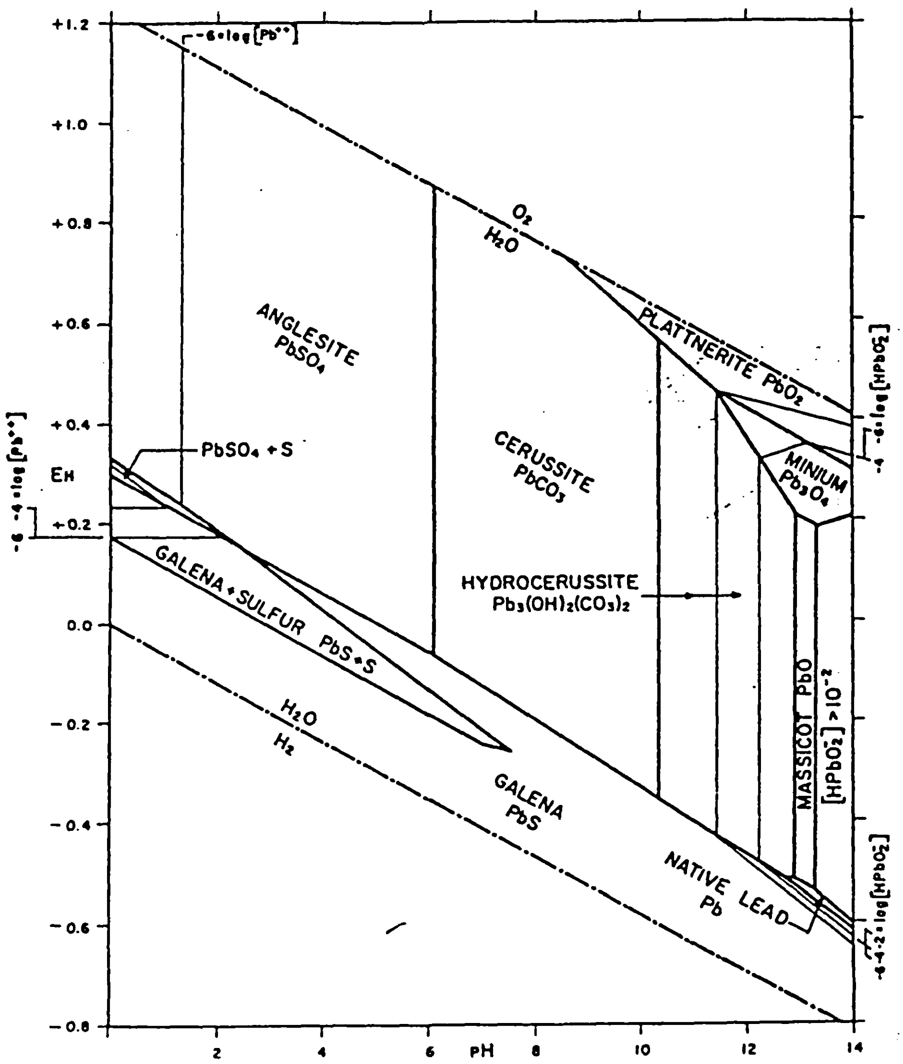

$\Sigma CO_2 = 0.1$, $\Sigma S = 10^{-1.5}$, t = 25°C, 1 atm pressure

Mann and Deutscher's (1980) theoretical study showed that at alkaline and neutral pH where cerussite is the solid limiting lead solubility, the solubility is virtually unchanged for an increase in f_{CO_2} to 10^{-2} bar (100kPa).* f_{CO_2} has only a small effect on lead solubility as compared to chloride and sulphate, which contrasts with the case for copper where dicarbonate complexes, in particular, have a strong influence on copper solubility in alkaline solution (Mann and Deutscher (1977)). The authors took the carbon dioxide content of natural waters to be controlled by the atmosphere, i.e. 0.03% ($f_{CO_2} = 10^{-3.5}$ bar = 3.2kPa), and carbonate values are related to this by

$$\log a_{CO_3^{2-}} = \log f_{CO_2} - 18.17 + 2pH \qquad (3.14)$$

A fixed total activity of combined carbonate species has been commonly used in calculations involving carbonate equilibria, for example, in the construction of Eh-pH diagrams (Garrels and Christ (1965)). Jenne (1968) pointed out that this is not a desirable assumption for surficial materials such as soils and streams, and that fixed partial pressures more closely approximate to natural systems. Field analyses of surface and near surface underground waters in varying geological environments usually show carbon dioxide partial pressures to be in the range $P_{CO_2} = 10^{-2}$ to 10^{-4} bar (100kPa to 1kPa). Mann and Deutscher (1978), in a study of drainage catchment in Western Australia, observed a mean P_{CO_2} of $10^{-2.01}$ bar (997.2kPa); values similar to this are commonly observed for groundwater in equilibrium with soil.

Recently, Abdul-Samad et al (1982) investigated the stability regions of leadhillite, $Pb_4SO_4(CO_3)_2(OH)_2$, hydrocerussite, $Pb_3(CO_3)_2(OH)_2$, anglesite, and cerussite in terms of pH and sulphate activity. The authors used the free energy change of the reaction,

$$3PbCO_3 + 2H_2O = Pb_3(CO_3)_2(OH)_2 + H_2CO_3^{\circ}(aq) \qquad (3.15)$$

to calculate the activity of $H_2CO_3^{\circ}$ at which hydrocerussite is stable with respect to cerussite. They found that, at $H_2CO_3^{\circ}$ activities greater than $10^{-4.4}$, cerussite is the stable phase, and vice versa.

---

* f_{CO_2} is the fugacity of carbon dioxide. Fugacity is the thermodynamically corrected gas 'activity' and is analogous to solution activity. For the purposes of this work, fugacity is taken to be equal to partial pressure, unless otherwise stated.

The authors chose to relate this stability boundary to the activity of $H_2CO_3°$ because they considered this species to be dependent only upon the partial pressure of carbon dioxide, whilst the activities of CO_3^{2-} and HCO_3^- are pH dependent. As described in section 3.3.4, in systems open to the atmosphere, all the aqueous carbon dioxide species are pH dependent. Further, $H_2CO_3°$ is the dominant solution species only at pH values below 6. Thus, the necessary activity of $H_2CO_3°$ to stabilise cerussite would only occur at quite acid pH, leaving a large hydrocerussite stability field. But, Garrels and Christ (1965) have shown that hydrocerussite has only a small stability field to the alkaline side of cerussite and only when a fixed carbon dioxide content is considered. Thus, it seems probable that the value of $H_2CO_3°$ activity of $10^{-4.4}$ represents total carbon dioxide content. Figure 3.5 shows the stability fields of anglesite, leadhillite, and cerussite as determined by Abdul-Samad et al (1982). The small leadhillite zone is seen to be dependent upon sulphate activity and pH. Cerussite is still seen to be the stable phase under the conditions encountered in the Dutchman dump.

3.3.5 Mechanism of galena oxidation by oxygen

The mechanism proposed by Eadington (1966), and later supported by Eadington and Prosser (1969), for the surface oxidation of lead sulphide (galena) by oxygen dissolved in water has received general acceptance. The reaction is considered to proceed in four stages:

1. An induction period, the length of which depends on the non-stoichiometry of the galena.
2. A short acceleratory period.
3. A period of steady-rate oxidation in which the rate depends on non-stoichiometry.
4. A period of retardation by a coating of lead sulphate.

1 The induction period

Initially, oxygen is rapidly chemisorbed* from solution onto the galena surface, withdrawing electrons from it and setting up an

---

* Adsorption denotes the process of concentration of any chemical species, i, occurring at an interfacial region separating two phases. If, at some stage, electrons are transferred during adsorption, then such adsorption becomes chemisorption (Leja (1982)).

Figure 3.5 Stability fields of anglesite and leadhillite in terms of pH and $a_{SO_4^{2-}}$ relative to hydrocerussite (firm line) at $a_{H_2CO_3^{\circ}} = 10^{-6.38}$, and to cerussite (dashed line) at $a_{H_2CO_3^{\circ}} \doteq 10^{-4.4}$ (from Abdul Samad et al (1982))

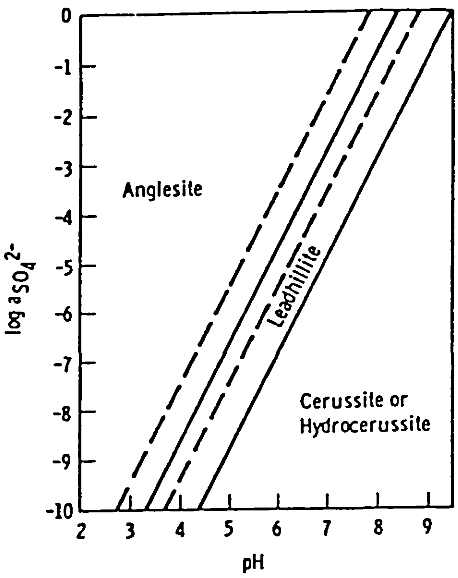

electrical space charge layer. Chemisorption continues until the space charge layer is established with the positive charge dispersed within the galena as positive holes, and the negative charge being associated with the chemisorbed oxygen atoms.

There then follows a slow process in which further electron transfer occurs to form O^{2-}, or perhaps O_2^{2-} initially, which reacts with water and desorbs as OH^-, or H_2O_2 and OH^-. The positive holes left in the galena associate with sulphide ions to form neutral sulphur atoms or, alternatively, associate with lead ions to form Pb^{3+} ions which remain in the galena lattice. Simultaneously, the galena surface loses a lead ion to the solution. The overall reaction is represented by:

$$PbS + O_{surface} + H_2O = Pb^{2+}_{(aq)} + S_{(PbS)} + 2OH^-_{(aq)} \qquad (3.16)$$

Since the transfer of Pb^{2+} and OH^- ions to the solution corresponds to a partial discharge of the electrical double layer, more oxygen can be chemisorbed. Also, the layer of galena near to the surface is now enriched in sulphur, i.e. the galena has been converted from n-type (if it was originally lead-rich) to p-type, and the number of positive holes is increased.

The outer layers of galena continue to oxidise slowly until they become supersaturated with sulphur (or excess sulphide ion).

2. The acceleratory period

The formation of elemental sulphur nuclei, which start to grow on the surface of the galena, marks the end of the induction period. Once a nucleus is formed, it quickly collects sulphur from the nearby supersaturated layer of galena and the sulphur content there falls to a level corresponding to a saturated solution. In other areas, away from the sulphur nuclei, the galena remains super-saturated with sulphur. These compositional differences correspond to changes in the positive hole density and, therefore, to an electrical potential difference between the areas adjacent to, and the areas away from, the sulphur phase. The potential difference accelerates the oxidation. The reaction is virtually the same as that which occurs during the induction period:

$$2PbS = 2Pb^{2+}_{(aq)} + 2S_{(sulphur)} + 4e^- \quad (3.17a)$$

$$O_{2(aq)} + 2H_2O + 4e^- = 4OH^-_{(aq)} \quad (3.17b)$$

The two reactions take place on different areas of the galena surface; the process being regarded as a form of electrolysis (Figure 3.6). At the electrode consisting of saturated galena near to the sulphur phase, more sulphur is formed by reaction (3.17a). Oxygen is reduced by reaction (3.17b) at the electrode consisting of super-saturated galena. Although the reaction is thermodynamically spontaneous, it is very slow in the absence of a catalyst. However, the other regions of the galena act as the catalyst.

3. The steady rate period

Reactions (3.17a) and (3.17b) occur during this period causing lead hydroxide to be precipitated near to the sulphur phase. The hydroxide and sulphur react according to:

$$4Pb^{2+} + 8OH^- + 4S = 2PbS + \underset{\text{basic lead thiosulphate}}{PbO.PbS_2O_3.nH_2O} + (4-n)H_2O \quad (3.18)$$

and thus sulphur is removed at approximately the same rate as it is formed. The super-saturated sulphur area, away from the sulphur phase, tends to be maintained by the oxygen in the same way that it was formed during the induction period.

The reduction of oxygen is assumed to be the rate determining step with its rate controlled by the potential difference between areas of the lead sulphide, as previously discussed. Continuing the analogy of electrolysis, the relationship between potential differences and rate of reaction is of the same form as that between overpotential and current density. Such a relationship leads to the sulphur activity ratio, $a_{supersat}/a_{sat}$, being greater than 10^3; this is high, but not impossible. For, the limit of solubility of sulphur in lead sulphide at 800°C is approximately 0.1 atomic percent, but at room temperature it is likely to be much less, probably less than 0.01 percent. Thus, the super-saturated region is required to contain approximately 10 atomic percent sulphur in a small region which could have been crystallographically near perfect before it became super-saturated.

Figure 3.6: Diagrammatic representation of the processes taking place during the steady rate period of galena oxidation (from Eadington and Prosser (1969))

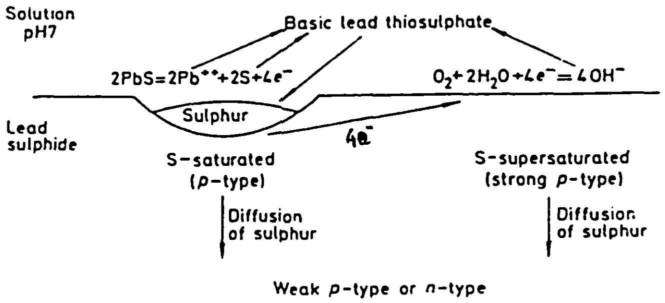
Solution pH7
Basic lead thiosulphate
$2PbS=2Pb^{++}+2S+4e^-$
$O_2+2H_2O+4e^-=4OH^-$
Sulphur
Lead sulphide
$4e^-$
S-saturated (p-type)
S-supersaturated (strong p-type)
Diffusion of sulphur
Diffusion of sulphur
Weak p-type or n-type

An important feature of the steady rate period is that is depends on the original non-stoichiometry of the galena. This implies that part of the galena, presumably the interior, is still much in its original state; however, sulphur diffuses into the interior from the outer regions that are saturated or super-saturated with sulphur. Eadington and Prosser (1969) suggested that a sulphur concentration gradient is set up over a distance of between 1 and 100nm in the crystal. If the distance is greater than 100nm, the whole crystal would effectively have been saturated with sulphur in Eadington's experiments. If the distance is comparable to or less than the S-S distance in the crystal then there would be no layer of sulphur-enriched lead sulphide as discussed in connection with the induction period. The apparent diffusion coefficient for sulphur calculated from this model using the concentration data referred to above was found to be $10^{-22} m^2 s^{-1}$. High temperature diffusion data extrapolated to 25°C gave 10^{-28} to 10^{-26} $m^2 s^{-1}$. If the activation energy changes at lower temperatures, it is expected to be a smaller value, and, hence, the extrapolated value is likely to be low.

The sulphur concentration adjacent to the sulphur phase is maintained at saturation level regardless of the composition of the underlying crystal; but, as a result of diffusion, the concentration in the supersaturated region tends to be reduced. This tendency is greatest in the crystals that are lead-rich in the interior, and, therefore, the concentration in the supersaturated zone is less for these crystals than for the sulphur-rich crystals. Consequently, the potential difference between the saturated and super-saturated zones is expected to be less and the reaction is found to be slower for lead-rich galena.

4. The retardation period

During this period, an oxidation film of lead sulphate has built up around the galena, inhibiting the passage of oxygen to the sulphide surface and exerting diffusion control on the oxidation system.

3.3.6 Effect on the oxidation rate of different variables

The following observations and conclusions are based on the work of Eadington (1966).

1. pH

The rates of oxidation of galena were similar and almost linear in all solutions until the formation of sulphate was detected. A significant decrease in reaction rate was observed following the formation of 1×10^{-9} moles of sulphate per square centimetre of surface area. The slowest overall rate was therefore observed in neutral solutions where sulphate was found to be the predominant oxidation species after 12 hours. Conversely, the fastest rate was found in acid solutions where the formation of sulphate was the slowest. The blocking effect of the sulphate is imperfectly understood. It is surprising that the formation of elemental sulphur, in relatively large quantities (in acid solution) has little effect on the oxidation rate in view of the well known poisoning of redox catalysts. Thus the sulphur formed is either sufficiently porous or is not attached to the surface and does not significantly hinder the transfer of the oxidising species to the surface.

2. Other reagents

An increase in the oxidation rate was observed upon the addition of potassium ethyl xanthate or potassium cyanide. This was attributed to the reaction of these compounds with the sulphur initially formed and so preventing the formation of the rate-controlling sulphate ions. Similar increases in oxidation rate upon the addition of ammonium acetate were attributed to the complexing of the insoluble lead salts causing them to dissolve, leaving the galena surface free for further oxidation. It is therefore expected that any reagent which either prevents or delays the formation of sulphate ions or renders them soluble will cause more extensive and faster oxidation.

Eadington and Prosser (1965) investigated the oxidation of copper sulphide (CuS) and found that, whilst the initial rate of oxidation was similar to that found for galena, the overall reaction rate was much faster since the initial rate was maintained in spite of extensive oxidation. Copper sulphide was shown to oxidise almost completely to the sulphate, which is readily soluble. The addition of xanthate during the oxidation of the sulphide caused a slower reaction. This was attributed to copper xanthate being relatively insoluble and causing a blockage of the surface.

These results show that one of the controlling factors of the overall oxidation of galena is the solubility of the oxidation products. In the absence of relatively insoluble surface coatings, oxidation can continue at the initial rate. The much smaller effects of surface coverings of sulphur or thiosulphate to those of sulphate led Eadington (1966) to suggest that the distribution of the oxidation products may also be an important factor in the blocking of oxidation.

3. Temperature

In the range 25°-50°C, the change in oxidation rate of galena was less than the 6% change due to sampling errors.

4. Oxygen pressure

The effect of variations in the oxygen pressure on the oxidation rate of galena in the range 20-760~~MM~~ mm Hg caused less than a 20% rate variation.

5. Surface area

The rate of oxidation was seen to be proportional to the solid-liquid interfacial area for samples taken from the same preparation batch.

6. Stoichiometry

Eadington (1966) concluded that structural imperfections have an important influence on the oxidation of galena. His results showed:

i) the rate of oxidation of galena varies with stoichiometry, sulphur-rich galena oxidising faster than sulphur-deficient.

ii) an induction period of variable length depending on stoichiometry; the longest period occurring with sulphur-deficient galena.

His analytical results showed that the products of oxidation are independent of stoichiometry, both qualitatively and quantitatively.

3.4 Mineralogy of galena alteration

The natural alteration of galena is generally considered to be of a simple type, with the ultimate formation of anglesite or cerussite depending on the prevailing conditions. However, most authors assume that galena cannot oxidise 'directly' to cerussite but must pass via anglesite; the common occurrence of mineral masses with a galena core surrounded by anglesite, which is in turn surrounded by cerussite is often quoted as evidence for this. Garrels (1954) explains these macroscopic observations on the basis that at the site of oxidation, an acid solution is formed, and the sulphide is converted into sulphate. The hydrogen ions move outward from the sulphide-sulphate reaction zone where they are neutralised by calcium carbonate and an outer zone of lead carbonate is built up by slow solution of the lead sulphate and precipitation of the carbonate.

Anderson (1930) states that galena first oxidises to anglesite and apparently that cerussite forms by replacement of anglesite and never of galena directly. More importantly, he notes the apparent absence of a volume change in the in situ conversion of galena to anglesite; the anglesite is usually dense (especially in the absence of limonite), it is homogeneous, and forms a knife-like contact with the galena. He did, however, note the presence of a 'narrow spongy zone' where the sulphate had been later attacked by iron or carbonate solutions.

Macroscopically-zoned, galena-anglesite-cerussite probably reflects a change in the oxidising environment rather than a fixed alteration route. Initially, acid conditions prevail and the sulphate is stable. Later, carbonate solutions are introduced and, under these new conditions, the carbonate is stable.

Park and Macdiarmid (1975) comment that the alteration of galena to cerussite may, or may not, involve intermediate anglesite. Freund (1966) notes that anglesite is frequently formed ahead of cerussite and that difficulties experienced in the froth flotation of galena could be attributed to the presence of extremely fine, microscopically non-determinable alteration products of unknown composition.

Ford and King (1965) and Ineson and Al-Kufaishi (1970) report galena altering directly to cerussite in limestone environments. This effect is expected under the conditions prevailing in the Dutchman dump.

3.5 Chemical considerations in the aqueous oxidation of chalcopyrite by oxygen

3.5.1 Neutral solutions

No detailed work like that carried out on galena by Eadington (1966) has been carried out on chalcopyrite or sphalerite. However, it is known that in neutral aqueous media, chalcopyrite is oxidised by oxygen to yield sulphates,

$$CuFeS_2 + O_2 \longrightarrow CuSO_{4(aq)} + FeSO_{4(aq)} \tag{3.19}$$

The reaction is slow at room temperature but rapid at higher temperatures (Habashi (1970)). Under the latter conditions, Fe^{2+} ions undergo hydrolysis and oxidation according to

$$Fe^{2+} + 2H_2O \longrightarrow Fe(OH)_2 + 2H^+ \tag{3.20}$$

$$2Fe(OH)_2 + H_2O + \tfrac{1}{2}O_2 \longrightarrow 2Fe(OH)_3 \tag{3.21}$$

It is also possible that oxidation precedes hydrolysis,

$$2Fe^{2+} + 2H^+ + \tfrac{1}{2}O_2 \longrightarrow 2Fe^{3+} + H_2O \tag{3.22}$$

$$Fe^{3+} + 2H_2O \longrightarrow Fe(OH)_3 + 3H^+ \tag{3.23}$$

Depending on temperature, iron (III) hydroxide undergoes rapid transformation to iron oxyhydroxide or iron (III) oxide according to

$$Fe(OH)_3 \longrightarrow FeO.OH + H_2O \tag{3.24}$$

$$2FeO.OH = Fe_2O_3 + H_2O \tag{3.25}$$

Brown (1971) notes that goethite (FeO.OH) is more stable than hematite (Fe_2O_3) below 40°C.

Steger and Desjardins (1978) studied the oxidation of chalcopyrite in air at 52°C and 68% relative humidity. They concluded that chalcopyrite is initially oxidised to a combination of iron(II) and copper(I) thiosulphates which undergo further oxidation to iron(III) and copper(II) sulphates. However, the products designated 'thiosulphates' can, in fact, be thiosulphate, sulfite, or polythionate since the authors' analytical methods could not distinguish among them. But, polythionate is, in general, a redox product of thiosulphate (Cotton and Wilkinson, (1962)), and it is reasonable to assume that the 'thiosulphate' is indeed thiosulphate or sulphite formed during the oxidation of chalcopyrite.

The authors found it impossible to determine the quantity of copper oxidised in the chalcopyrite and therefore assumed it to be essentially the same as the quantity of oxidised iron:

$$CuFeS_2 + 2O_2 \longrightarrow FeS_2O_3 + CuO, \text{ or} \tag{3.26}$$

$$4CuFeS_2 + 7\tfrac{1}{2}O_2 \longrightarrow 2FeS_2O_3 + 2Cu_2S_2O_3 + Fe_2O_3 \tag{3.27}$$

Their results suggested that approximately 15% of the oxidised sulphur does not form sulphate. That is consistent with

$$4CuFeS_2 + 15\tfrac{1}{2}O_2 \longrightarrow Fe_2(SO_4)_3 + Fe_2O_3 + 4CuSO_4 + S \tag{3.28}$$

There was also some evidence to suggest that some water of hydration is associated with the oxidised metal species.

Both thiosulphate and sulfite can reduce iron(III) to iron(II) and copper(II) to copper(I) species respectively (Kolthoff and Belcher (1957)). Steger and Desjardins (1978) therefore assumed that the oxidised product designated 'thiosulphate' must be associated with the lower valence metal ions. The authors found that the average values of 'thiosulphate' for the oxidised samples were consistent with their iron(II) and copper(I) contents. The same consistency was observed between 'thiosulphate' and iron(II) in the oxidation of pyrite and pyrrhotite under the same conditions. This led the authors to suggest that there is a limit on the amount of lower valance metal that can be present in the oxidation products under the conditions used. This limitation is thought to apply to the metal rather than to the 'thiosulphate' since the amount of metal exceeds that of 'thiosulphate' in the unoxidised samples.

3.5.2 Acidic solutions

Ichikuni (1960) showed that at temperatures greater than 80°C, acidity increases the rate of aqueous oxidation of chalcopyrite. In 0.1M dm^{-3} hydrochloric acid, the amount of sulphate ion formed in solution is negligible compared with Cu^{2+} and Fe^{2+} ions. This is because under these conditions, appreciable amounts of sulphur are formed according to

$$CuFeS_2 + 4H^+ + O_2 \longrightarrow Cu^{2+} + Fe^{2+} + 2S + 2H_2O \tag{3.29}$$

The sulphur is then oxidised to sulphate, with the reaction being favoured by increased temperature and low acidity,

$$S + H_2O + 1\frac{1}{2}O_2 \longrightarrow 2H^+ + SO_4^{2-} \quad (3.30)$$

Vizsolyi et al (1967) showed that at 120°C and 3400kPa oxygen partial pressure, chalcopyrite is oxidised thus,

$$CuFeS_2 + 2H^+ + 1^1/4\ O_2 \longrightarrow Cu^{2+} + FeO.OH + \frac{1}{2}H_2O + S \quad (3.31)$$

Under certain conditions of pH and temperature, aqueous sulphate ions enter into the crystal structure of the iron oxyhydroxide (goethite) forming a basic sulphate such as $Fe(OH)SO_4$.

Hiskey and Wadsworth (1975) note that, during the acid oxidation of chalcopyrite, the remnant particles retain the same geometrical shape as the parent particles with sharp corners being preserved during the reaction. This observation is important since sharp corners indicate surface controlled kinetics; diffusional processes tend to round off sharp corners and edges. Bauer et al (1972), however, found that the rate of dissolution of chalcopyrite in the presence of Fe^{3+} ions depends upon the diffusion of those ions through a deposited sulphur film resulting from the anodic dissolution of chalcopyrite.

$$CuFeS_2 \longrightarrow Cu^{2+} + Fe^{2+} + 2S^\circ + 4e^- \quad (3.32)$$

Blain and Andrew (1977) propose a similar anodic oxidation of chalcopyrite leading to the formation of geothite:

anode: $CuFeS_2 + H_2O \longrightarrow FeO.OH + Cu^{2+} + 19H^+ + 2SO_4^{2-} + 17e^-$ (3.33)

cathode: $4^1/4\ O_2 + 8\frac{1}{2}H_2O + 17e^- \longrightarrow 17OH^-$ (3.34)

net: $CuFeS_2 + 1\frac{1}{2}H_2O + 4\frac{1}{2}O_2 \longrightarrow FeO.OH + Cu^{2+} + 2H^+ + 2SO_4^{2-}$ (3.35)

Wadsworth (1972), in a comparison of the oxidation of several copper-sulphide minerals by different methods, found the results for chalcopyrite to be distinct for a variety of reasons:

1. transport control is indicated at lower temperatures, under non-autoclave conditions, in which the oxidant must diffuse through the oxidation products;
2. the activation energy for oxygen oxidation is approximately half that for oxidation by the Fe^{3+} ion;

3. the magnitude of the activation energy is very large for diffusion through liquid-filled pores in the product layer, which would be a condition that would have to be satisfied if electrochemical processes are important, since a dense sulphur layer would be non-conducting.

Wadsworth (1972) concluded that the importance of electrochemical reactions in the oxidation of chalcopyrite is not clear from the observed kinetics. The large activation energy associated with parabolic kinetics suggests solid-state diffusion of oxidant through product layers. If an electrochemical mechanism is operative, then the physical nature of the products formed would have to be unique in that the pores would have to be extremely small, limiting the diffusion of the oxidant. Thus, partial dehydration of diffusion ions or the flow of polymeric sulphur units in the product layer might be involved.

The role of initial acidity (sulphuric acid) was studied by Braithwaite and Wadsworth (1976). They found that a constant pH is established during the oxidation of chalcopyrite because the acid consumed during the dissolution equals that produced by the hydrolysis of Fe^{2+} and Fe^{3+} ions. This constant pH decreases with increasing temperature. The dissolution of copper and the precipitation of iron phases was found to be faster in hydrochloric acid than in sulphuric acid (Habashi (1978)). This was attributed to the formation of chlorine which rapidly oxidises the chalcopyrite.

3.5.3 Alkaline solutions

Little work has been carried out on the oxidation of chalcopyrite in alkaline media. Haskett et al (1975) found that it reacts with sodium hydroxide solutions at 60° to 120°C under an oxygen partial pressure of 500 to 1500kPa according to:

$$2CuFeS_2 + 12NaOH + 8\tfrac{1}{2}O_2 \longrightarrow 2Na_2Cu(OH)_4 + Fe_2O_3 + 4Na_2SO_4 + 2H_2O \quad (3.36)$$

In ammoniacal media, the oxidation of chalcopyrite leads to the complexation of copper ions with the amine complex and the precipitation of iron as hydroxide, with sulphur being solubilised as sulphate, via many intermediates (Habashi (1978)).

The oxidation rates of chalcopyrite in all media are affected if other sulphide minerals are in contact with it forming a galvanic cell. As stated in section 3.1, when sulphides are in contact, the sulphide having the lowest electrode potential is preferentially oxidised. Although the electrode potentials of particular sulphide minerals vary as a function of the sulphur activity of the sulphide (Sato (1966)), and the composition of the electrolyte, in general the electrode potentials increase in the order sphalerite, galena, chalcopyrite, and pyrite (Govett et al (1976)).

3.5.4 Carbonate solutions

The aqueous oxidation of chalcopyrite leads to the formation of various copper, iron, and sulphur species. In carbonate solutions, the behaviour of sulphur from chalcopyrite is probably the same as that from galena (section 3.3.4). The behaviour of the copper species depends upon pH and carbonate species concentration. It also depends upon sulphate ion concentration since, at any given pH, the solubility of copper may vary by nearly two orders of magnitude depending on the sulphate concentration (Mann and Deutscher (1977)). But, high acidity and high sulphate concentrations favour the solution transport of copper.

Mann and Deutscher (1977), in a theoretical study of geochemical copper behaviour, showed that malachite, $Cu_2CO_3(OH)_2$, is the phase which limits copper solubility (i.e. it is the least soluble, and therefore, the most stable phase) over the pH range of 2 to 12 studied. In solutions containing sulphate ions in addition to carbonate species, antlerite, $Cu_3(OH)_4SO_4$, and brochantite, $Cu(OH)_{1.5}(SO_4)_{0.25}$, limit copper solubility at low pH values.

Rickard (1971) studied theoretically the $Cu\text{-}H_2O\text{-}CO_2\text{-}O_2$ system. Within this system, neither copper(I) nor copper(II) carbonates have been isolated as solids. The stable compounds are copper(II) oxy-carbonates. The relationship between the dissolved species in this system are shown in Figure 3.7. It is seen that copper carbonate complexes first appear at a total dissolved carbonate activity of $10^{-5.3}$ and at a pH of 8.9. In weakly acid to alkaline waters, the copper carbonate complexes become of major importance in the solution chemistry of copper as the total carbonate activity increases. In particular, the formation of undissociated copper(II) carbonate, and the binegative copper(II) carbonate

Figure 3.7: Relationships between dissolved copper carbonate species as a function of $p^{[CO_3]}$ and pH at 25°C and 1 atm pressure (from Rickard (1971)).

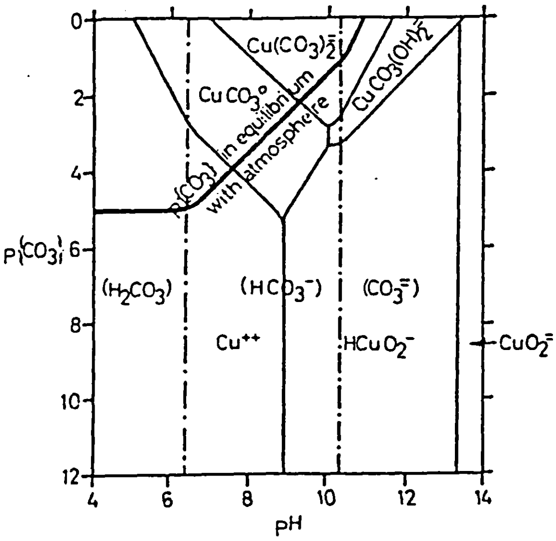
0
2
4
6
8
10
12
p{CO3}
Cu(CO3)2=
CuCO3°
CuCO3(OH)2=
p{CO3} in equilibrium with atmosphere
(H2CO3)
(HCO3-)
(CO3=)
Cu++
HCuO2-
CuO2=
4
6
8
10
12
14
pH

Figure 3.8: Relationships in the Cu-H_2O-O_2-CO_2 system as a function of pH, $p^{[CO_3]}$, and Eh at $p^{[Cu]}$ = 6, 25°C, and 1 atm pressure (from Rickard (1971))

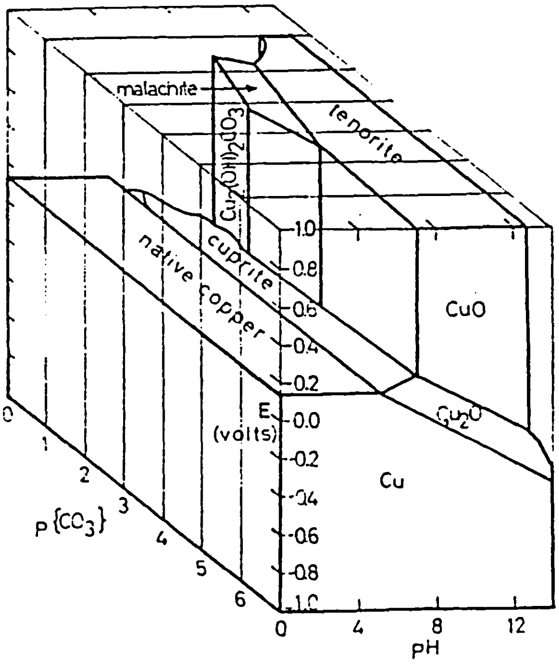
malachite
Cu2(OH)2CO3
tenorite
native copper
cuprite
CuO
Cu2O
Cu
E (volts)
1.0
0.8
0.6
0.4
0.2
0.0
-0.2
-0.4
-0.6
-0.8
-1.0
p{CO3}
0
1
2
3
4
5
6
0
4
8
12
pH

complex play major roles in determining the solubility of the copper minerals as shown in Figure 3.8. Note the complete disappearance of the tenorite field at $p[CO_3] > 0.9$, and the limitation of the malachite field. As pointed out by Garrels and Christ (1965), azurite is stable relative to malachite at carbon dioxide partial pressures above the normal atmospheric level, or where the activity of water is reduced.

Figure 3.9 shows the activity of copper species in equilibrium with azurite, malachite, and tenorite. Note that when $p[Cu] = 6$, azurite has no stability field, and at $p[Cu] = 7$, malachite ($K_{sp} = 1.7 \times 10^{-34}$, Mann and Deutscher (1977)) has no stability field, even at high total carbonate activities.

Rickard (1971) also analysed the $Cu\text{-}H_2O\text{-}O_2\text{-}S$ system. Figure 3.10 shows the values of p[Cu] in equilibrium with the major oxidised minerals in this system at various $p[SO_4^{2-}]$ values. It is seen that tenorite is the stable phase at neutral to alkaline pH and at sulphate activities expected in natural carbonate environments. Although carbon dioxide species are excluded from this analysis, it can be argued that, on superimposition of the two stability diagrams, since malachite is stable relative to tenorite in most carbonate environments (see above), malachite would also be the stable phase at neutral to alkaline pH in the $Cu\text{-}H_2O\text{-}O_2\text{-}S\text{-}CO_2$ system, as determined by Mann and Deutscher (1977).

Mann and Deutscher (1977) calculated the theoretical total soluble copper content of various solutions as a function of pH using the equation

$$\log a_{CO_3^{2-}} = \log f_{CO_2} - 18.17 + 2pH \qquad (3.14)$$

to relate pH and carbonate ion activity (section 3.3.4). In general, when plotted, the shapes of these curves (Figure 3.11) are dominated by the concentrations of hydroxide and carbonate species in solution, and only to a lesser extent are they modified by the presence of sulphate. The curve, with a distinct minimum near a pH of 9, arises because the activity of copper in equilibrium with malachite increases rapidly with decreasing pH at values below a pH of 7 as the carbonate content of the water decreases, and because at pH values greater than 7 and 9 respectively, the authors consider that the undissociated dihydroxy complex and the binegative copper(II) carbonate complex ions become the

Figure 3.9: Values of $p^{[Cu]}$ in equilibrium with tenorite, malachite, and azurite in term of $p^{[CO_3]}$ and pH at 25°C and 1 atm pressure (from Rickard (1971))

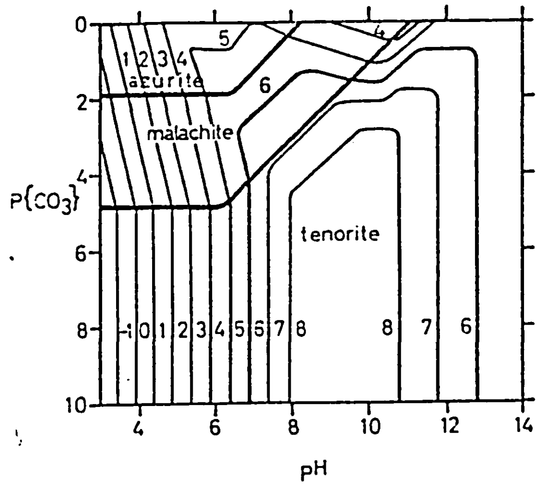

Figure 3.10: Values of $p^{[Cu]}$ in equilibrium with the major oxidised phases in the $Cu-H_2O-O_2-S$ system at various $p^{[SO_4^{2-}]}$ values at 25°C and 1 atm pressure (from Rickard (1971))

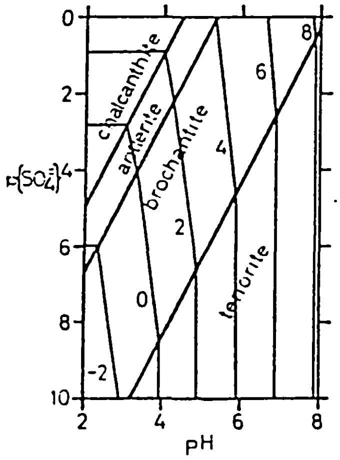

Figure 3.11: Effect of sulphate activity on Cu solubility (from Mann and Deutscher (1977))

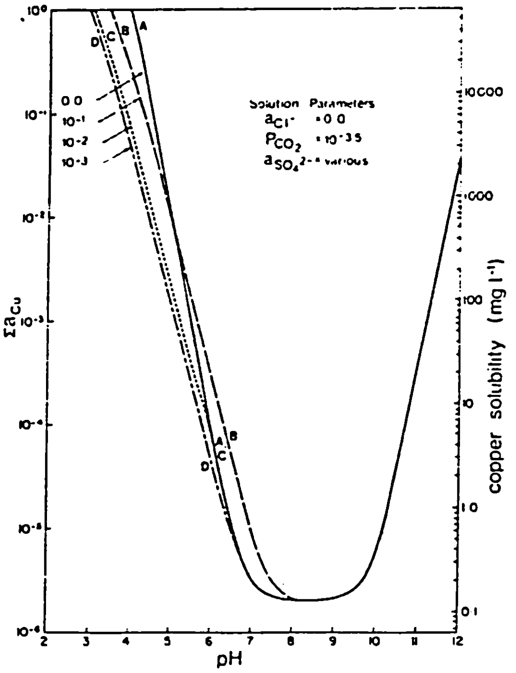

Curve A, sulphate-free

Curve B, $a_{SO_4^{2-}} = 10^{-1}$

Curve C, $a_{SO_4^{2-}} = 10^{-2}$

Curve D, $a_{SO_4^{2-}} = 10^{-3}$

dominant soluble copper species.

An increase in the carbon dioxide partial pressure from $10^{-3.5}$ to $10^{-3.0}$ bar (3.2 to 10kPa), a value still within the range commonly observed for groundwaters and surface waters, is calculated by Mann and Deutscher (1977) to have a two-fold effect on copper solubility, particularly when sulphate activities are low. At low pH values, copper solubility is decreased because it is governed by the dissociation of malachite which is carbonate ion dependent. However, at neutral and alkaline pH values, this effect is more than compensated for by an increase in concentration of the complex species $CuCO_3^{\circ}$ and $Cu(CO_3)_2^{2-}$, and there is a significant increase in the copper content of solutions at higher pH values with the increase in carbon dioxide partial pressure. This is in accord with the work of Rickard (1971).

Copper solubility in sulphate-free solutions at a low carbon dioxide partial pressure of $10^{-4.0}$ bar (1kPa) is increased in acid solutions and decreased in alkaline solutions; tenorite is the copper solubility-limiting phase (Mann and Deutscher (1977)). This was also shown by Rickard (1971).

The solution geochemistry of most trace metals, including copper, is, however, generally far more complicated than can be appreciated by considering equilibrium behaviour in solutions containing only the major anions. Copper concentrations in solution will often be influenced by its adsorption onto clays and hydrous oxides of iron and manganese (Jenne (1968)) and by complex ion formation with other inorganic and particularly organic species, so that only in rare circumstances will natural waters contain copper in solution at the quoted activities. Collins (1973) in a study of the concentration control of soluble copper in a mine tailings drainage stream found that soluble copper was not lost from solution by precipitation but by adsorption onto stream sediment.

One of the most complete studies on adsorption from the point of view of the natural aqueous environment was made by Krauskopf (1956). He used solutions containing a total dissolved copper activity of approximately 10^{-5} at a pH of approximately 8. Under these conditions, only oxides (and hydroxides), oxy-carbonates, oxy-chlorides, and oxy-sulphates of copper are stable. Krauskopf found no significant difference between the adsorption capacities of iron and manganese oxides, which he took to be oppositely charged in the colloidal state. This would not be expected if all the copper was ionic. Therefore, it would appear that Krauskopf's systems contained solid copper phases and the degree of copper adsorption was probably modified by the equilibrium between the solid phases and the ionic copper species. This process was recognised by Mitrofanov and Bazanova (1959) in their studies of the adsorption of copper on sphalerite. They showed that adsorption on sphalerite was at a maximum at a pH of 5.7 and at a minimum at a pH of 8. At pH values greater than 6, adsorption was independent of the initial copper concentration and was determined by the solubility of copper(II) hydroxide. Even in the absence of solid copper phases, an equilibrium is reached between the ions adsorbed and those remaining in solution. In both inorganic and organic systems, it has been shown that initial high copper adsorption is followed by a release of copper into solution (Riley (1939); Krauskopf (1956)). All other variables being constant, the position of the equilibrium is determined by the amount of adsorbent present and the concentration of adsorbate in solution. If fresh amounts of adsorbent are added, a new equilibrium is established. This has been observed in streams by DeGrys (1962), where increased stream velocity may give an increase in sediment load and a decrease in the concentration of dissolved constituents.

It has also been shown (Gorlich and Gorlich (1958)) that metal ions are adsorbed onto calcium carbonate and natural limestones; the Cu^+ species was the third most readily adsorbed after Fe^{3+} and Pb^{2+} species.

Iron migrates in the aqueous state where the solutions are strongly acidic or deficient in oxygen (Park and MacDiarmid (1975)). Giblin (1978) notes that at pH values above 4, at sufficiently high oxygen activities, most iron will be immobilised as species of hydrous iron(III) oxide with a solubility product of about 10^{-36} at 25°C.

Posnjak and Merwin (1919) have shown that there is no mineral species 'limonite', $2Fe_2O_3.3H_2O$. The only members of the hydrous iron oxide series are the iron(III) oxide, hematite, and the monohydrate, $Fe_2O_3.H_2O$, which exists in two forms, goethite (α-FeO.OH), and lepidocrocite (β-FeO.OH), which have different crystalline forms. Blain and Andrew (1977) claim that the series shows a continuous range of adsorbed water. So-called limonite is goethite or lepidocrocite with or without hematite, adsorbed water, jarosite, and nontronite.

Garrels and Christ (1965) calculated the stability fields of the major iron minerals as a function of Eh, pH and carbon dioxide partial pressure (Figure 3.12). Although geothite is not apparently represented on this diagram, it can be taken as occupying the hematite stability field. For, diagrams of this type are valid only for the species considered; they do not reveal whether species not considered may be stable relative to those used. Garrels and Christ (1965) considered the hematite - water-goethite system to be a case in point because the hematite plus water field may be unstable to the reaction

$$Fe_2O_3 + H_2O \longrightarrow 2FeO.OH \qquad (3.37)$$

Brown (1971) notes that geothite is more stable than hematite below 40°C. Thus, the hematite plus water field would disappear in favour of a possibly-larger geothite plus water field.

Figures 3.13 and 3.14 show the stability ranges of iron minerals in carbonate systems calculated by different methods; Figure 3.13 at constant carbon dioxide partial pressure, and Figure 3.14 at a fixed total dissolved carbonate activity. As seen, the different methods of calculation produce little change in the stability fields at oxidising, alkaline conditions. A change in the carbon dioxide partial pressure to $10^{-3.5}$ bar (3.2kPa, i.e. atmospheric) in Figure 3.13 causes the siderite field to be so small that it barely gets above the stability limit of water. Additions of sulphur to the system also barely changes the hematite stability field (Garrels and Christ (1965)). Therefore, it is seen that geothite is the theoretically stable iron phase in oxidising, carbonate systems.

The iron phases grouped under the term 'limonite' may either become fixed at the site of the former sulphide, or be transported in solution and be precipitated elsewhere. The former is termed indigenous limonite, and the latter, transported limonite. Exotic limonite is that formed at a great distance from the source sulphide(s).

Figure 3.12: Stability of hematite, magnetite, and siderite as functions of Eh, pH and P_{CO_2} at 25°C and 1 atm total pressure (from Garrels and Christ (1965))

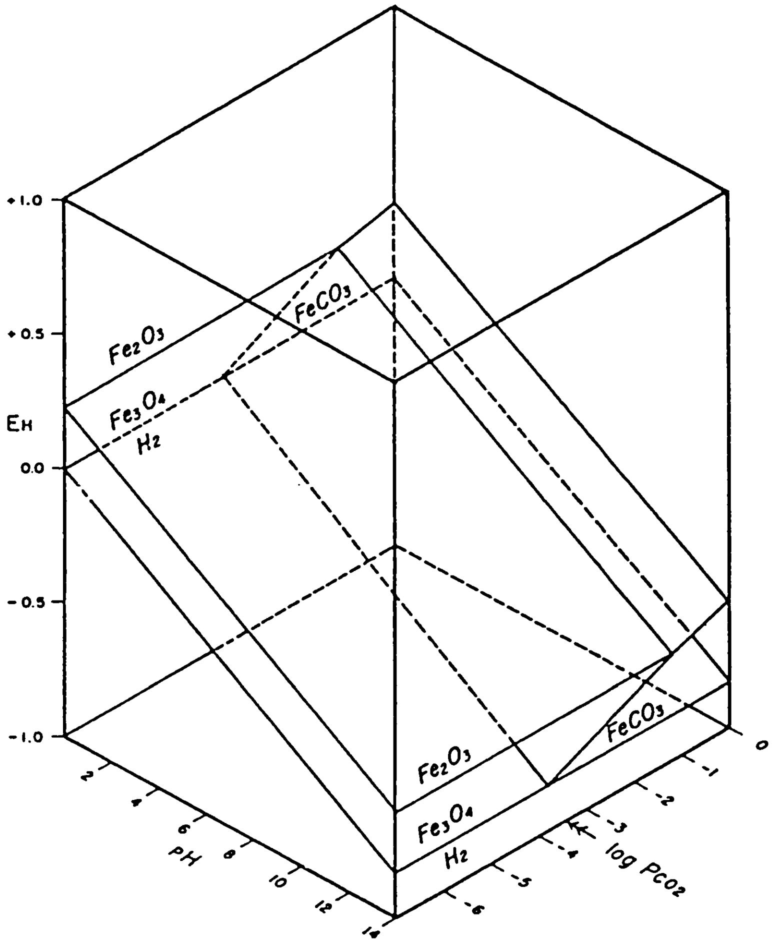
+1.0
+0.5
EH
0.0
-0.5
-1.0
Fe_2O_3
Fe_3O_4
H_2
$FeCO_3$
Fe_2O_3
Fe_3O_4
H_2
$FeCO_3$
pH
2
4
6
8
10
12
14
log P_{CO_2}
0
-1
-2
-3
-4
-5
-6

arrowed P_{CO_2} = atmospheric

Figure 3.13 Stability of iron minerals at 25°C, $p_{CO_2} = 10^{-2.0}$ and 1 atm total pressure (from Garrels and Christ (1965))

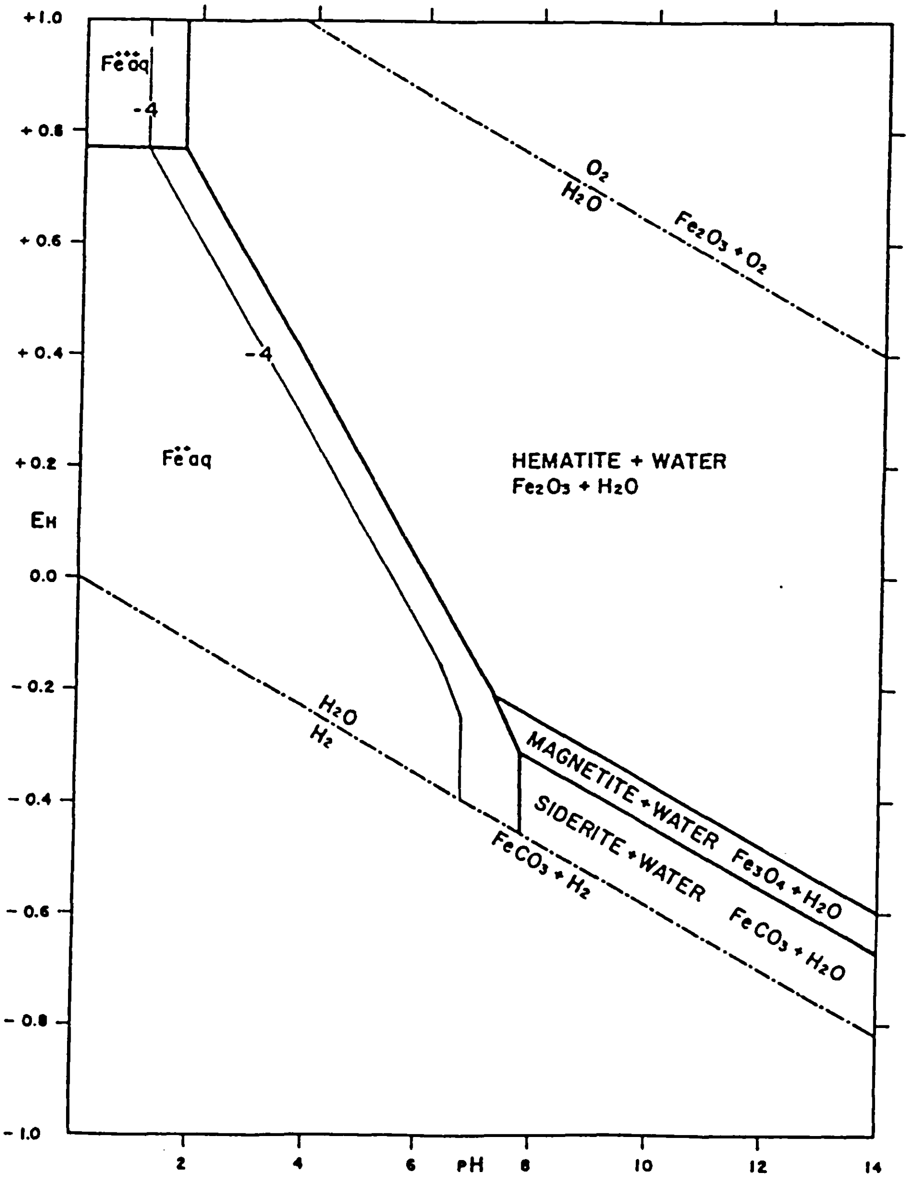

Boundaries of solids at total ionic activity of 10^{-6}. Contour is for total ionic activity of 10^{-4}

Figure 3.14: Stability of hematite, magnetite and siderite in aqueous solution containing total dissolved carbonate species of 10^{-2}M at 25°C and 1 atm total pressure (from Garrels and Christ (1965))

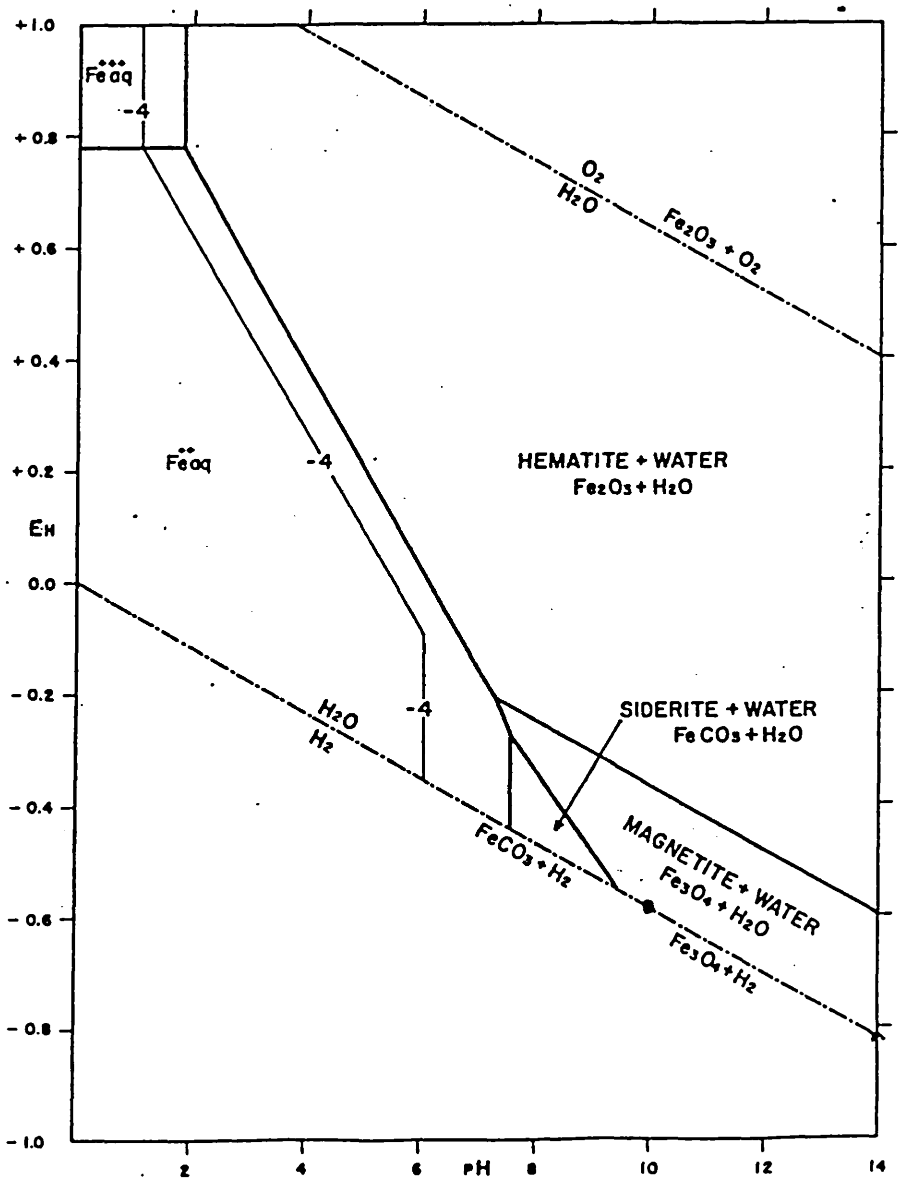

Boundaries of solids at total ionic activity of 10^{-6}. Contour is for total ionic activity of 10^{-4}

The indigenous limonite is precipitated in the iron(III) state, whilst the transported limonite is carried in the iron(II) state. Posnjak and Merwin (1922) showed that the oxidation of iron(II) to iron(III) is retarded by free sulphuric acid and is accelerated by the presence of copper; the deposition of iron(III) oxides is likewise retarded by free acid and aided by copper. Therefore, the oxidation of pyrite leads to soluble, removable iron but chalcopyrite yields iron(III) which is rapidly oxidised in situ to goethite. Thus, as noted by Bateman (1965), indigenous limonite indicates the former presence of copper, and transported limonite indicates a former high iron:copper ratio, or else a lack of copper. Blanchard and Boswell (1925) state that as the chalcopyrite approaches purity, the iron of the indigenous limonite, though variable, approaches $^1/4$ to $^1/3$ that of the sulphide, the rest being removed. Higher values would be expected in a rapidly precipitating solution such as a bicarbonate solution.

Indigenous limonite of sulphide derivation occupies the voids left by the former sulphides (Bateman (1965)). It does not occur outside the voids. Its characteristic structure denotes the kind of predecessor sulphide. It is generally compact and hard, and has a subdued colour.

Transported limonite may have been moved no further than beyond the rim of the void, or it may have been transported hundreds of metres from the parent sulphide (exotic limonite). The distance of transportation depends largely on the precipitating power of the rock through which the solutions pass; limestone being a strong, rapidly reacting precipitant. Transported limonite may thus form haloes around the empty voids or it may thoroughly permeate the enclosing rock. A little of it makes a conspicuous and exaggerated showing in varied structural forms, colours and positions.

Silica incorporated into the 'limonite' gives rise to variable 'limonitic jasper', a pervasive phase which is difficultly soluble both in acids and bicarbonate solutions (Blanchard and Boswell (1934)). Other species in solution can also co-precipitate with geothite, e.g. hydrous manganese oxides. Goethite can also adsorb species from solution, especially copper (Rickard (1971)). The mechanism of adsorption of copper is unclear. Geothite has a zero point of charge at a pH of about 8 (Nickel (1982)) so that below this pH, the geothite surface is positively charged and above it, negatively charged. The colloidal-like nature of the geothite presents a large surface area for adsorption. It is also possible that the amorphous structure of 'limonite' is a favourable location for Cu^{2+} ions because copper prefers distorted, octahedral coordination (Orgel (1966)). Collins (1973) presumes that some form of specific adsorption or incorporation of copper species into the goethite structure must occur. Should the primary mineral be chalcopyrite, which contains iron(III), then dissolution will result in direct formation of goethite, which, in turn, would adsorb some of the released copper. The capacity of goethite to immobilise copper and other metals by adsorbing them from solution has a great influence on the metal content of associated groundwaters.

3.5.5 Mechanism

The mechanism of the aqueous oxidation of chalcopyrite by oxygen is not well defined. Eadington (1977), who studied the oxidation layers of chalcopyrite using Auger electron spectroscopy, suggested that the initial adsorption of oxygen is associated with the iron, rather than the copper sites. He also found that the rate of oxidation in deionised water is approximately 30 times faster than by dry oxidation.

Figure 3.15 is an elemental profile measured across the 10nm thick oxidation layer produced after 30 minutes of wet oxidation in deionised water. The carbon peak was found to be unstable under the electron beam, and the peak height was reduced by 50% over a period of 10 minutes. This instability suggests that the carbon was in the form of organic material adsorbed at the surface of the oxidation layer. The adsorbed layer was found to be about a monolayer in depth, and, immediately beneath it, was a region of high copper:iron ratio. Thinning of the oxidation layer revealed that the copper:iron ratio decreased from 5.5:1 to 0.4:1 before rising to 1:1 in the bulk chalcopyrite. Eadington (1977) concluded that this is due to the leaching of soluble copper salts from the oxidation layer, followed by re-adsorption at the surface. Oxidation layer profiles from naturally weathered pieces of chalcopyrite show similar results, although much thicker layers of products are found in the samples, together with a greater variation between samples (Eadington (1977)).

Figure 3.15 Element concentration profiles (measured by Auger electron spectroscopy) in the oxide layer formed on chalcopyrite after 30 minutes of wet oxidation (from Eadington (1977))

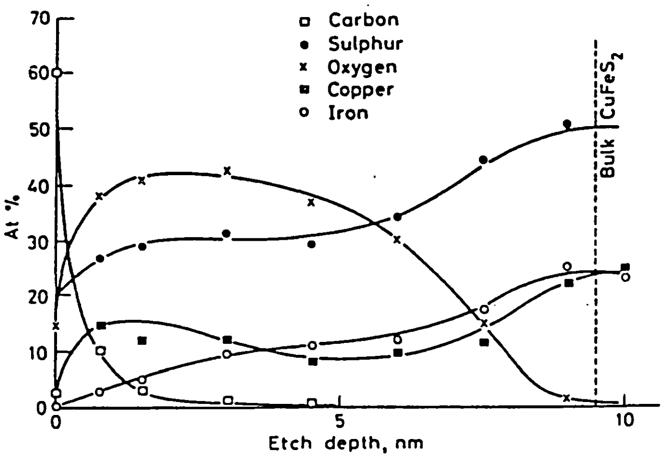

Figure 3.16 Element concentration profiles (determined by microprobe analysis) across a chalcopyrite oxidation rim (from Mallio (1981))

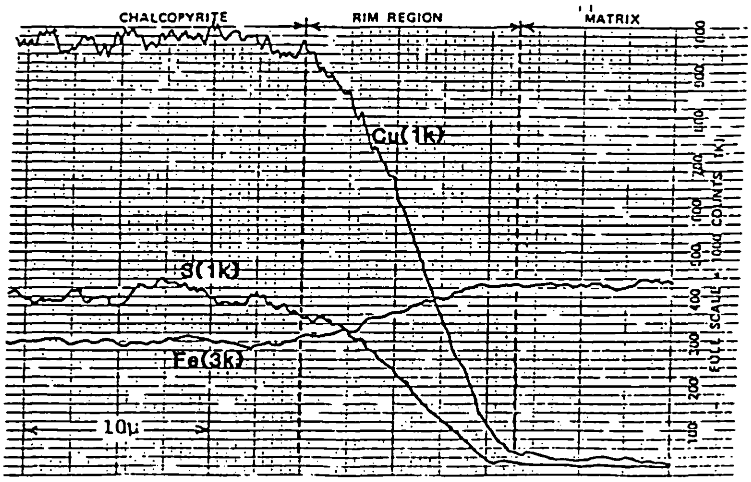

Mallio et al (1981) in a study of in situ copper leaching stated that the oxidation of chalcopyrite takes place by the reaction of oxidising agents with the sulphur to form sulphate and the complexation and removal of copper at the reaction interface, leaving spongy amorphous iron oxide behind. The reaction was seen to proceed from the surface of a grain and progress inward with the leaching interface essentially parallel to the shape of the grain. In some cases, the oxidation takes place without the immediate solution of the copper but by the slow diffusion of copper (Figure 3.16)

Electron microprobe analyses indicated that, often, 98-100% copper solubilisation from the chalcopyrite takes place. The outer rim of the leached residue was seen to be richest in copper (0.7-0.8%), silicon (1.4-1.8%), aluminium (0-0.6%), calcium (0.4-1.0%), and sulphur (0-0.7%). Mallio et al (1981) suggest that these elements are apparently occluded or exchanged for H^+ in the hydrous iron oxide residues by reaction with leach solutions.

Mallio et al (1981) also considered the effects of copper-rich leach solutions on other minerals. These reactions involve the formation of new minerals, removal of copper by ion exchangers, and the secondary enrichment of copper sulphide phases. Secondary enrichment of bornite to covellite was seen to occur at some distance away from the fluid injection points. Malachite was seen to be forming where the copper-rich solutions contacted calcareous neutralisers, and copper was seen to exchange with calcium in zeolites. Some zeolites, such as stilibite, were found to contain as much as 9-10% copper by mass.

It is therefore expected that the aqueous oxidation of chalcopyrite in a carbonate environment will lead to the formation of three groups of products. Copper, in the aqueous forms detailed in section 3.5.4, will precipitate out as malachite if sufficient concentrations exist, or be lost in solution together with the oxidised sulphur species. A residue of spongy, amorphous goethite material will be left by the relatively immobile iron content of the chalcopyrite grains.

3.6 Chemical considerations in the aqueous oxidation of sphalerite by oxygen

The oxidation of sphalerite has received little attention in the literature. The work of Wang (1915), although suffering from the technical constraints of its day, presents some valid observations based on simple laboratory experiments. He found no appreciable change in sphalerite samples which had been immersed in carbonate and bicarbonate solutions for two months. But, when he mixed limestone with zinc sulphate solutions he found that smithsonite, $ZnCO_3$, 'replaced' the limestone and that the replacement was more rapid with impure rather than pure limestone; this was attributed to the action of organic material in the impure limestone. He also found that when a solution of an alkali or calcium bicarbonate was mixed with a solution of zinc sulphate or chloride, smithsonite was precipitated but that when a solution of a normal carbonate, such as sodium carbonate, was used, a basic carbonate or hydrozincite was obtained.

From these, and other observations, Wang (1915) concluded that smithsonite is not formed directly from sphalerite in situ but that sphalerite is first oxidised to the sulphate which migrates in solution before carbonation takes place on contacting calcareous material or solutions. Observations of smithsonite in the cleavage cracks of sphalerite were explained by Wang (1915) as having been caused by a fracturing of the unaltered sulphide permitting solutions containing smithsonite to infiltrate and deposit smithsonite, rather than by direct oxidation. However, Wang considered that iron(III) sulphate, from the oxidation of associated iron-bearing sulphides, in the presence of dissolved air is responsible for the oxidation of sphalerite. Whilst oxidation by iron(III) species is indeed an important process in massive, iron-bearing sulphide deposits and also in some commercial processes, it is not considered to be a major oxidising force in material such as that which makes up the Dutchman dump. Wang (1915) considered that the following sequence of oxidation takes place:

$$FeS_2 + \tfrac{1}{2}O_2 + H_2O \longrightarrow FeSO_{4(aq)} + H_2SO_4 \qquad (3.38)$$

$$2FeSO_4 + H_2SO_4 + \tfrac{1}{2}O_2 \longrightarrow Fe_2(SO_4)_3 + H_2O \qquad (3.39)$$

and then, if no sphalerite is present

$$Fe_2(SO_4)_3 + 3H_2O \longrightarrow Fe_2O_3 + H_2SO_4 \qquad (3.40)$$

or, if sphalerite is present

$$Fe_2(SO_4)_3 + ZnS \longrightarrow 2FeSO_4 + ZnSO_4 + S \qquad (3.41)$$

Pawlek (1969) in a pressure leaching study, proposed an electrochemical model for sphalerite oxidation in which it reacts anodically according to

$$ZnS \longrightarrow Zn^{2+} + S^\circ + 2e^- \qquad (3.42)$$

The cathodic reduction of chemisorbed oxygen, the presence of which may vary with the number of charge carriers within the sphalerite owing to its semi-conductor properties, is described by:

$$\tfrac{1}{2}O_2 + 2H^+ + 2e^- \longrightarrow H_2O \qquad (3.43)$$

This semi-conductor model was tested by Pawlek (1964) by introducing ultraviolet radiation into the system that, in the case of doped ZnS, showed an appreciable increase in the rate of dissolution. The overall kinetics were not explained on the basis of electronic conduction alone, indicating that other rate processes were involved. The initial dissolution of sphalerite was seen to result in the formation of H_2S which retards the dissolution. The following reactions were proposed for the oxidation of H_2S:

$$H_2S + H_2SO_4 \longrightarrow H_2SO_3 + H_2O + S^\circ \qquad (3.44)$$

$$2H_2S + O_2 \longleftrightarrow 2H_2O + 2S^\circ \qquad (3.45)$$

$$H_2S + 2O_2 \longrightarrow SO_4^{2-} + 2H^+ \qquad (3.46)$$

of which (3.44) is the most important in highly acidic solutions, (3.46) is the most important at high temperatures, and (3.45) is slower and rate controlling.

Scott and Dyson (1968) investigated the effect of various catalysts on the pressure leaching of sphalerite, which was found to oxidise according to

$$ZnS + \tfrac{1}{2}O_2 + H_2SO_4 \longrightarrow ZnSO_4 + S + 2H_2O \qquad (3.47)$$

$$ZnS + 2O_2 \longrightarrow ZnSO_4 \qquad (3.48)$$

with the latter occurring in the absence of acid. Several metals in solution catalysed the acid reaction, with the metals increasing in catalytic activity in the order Fe < Mo < Ru < Bi < Cu. Copper and ruthenium were found to have appreciable catalytic properties in the absence of acid. Although many other ions, in addition to those listed, have the correct ionic radii to exchange with zinc in the sphalerite lattice (e.g. Ag, Hg, Pb, Sn) they did not influence the kinetics of dissolution. The effect of the catalysts was attributed to penetration to sufficient depth to influence the electrical conductivity of the lattice thus permitting electrochemical dissolution to occur according to equation (3.42). The specific catalytic activity was attributed to the effect of the catalyst on the discharge of oxygen at active surface sites. Some sulphate was formed (15 to 30%) which was attributed to the oxidation of intermediate H_2S. No systematic correlation between half-cell potentials or related electrochemical effects was observed.

Steger and Desjardins (1980) found that the limited literature assumes that sphalerite is initially oxidised to zinc sulphate. The authors studied the oxidation in air and found it to be described by equation (3.48) with the sulphate probably being hydrated. This reaction, however, does not take into account the oxidation of iron, which is always present in sphalerite to some degree. Good experimental agreement between oxidised zinc and sulphate contents led the authors to think that the sulphur associated with the iron is oxidised to SO_2, or to S°, and is lost by subsequent sublimation. The loss of much larger quantities of S° than those formed in the oxidation of the high-iron sphalerite was demonstrated in the oxidation of pyrrhotite (Steger and Desjardins (1978)). The authors therefore described the oxidation of iron-bearing sphalerite by

$$Zn(Fe)S + O_2 + H_2O \longrightarrow ZnSO_4 + (Fe_2O_3.nH_2O) + S^\circ \text{ or } SO_2 \qquad (3.49)$$

They assumed that the iron is oxidised to the iron(III) state and they made no attempt to balance the equation. The reaction was found to proceed according to a linear rate law. The assumption regarding the formation of hydrated iron(III) oxide, or more likely, goethite, appears valid considering the analysis of iron behaviour previously presented.

Garrels (1954) pointed out that the aqueous behaviour of zinc differs from that of lead and copper because there are important aqueous zinc complexes expected in natural systems. The effect of these complexes formed in alkaline solution can be included in a separate 'solubility' diagram that serves to show the important differences in solubility caused by the presence of complexes with low dissociation constants. Figure 3.17 shows the zinc ion activity diagram, and Figure 3.18 the zinc 'solubility' diagram. Figure 3.18 is not, of course, a true solubility diagram but one in which the activity of the important ZnO_2^{2-} complex is added to the activity of the zinc ion. The zinc ion activity (Figure 3.17) is similar to that for lead. The major differences are the absence of an insoluble sulphate in the zinc system and the considerably greater activity of zinc in equilibrium with the sulphide. Only the carbonate and the sulphide appear on the diagram; in systems saturated with carbon dioxide, the carbonate ($K_{sp} = 1.7 \times 10^{-11}$, Mann and Deutscher (1980)) is more stable at all values of pH than the hydroxide (Garrels (1954)). Figure 3.18 shows the effect of the ZnO_2^{2-} complex ion. The 'solubility' reversal at a pH of about 7 is present in both the carbonate and sulphide stability fields. The commonly observed active migration of zinc in the zone of oxidation of sphalerite is readily understood on the basis of the solubility minimum of the carbonate of about 10^{-4} moles per litre (Garrels (1954)). This figure would not be affected, of course, by an assumption of the total soluble sulphur in the system.

Takahashi (1960) noted that when smithsonite is dissolved in solution, the total zinc concentration in solution is not only a function of the simple zinc ion but also of undissociated zinc carbonate and various zinc complex ions. However, he considered only $ZnOH^+$ to be significant, and that the concentrations of the undissociated carbonate and other complex ions are negligibly small compared with the concentration of Zn^{2+} in a pH range of 5 to 10.

Takahashi (1960) analysed the stability fields of supergene zinc minerals within the smithsonite field calculated by Garrels (1954). The factors involved in the formation of the most common supergene zinc minerals, smithsonite, hemimorphite, and hydrozincite, are pH, Eh, total carbon dioxide (in solution, or partial pressure), concentration of silica, temperature, and pressure. However, Eh is not related to

Figure 3.17 Stability fields of sphalerite and smithsonite as functions of pH and Eh, ΣCO_2 = 0.03 (from Garrels (1954))

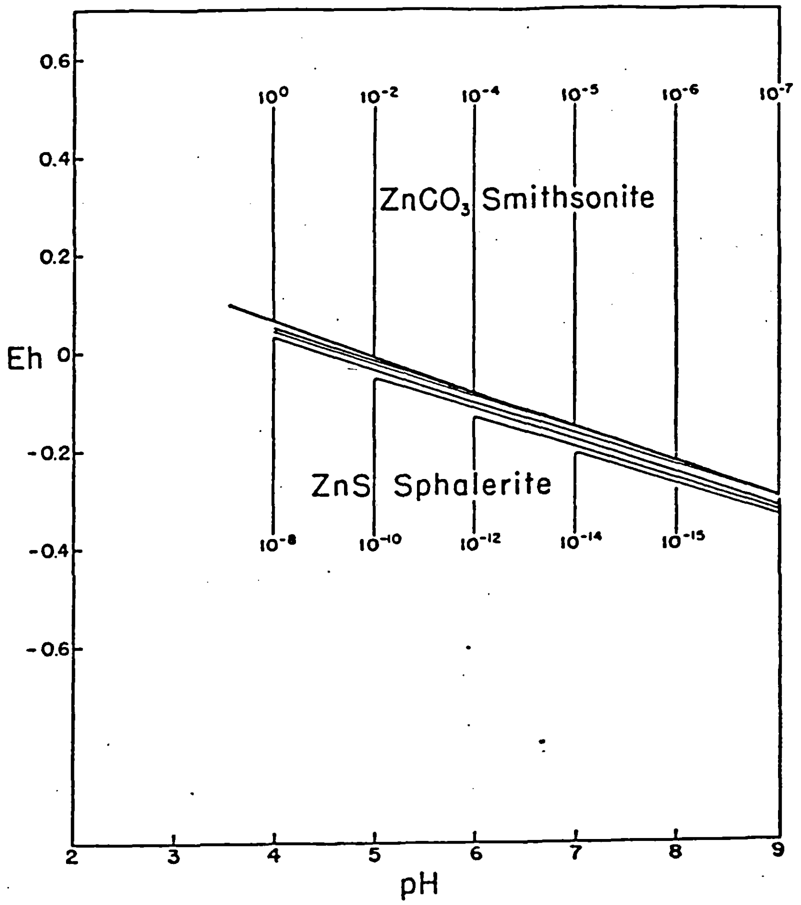

Contours are for activity of Zn^{2+}

ΣCO_2 = 0.03, ΣS = 0.1, t = 25°C

Figure 3.18 Stability fields of sphalerite and smithsonite as functions of pH and Eh (from Garrels (1954))

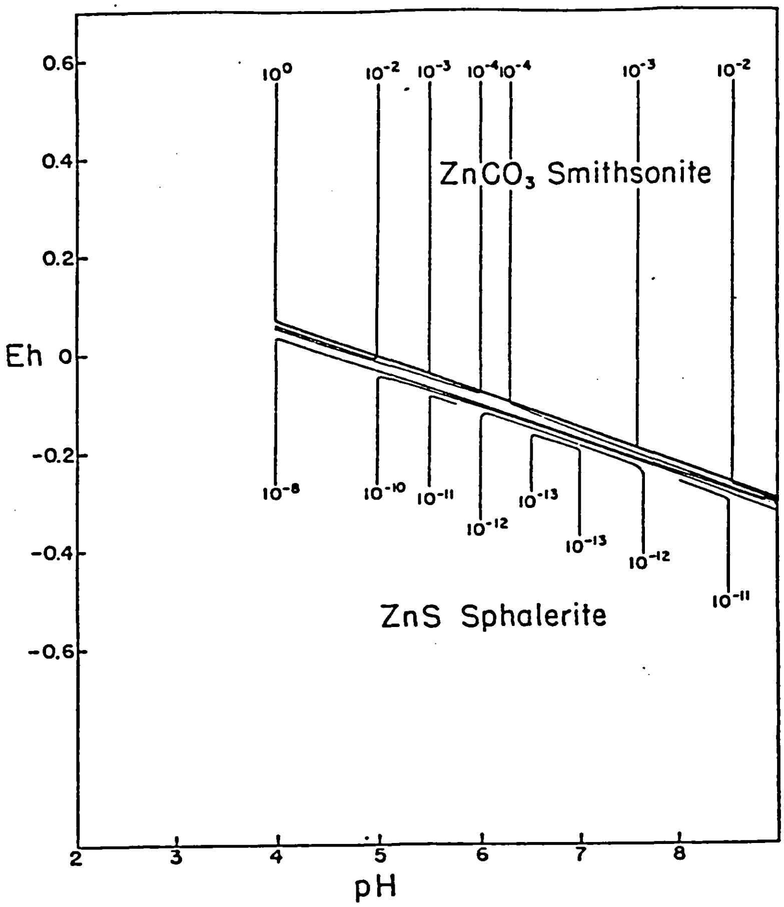

Contours are for activity of Zn^{2+} and ZnO_2^{2-}

$\Sigma CO_2 = 0.03$, $\Sigma S = 0.1$, $t = 25°C$

Figure 3.19 Stability fields of smithsonite, hydrozincite, and zinc hydroxide in solutions free from silica at 25°C (from Takahashi (1960)).

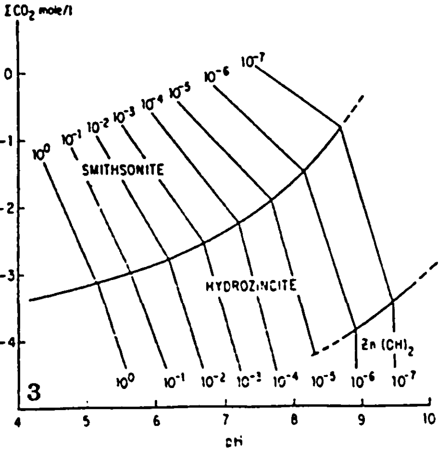

Numbers indicate the concentrations of Zn (Mdm^{-3})

the stability boundaries between these minerals since there is no change in the valencies of the elements involved in the formation of these minerals, and temperature and pressure may be assumed to be constant. Thus, pH, carbon dioxide concentration, carbon dioxide partial pressure, and aqueous silica concentration are considered to be the most important factors. Takahashi (1960) had insufficient data on Si-O species to determine the stability fields of zinc silicate minerals. However, he did determine the stability fields of smithsonite and hydrozincite, and the probable maximum field of hemimorphite was determined in terms of pH and total carbon dioxide in solution. For solutions in equilibrium with the atmosphere:

pH	Stable zinc phase
<6.2	hemimorphite
6.2-8.1	smithsonite
>8.1	hydrozincite

The absence of zinc hydroxide can be readily understood by its stability field as shown in Figure 3.19. When the total carbon dioxide activity in solution is 10^{-3} of its value under atmospheric conditions at 25°C, it becomes the stable mineral above a pH of 8.3; when the activity is 10^{-2} of that under atmospheric conditions, it becomes the stable phase above a pH of 9.5. Such conditions are extremely rare in nature.

Hem (1972) calculated that the influence of carbonate species on the solubility of zinc decreases when the total dissolved carbon dioxide content is about 10^{-4}Mdm^{-3}, and that smithsonite will not be stable at any pH if the total carbon dioxide content is less than about $10^{-4.8}$ Mdm^{-3}. This is equivalent to a carbon dioxide partial pressure of $10^{-3.3}$ bar (5kPa) in a system open to the atmosphere, which is a little above the normal value of ordinary air.

From these observations, Hem (1972) concluded that smithsonite and the hydroxide are too soluble to exert a very effective control on the zinc concentrations of natural waters unless there is an 'unusually' high activity of dissolved carbon dioxide species present. The author postulated zinc concentration control by zinc silicates, such as willemite, but the argument was not developed in full because of insufficient data.

The theoretical analyses of Mann and Deutscher (1980) also showed smithsonite to be the stable phase relative to the hydroxide at carbon dioxide partial pressures above atmospheric. The authors concluded that the carbonate assemblage, malachite-cerussite-smithsonite, is the stable copper-lead-zinc system in all solutions for a pH above 8, and in chloride- and sulphate-free solutions for a pH above 5 where the carbon dioxide partial pressure is 10^{-2} bar (100kPa).

In tests to evaluate the use of crushed limestone in soils to control the rate of migration of various metals contained in municipal, solid-waste, landfill leachate by Artiola and Fuller (1980), zinc behaved erratically. Like the other metals studied (Be, Cd, Fe, Ni), zinc migrated more slowly in clay-rich than in sandy soils, both in the presence and absence of limestone. Limestone alone was found to retain zinc, but less so than for most of the metals studied. The mobility of zinc in soils and clay minerals depends upon solution pH, ionic strength, and cation exchange capacity at pH values around 6, with precipitation of solid phases becoming more important than cation exchange capacity at pH values above 7 (Griffin and Shimp (1978)).

3.7 Conclusions

The major soluble minerals in the Dutchman dump are calcite, galena, sphalerite and chalcopyrite. Galena, chalcopyrite, and sphalerite are unstable under the oxidising, bicarbonate conditions found where calcium carbonate is in equilibrium with water and the atmosphere. By considering the physical chemistry of the species likely to be formed during the oxidation of the sulphides and by assuming equilibrium conditions, the probable secondary, oxidate minerals can be predicted.

These predictions suggest that the relatively water-insoluble galena is probably oxidised, by dissolved oxygen, to cerussite, via lead hydroxide and basic lead thiosulphate, without the formation of intermediate anglesite; sulphur is lost a~~r~~s oxidised aqueous species. The immobility of lead in solution should cause little lead migration from the parent sulphide and secondary carbonate. The rate of oxidation of galena is probably less than 10^{-10} moles per square centimetre per hour, which corresponds to a rate of approximately 10^{-10}m depth of surface per hour. This was the rate measured by Eadington (1966) in an agitated water-oxygen system where no product layers built up on the galena surface to limit the reaction rate.

Chalcopyrite is expected to oxidise to leave a goethitic remnant of the parent sulphide and to lose sulphur as aqueous oxidised species. Copper is expected to be solubilised, but will precipitate nearby as malachite.

Sphalerite is thought to oxidise rapidly and to give rise to aqueous zinc species and aqueous sulphur species. Zinc is expected to be mobile in solution and to be able to travel far from the parent sulphide before precipitating as smithsonite. The probable rates of oxidation of chalcopyrite and sphalerite are unknown, but they are expected to be faster than that of galena.

The carbonate assemblage, cerussite, malachite, and smithsonite, is stable under the expected conditions. Field relations also bear this out (Blain and Andrew (1977).

CHAPTER FOUR

Preliminary Results

4.1 Size and chemical analyses

4.1.1 Mineral samples

The four working samples (section 2.5), designated A1, A2, B, and C were wet screened down to 53µm. The designations reflect the sampling locations, viz:

A1 - near the base of the dump
A2 - 4m above A1
B - 4m above A2
C - 4m above B.

These samples were not meant to be representative of the dump as a whole but only of the finer-material zone.

The very similar size distributions of these samples are shown in Appendix 3. The small differences between the samples can be ascribed to sampling variance and variations in the original material.

Microscopical examination of the size fractions showed that the base-metal mineralisation was effectively restricted to the material finer than 2.3mm. This mineralisation occurred in the form of carbonates (cerussite, malachite, and smithsonite) and carbonate-coated sulphide grains (galena and chalcopyrite); much of the mineralisation appeared to be liberated or associated with baryte. Other phases identified were calcite, dolomite, fluorite, geothite, quartz, and other silicates.

The material coarser than 2.3mm was not considered further.

Subsamples of the -2.3mm size fractions were riffled and ground to unit micrometre size in a laboratory mill. Samples (0.4-0.5g) of the ground material were dissolved in nitric acid and the solutes were analysed for Cu, Pb, Zn, Fe, Ca and Mg content by atomic absorption spectroscopy (AAS). Additional subsamples were analysed for 'simple' carbonate content by dissolution in cold, 0.1Mdm^{-3} hydrochloric acid. The insoluble mineral residues from these procedures were analysed by X-ray diffraction (XRD) and by semi-quantitative X-ray fluorescence spectrometry (XRF) to determine their major insoluble mineral contents, and their chemical compositions, respectively. The results of these analyses are shown in Appendix 4.

The results show that the 'simple' carbonate content of the material was in the range 50-80 mass %.

The nitric acid-soluble content of the material was seen to be in the range 60-90 mass %. Only two fractions showed a lower solubility in nitric acid than in dilute hydrochloric acid - an effect caused by sampling variation. Different primary sub-samples of the same material showed variations up to ±6% (relative) in the base-metal contents. Analytical variations, determined by replicate analyses, were found to be better than ±3% (relative).

XRD analyses showed that baryte and fluorite were the major minerals present in the dilute hydrochloric acid residues. Baryte alone was seen to dominate the nitric acid residues.

XRF analyses showed major amounts of barium and calcium in the dilute hydrochloric acid residues, most probably as baryte and fluorite respectively. The copper, lead and zinc detected represented their sulphide minerals. The sulphur content was incorporated in baryte and the sulphides. The iron was seen to occur as sulphides and oxides, manganese as wad, and silicon as quartz and other silicates. Strontium may have occurred as the sulphate, celestite, since no strontium was solubilised by hydrochloric acid. The traces of potassium, chlorine, and nickel were unaccounted for.

The nitric acid residues gave similar XRF results to those obtained from the hydrochloric acid residues. Barium and sulphur (probably as baryte) were the major elements present - the fluorite having dissolved. The silicon was seen to occur as quartz and other silicates. Strontium probably occurred as celestite since no strontium was solubilised by nitric acid. The traces of zinc occurred in an unknown form, and the traces of potassium, iron, chlorine, calcium, and bromine were also unaccounted for.

The AAS analyses for copper, lead, and zinc showed that the proportion of these elements increased with decreasing particle size, along with increasing insoluble mineral contents. The actual metal contents were seen to be very low.

Overall, the samples were chemically and physically very similar and were dominantly carbonates.

4.1.2 Water samples

The results of the analyses of the water samples collected in February 1982 are shown in Table 4.1. Sample designations refer to the following locations:

E1 - point of issue of the stream from the Dutchman adit.
E2 - 4m from E1.
E3 - Just above the point of entry of the stream into the Dutchman dump (4m from E2).
E4 - Discharge stream from the Ecton Deep Adit into the River Manifold.
E5 - River Manifold upstream of E4.

Table 4.1: Results of the analyses of Ecton water samples

		Concentration of metal in solution (ppm)					
Sample	pH	Ca	Mg	Cu	Pb	Zn	Fe
E1	8.3	66	12.5	0.0(6)	0.0(6)	0	0.2
E2	8.3	67	12.5	0.0(6)	0.0(8)	0	0.2
E3	8.4	64	12.5	0.1(1)	0.1(1)	0	0.4
E4	8.0	52	11.0	0.0(3)	0.1(0)	0	0.3
E5	7.2	17	3.2	0.0(6)	0.0(6)	0	0.3

Analytical error: better than 3% relative

Ca and Mg results confirmed by Analytical Services Lab., RSM.

All the bulk water samples were sealed in polypropylene containers for transportation to London, where the pHs of the samples were measured before the samples were filtered through a 0.5µm millipore filter. The filtrates were acidified and then analysed by AAS.

Samples E1, E2 and E3 represent points along the course of the stream that issues from the Dutchman adit and runs into the dump: the only non-precipitation source of water that reaches the dump. The water is seen to be in equilibrium with calcite, though its calcium content is higher than that predicted from equilibrium relations (section 3.3.4), which is not uncommon in natural systems. Sample E5 differs from the others because the river flows through a siliceous rock zone upstream from the sampling point.

4.2 Heavy liquid separation

The low concentrations, and the apparent high degree of liberation, of the base-metal mineralisation, together with the association of the unliberated material with baryte, enabled heavy liquid separations to be made on sub-samples of the size fractions to provide more concentrated study material. The separations were carried out at a density of 2.96gcm^{-3} using 1,1,2,2-tetrabromoethane; the results are shown in Table 4.2.

Optical examination of the products of the separations showed that the base-metal mineralisation had been effectively concentrated in the denser fractions. XRD analysis of the products from a randomly chosen size fraction (A1 -2.3 + 1.7mm) showed baryte, smithsonite, and fluorite to be the major minerals present in the 'sink' product, and calcite, dolomite, and quartz to be the major minerals present in the 'float' product.

Table 4.2: Heavy liquid separation results

	Mass % of sample size fraction denser than 2.96gcm^{-3}			
Size fraction (μm)	A1	A2	B	C
-2300 + 1700	35.2	32.8	38.9	36.3
-1700 + 1180	37.6	35.0	40.5	40.1
-1180 + 850	41.7	41.0	47.0	40.3
-850 + 600	39.8	40.9	49.8	44.7
-600 + 420	46.1	44.8	46.6	51.1
-420 + 300	49.8	45.4	50.9	56.6
-300 + 210	49.5	48.4	51.7	53.9
-210 + 150	52.0	51.6	52.8	58.3
-150 + 104	50.8	58.8	69.0	64.5
-104 + 75	61.5	53.4	56.4	84.4
-75 + 53	65.8	72.5	56.7	64.8

4.3 Optical mineralogy

Examination of the +2.96SG fractions showed the presence of baryte, fluorite, galena, cerussite, chalcopyrite, malachite, smithsonite, goethite, and minor calcite and silicates. The -2.96SG fractions were composed mainly of calcite and dolomite with some silicates but negligible base-metal mineralisation.

Sub-samples of the density fractions were made into polished sections for more detailed study.

Lead minerals

The only lead minerals detected were galena and cerussite. These phases commonly occurred in cuboid particles with cerussite surrounding a galena core (Figure 4.1). No unaltered galena was seen. Most of the galena-cerussite particles were apparently liberated, the rest were associated with smithsonite or occurred as small inclusions in baryte.

The galena-cerussite contact appeared sharp with no interposed phases, such as anglesite. This sharp contact was also seen in thin sections of +2.96SG material.

Copper minerals

Chalcopyrite and malachite were the only copper minerals detected. The chalcopyrite occurred either as apparently liberated grains or as small inclusions in calcite. No unaltered chalcopyrite was seen. In all instances, the chalcopyrite grains showed concentric alteration to goethite with efflorescent, (in the case of apparently liberated grains) or cleavage crack-filled, malachite (in calcite). Figure 4.2 shows these features. Numerous grains showing complete alteration to goethite were seen. Smears and stains of malachite were also common. No azurite was seen - this accords with the study by Sarjeant (1956) of the Ecton waste dumps in which azurite was seen as a trace in one dump only.

Zinc minerals

The only zinc mineral seen was smithsonite. This occurred as apparently liberated grains (Figure 4.3) and also associated with cerussite, baryte, and fluorite. No sphalerite was seen in any section.

Other sulphides

Pyrite was the only other sulphide mineral to be seen in any quantity. It occurred as cubic and sub-cubic, apparently liberated grains and also as very small inclusions in baryte. The apparently liberated grains showed alteration to geothite along cleavage and fracture lines, whilst the alteration seen in the enclosed grains was of a concentric form.

Other minerals

The other major minerals seen, excepting calcite and dolomite, were baryte and fluorite. The baryte appeared largely liberated though some grains contained inclusions of sulphides and their alteration products. Most baryte grains were of a fractured cockscomb-type. No alteration products of baryte (e.g. witherite) were seen, though the calcite and dolomite contained up to 5% barium. The fluorite occurred mainly as apparently liberated cubic grains or associated with cerussite-galena. Some fluorite grains showed solution effects.

Figure 4.1 Typical altered cuboid galena grains

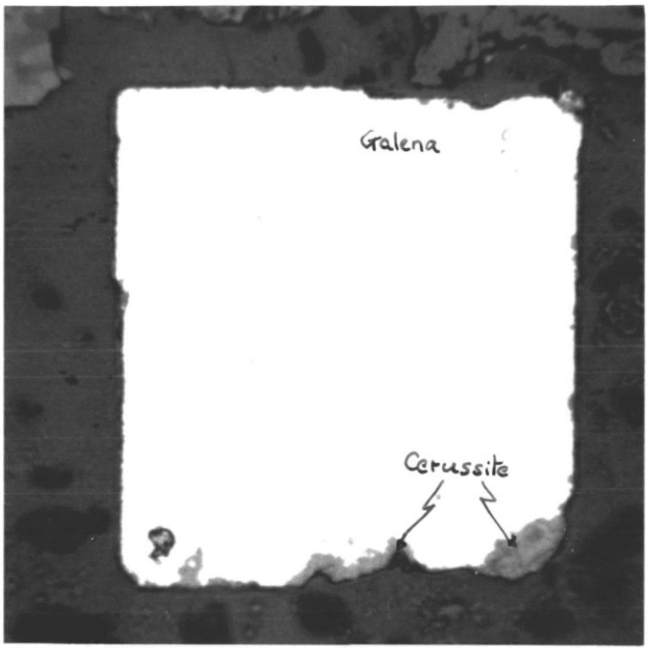
Galena
Cerussite
500 µm

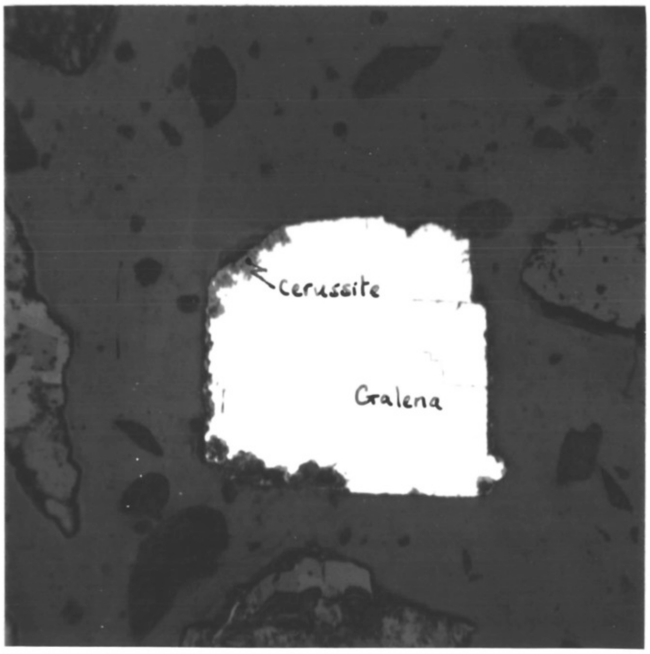
Cerussite
Galena
400 µm

Figure 4.2 Typical altered chalcopyrite grains

(i) Alteration to goethite with efflorescent malachite

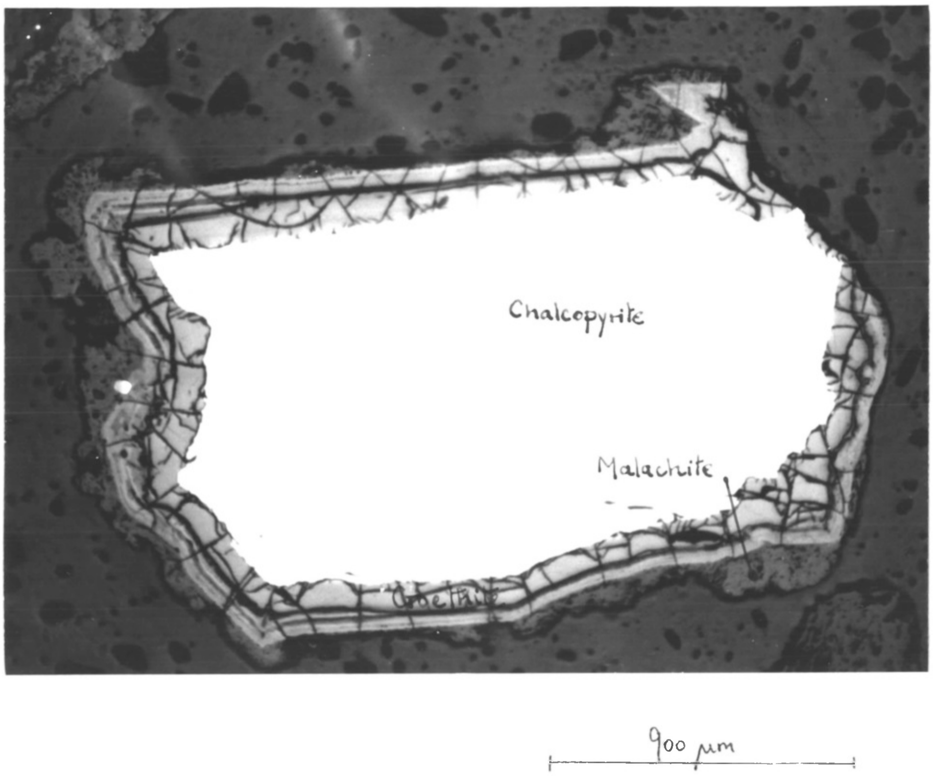
Chalcopyrite
Malachite
Goethite
900 µm

(ii) Alteration (in calcite) to goethite and malachite

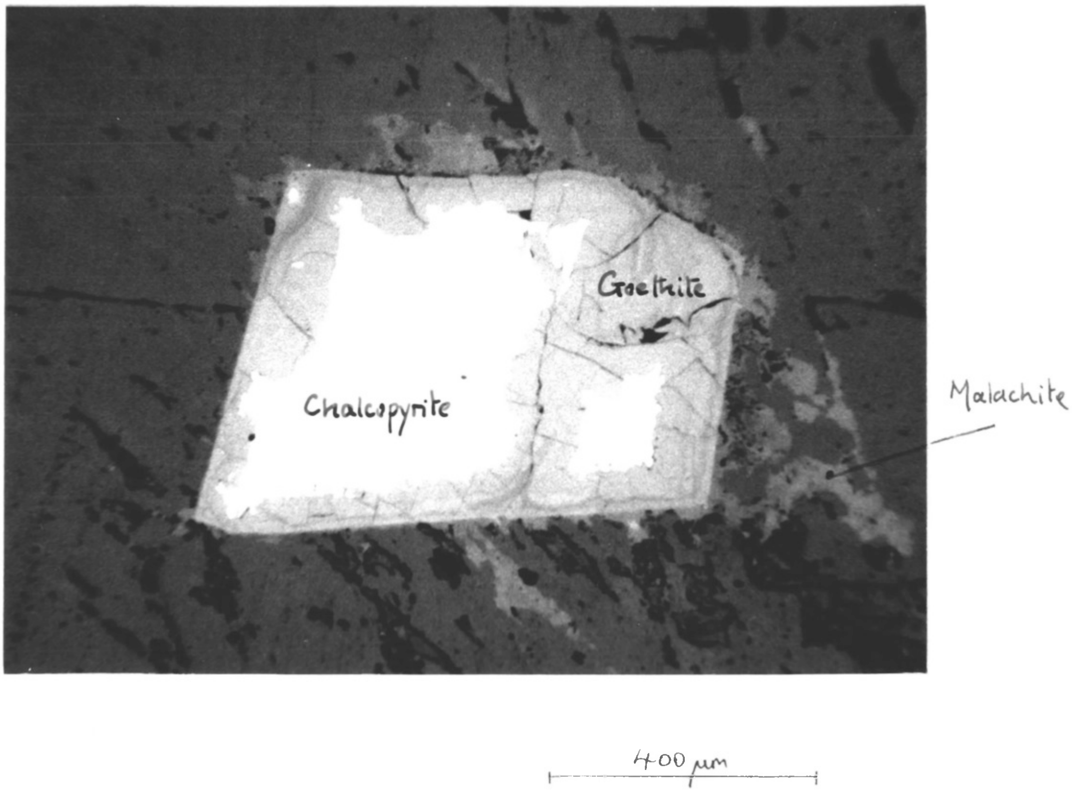
Goethite
Chalcopyrite
Malachite
400 µm

Figure 4.3 A typical smithsonite grain

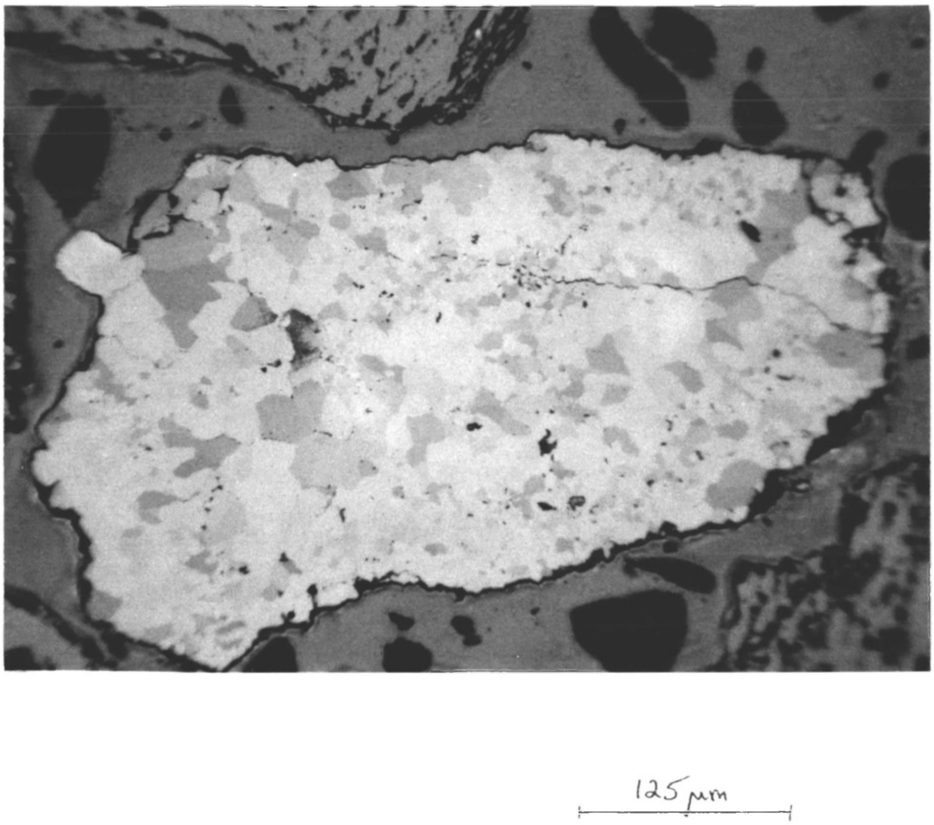

4.4 Summary

The mineral samples collected from the Dutchman dump were seen to be both chemically and mineralogically very similar to each other.

The original base-metal sulphide minerals in the dump were seen to have undergone varying degrees of alteration. The alteration occurred in a chemical environment characterised by calcite which was in equilibrium with water and the atmosphere. The predicted stable oxidate mineral assemblage under these conditions (viz, malachite, goethite, cerussite, and smithsonite) was found to occur in the samples.

The alteration of the base-metal sulphides appeared to be mineralogically simple:

galena altered directly to cerussite;
chalcopyrite altered directly to goethite and malachite; and
sphalerite altered to smithsonite.

Qualitatively, the relative alteration states of the base-metal sulphides appeared to be $Zn >> Cu \geqslant Pb$, and this is in accord with the predictions of Mann and Deutscher (1980).

CHAPTER FIVE

Quantification of galena alteration

5.1 Introduction

The nature and amount of the galena alteration described in section 4.3 can be quantified by two methods:

1. Image analysis of polished mineral sections, and
2. Chemical analysis based on the different solubilities of cerussite and galena.

5.2 Image analysis

Image analysis is the quantitative measurement of the geometrical features visible on two-dimensional images (Jones (1977)); in this instance, the images represent plane sections of minerals.

Early workers demonstrated that:

1. the area proportion of a phase in a polished section (A_a), and
2. the linear intercept proportion of a phase in a polished section (L_l), and
3. the point proportion of a phase in a polished section (P_p), are

equal to the true volumetric proportion of that phase in a rock mass, provided that statistically adequate numbers of measurements are made on large enough random surfaces. Thus,

$$P_p = L_l = A_a = V_v \qquad (5.1)$$

Recently, computer-controlled, automatic measuring systems have been developed which can swiftly produce large amounts of precise data which are objective and within statistically definable confidence limits. Hence, it is now possible to carry out automatic area (Fisher and Cole (1968)), line (Jones and Gavrilovic (1970)), and point measurements (section 6.2). In addition, these techniques enable parameters to be calculated that could not previously be determined and they also allow stereological transformations (the extrapolation of three-dimensional reality from two-dimensional data) to be more readily carried out.

5.3 Area image analysis

5.3.1 Equipment and procedure

The instrument used for these analyses was a Bausch and Lamb, model Omnicon 3000, optical image analyser of the Dept of Metallurgy and Materials Science, Imperial College. The instrument employs a video camera mounted on a microscope to provide images which are displayed on a monitor and processed by a dedicated computer.

The instrument was used in a semi-automatic, reflected light mode. The sections analysed were those of sample AI material with a density greater than 2.96 gcm^{-3} (section 4.3). The measuring system was calibrated with standards before each section was analysed. The whole surface of each 2.5cm diameter section was examined to locate every particle containing cerussite and galena: when a particle of interest was located, a light-pen was used to initiate a program which calculated the separate areas of both the galena and the cerussite. It was necessary to locate these particles manually because the optical properties of the cerussite were very variable and, in the automatic search mode, the instrument was unable to differentiate between cerussite and other carbonates, especially smithsonite, and baryte.

5.3.2 Results

The small numbers of galena- and cerussite-bearing particles found in the coarser size fractions made statistical analysis of the results meaningless; Table 5.1 summarises the results. For the purposes of these analyses, 'apparently liberated' lead-bearing grains included liberated galena-plus-cerussite particles. These particles tended to square in shape - with cerussite surrounding a galena core.

A major difficulty was encountered during the area analyses. The difficulty arose because of an inability to identify particles of cerussite when they occurred without cores of galena. Therefore, the results obtained from the area-measuring system are of limited value.

In view of the instrumental limitations with this material, the method of analysis was not continued.

Table 5.1: Area analysis - summary. Sample A1, +2.96SG material

Particle size (μm)	No. of lead-bearing particles	No. of lead-bearing particles that were apparently liberated	Range of apparent alteration (area %)	Area-weighted mean alteration (area %)
-1700+1180	14	6	5-74	27
-1180+ 850	19	5	1-72	29
-850+ 600	26	18	9-90	42
-600+ 420	65	51	1-96	32
-420+ 300	117	98	1-96	20
-300+ 210	95	88	5-90	24

5.4 Linear image analysis

5.4.1 The linear image analyser

The instrument used for these analyses was a Camebax-Micro, electron probe X-ray microanalyser of the Mineral Technology Section, Imperial College.

The principles of the electron probe X-ray microanalyser (microprobe) are described by Long (1977), whilst Jones (1982a, b) describes its application in mineralogical analysis. Minerals bombarded by high energy electron beams give off X-rays which are characteristic of the elements in the minerals. In the microprobe, a focussed beam of electrons, about 1 µm in diameter, is directed onto a mineral which is thus identified by its characteristic X-rays.

The development of the Camebax-Micro as a linear image analyser is described by Jones (1982a). The Camebax-Micro is a 4-spectrometer instrument controlled by a Motorola 6802 microprocessor linked to a DEC PDP 11/23 minicomputer (Figure 5.1).

When used as an automatic, linear image analyser, the instrument makes very rapid, qualitative analyses of a large number of linearly contiguous 'points' spaced at 2 µm intervals. The mineral at each point is identified, or rather, it is distinguished from the other minerals (Jones (1982b)), in milliseconds.

5.4.2 Procedure

In view of the small numbers of particles of interest found in the coarser size fractions during the area analysis, only the sections of material finer than 150 µm were analysed.

The linear analyses were carried out with a beam accelerating voltage of 15 kV and a ~~filament~~ beam current of 0.16mA. ~~These are~~ The current value is unusually high ~~values~~ but ~~they are~~ it is necessary because of the small numbers of X-ray quanta produced in the short (20ms) counting period used for each analysed point. The elements sought were lead, sulphur, and zinc; the following differentiations were therefore possible:

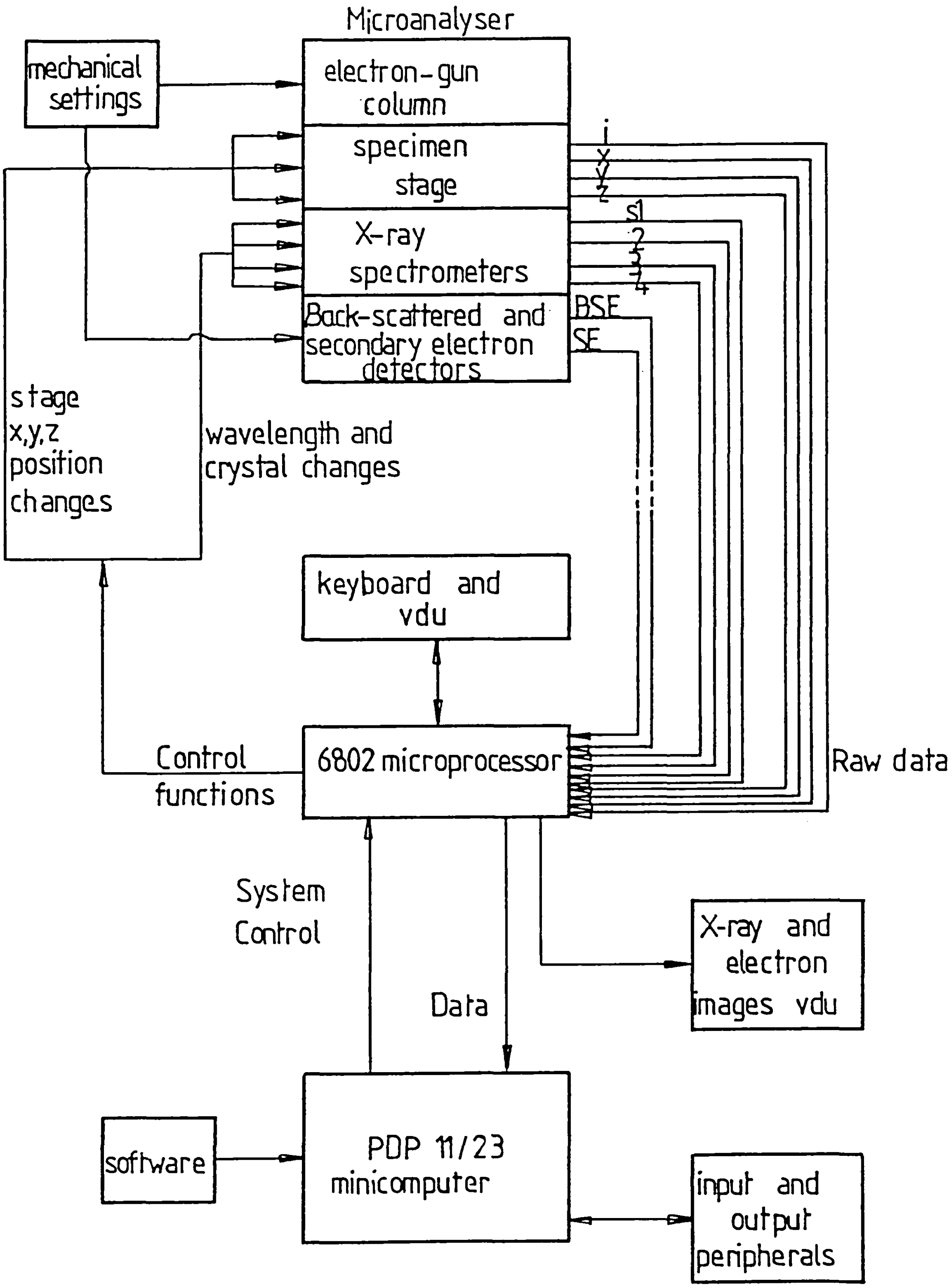
Microanalyser
mechanical settings
electron-gun column
specimen stage
X-ray spectrometers
Back-scattered and secondary electron detectors
i
x
y
z
s1
2
3
4
BSE
SE
stage x,y,z position changes
wavelength and crystal changes
keyboard and vdu
Control functions
6802 microprocessor
Raw data
System Control
Data
X-ray and electron images vdu
software
PDP 11/23 minicomputer
input and output peripherals

Figure 5.1 Cameca CAMEBAX-MICRO control system architecture

lead, plus sulphur = galena
lead, but no sulphur = cerussite
zinc, plus sulphur = sphalerite
zinc, but no sulphur = smithsonite
sulphur, but no lead or zinc = baryte (plus minor sulphides)

5.4.3 Results

The quantity of data produced from a linear analysis is extremely large and, therefore, only summaries of the relevant data are presented. Appendix 5 shows a print-out from a linear analysis. Appendix 6 contains the modal analyses for each of the sections analysed, together with the linear grade (or alteration) distributions of the cerussite-galena particles. It should be remembered that 'apparently liberated' in the context of these measurements refers only to the state of liberation with respect to only lead-, sulphur- and zinc-bearing phases; all other phases were recorded as matrix. Whilst it is difficult to determine the absolute accuracy of the measurements without using independent standards, the results are seen to be self-consistent.

The cerussite linear distribution data, Table 5.2, shows that the majority of the cerussite appears to be liberated but that almost all of the unliberated cerussite is associated with galena. The overall linear ratios, and hence the volumetric ratios, of cerussite to galena are seen to increase with decreasing particle size, i.e. the galena, as expected, shows a higher proportion of alteration at finer sizes. The differences between the results for different samples of a particular size fraction reflect differences in the original material.

The linear distribution data for the galena, Table 5.3, show that more than 95% of this material is associated with cerussite. No apparently liberated (i.e. unaltered) galena was detected. The galena grains which were not associated with cerussite were observed to occur as small inclusions within large, unfractured grains of baryte. However, most of these galena grains showed a very thin, unidentified alteration coating.

Tables 5.4 and 5.5 show the linear distribution data for smithsonite and baryte. 95% of the smithsonite was apparently liberated, whilst over 99% of the baryte was apparently liberated.

Table 5.2: Cerussite linear distribution data

a) -150 + 104 μm + 2.96 SG

			Sample		
	A1	A2	B	C	Total
ΣL cerussite (μm)	12590	2608	14704	37292	67194
L apparently liberated (μm)	9506	1662	10730	27212	49110
Linear ratio, cerussite:galena	2.6:1	3.1:1	2.4:1	2.8:1	2.7:1
L% apparently liberated	75.5	63.7	73.0	73.0	73.1
L% in composite particles:					
Cerussite + galena	17.8	26.9	18.9	22.0	20.7
Cerussite + smithsonite	5.6	7.8	7.3	3.1	4.7
Cerussite + baryte	0	1.6	0.7	0.7	0.6
Cerussite + galena + baryte	1.1	0	0	0.6	0.5
Cerussite + smithsonite + baryte	0	0	0.1	0	tr
Cerussite + galena + smithsonite	0	0	0	0.6	0.3
TOTAL	100	100	100	100	100

b) -104 + 75 μm + 2.96 SG

	A1	A2	B	C	Total
ΣL cerussite (μm)	10308	13048	15188	14716	53260
L apparently liberated (μm)	6762	9396	11100	12082	39340
Linear ratio, cerussite:galena	3.4:1	5.1:1	2.5:1	3.9:1	3.4:1
L% apparently liberated	65.6	72.0	73.1	82.0	73.9
L% in composite particles:					
Cerussite + galena	23.8	23.1	21.3	16.7	21.0
Cerussite + smithsonite	9.1	4.4	4.6	0.9	4.4
Cerussite + baryte	0.7	0.1	0.8	tr	0.2
Cerussite + smithsonite + baryte	0	0	0.2	0	0.1
Cerussite + galena + smithsonite	0.8	0.1	0	0	0.2
Cerussite + galena + baryte	0	0.3	tr	0.4	0.2
TOTAL	100	100	100	100	100

c) -75 μm + 53 μm + 2.96 SG

	A1	A2	B	C	Total
ΣL cerussite (μm)	14026	19912	27558	55812	117308
L apparently liberated (μm)	10176	14338	21626	43816	89956
Linear ratio, cerussite:galena	5.2:1	4.6:1	4.4:1	4.2:1	4.7:1
L% apparently liberated	72.6	72.0	78.5	78.5	76.7
L% in composite particles:					
Cerussite + galena	20.8	19.2	19.7	19.1	19.5
Cerussite + smithsonite	5.9	8.8	0.5	1.5	3.8
Cerussite + baryte	0.8		0.7	0.6	
Cerussite + galena + baryte	0		0.6	0.3	

Table 5.3: Galena linear distribution data

a) -150 + 104 μm + 2.96 SG

			Sample		
	A1	A2	B	C	Total
ΣL galena (μm)	4880	834	6128	13228	25070
L% in composite particles:					
Galena + cerussite	94.2	99.8	99.9	94.4	95.9
Galena + baryte	tr	0.2	0.1	0	tr
Galena + cerussite + baryte	5.8	0	0	5.0	3.8
Galena + cerussite + smithsonite	0	0	0	0.6	0.3
TOTAL	100	100	100	100	100

b) -104 + 75 μm + 2.96 SG

	A1	A2	B	C	Total
ΣL galena (μm)	3078	2540	6002	3798	15418
L% in composite particles:					
Galena + cerussite	98.3	98.5	99.2	96.0	98.1
Galena + baryte	0.1	0	0	0	tr
Galena + cerussite + baryte	0	0.7	0.8	4.0	1.4
Galena + cerussite + smithsonite	1.6	0.8	0	0	0.4
TOTAL	100	100	100	100	100

c) -75 + 53 μm + 2.96 SG

	A1	A2	B	C	Total
ΣL galena (μm)	2708	4294	6230	13440	26672
L% in composite particles:					
Galena + cerussite	100	99.3	95.4	97.4	97.5
Galena + baryte	0	0.7	0	0.4	2.5
Galena + cerussite + baryte	0		4.6	2.0	
Galena + cerussite + smithsonite	0	0	0	0.2	
TOTAL	100	100	100	100	100

Table 5.4: Smithsonite linear distribution data

a) -150 + 104 μm + 2.96 SG

			Sample		
	A1	A2	B	C	Total
ΣL smithsonite (μm)	53608	14568	27116	17416	112708
L apparently liberated (μm)	52052	14104	25988	16462	108606
L% apparently liberated	97.1	96.8	95.8	94.5	96.4
L% in composite particles:					
Smithsonite + cerussite	2.3	1.4	2.2	3.3	2.3
Smithsonite + baryte	0.6	1.8	1.3	1.5	1.1
Smithsonite + sphalerite	0	0	0.4	0	0.1
Smithsonite + sphalerite + baryte	0	0	0.2	0	tr
Smithsonite + baryte + cerussite	0	0	0.1	0	tr
Smithsonite + galena + cerussite	0	0	0	0.7	0.1
TOTAL	100	100	100	100	100

b) -104 + 75 μm + 2.96 SG

	A1	A2	B	C	Total
ΣL smithsonite (μm)	30664	29118	21174	23176	104132
L apparently liberated (μm)	29634	28184	19962	23050	100830
L% apparently liberated	96.6	96.8	94.3	99.5	96.8
L% in composite particles:					
Smithsonite + cerussite	1.9	2.5	3.5	0.5	2.1
Smithsonite + baryte	1.3	0.7	2.0	0	1.0
Smithsonite + galena + cerussite	0.2	tr	0	0	0.1
Smithsonite + baryte + cerussite	0	0	0.2	0	tr
TOTAL	100	100	100	100	100

c) -75 + 53 μm + 2.96 SG

	A1	A2	B	C	Total
ΣL smithsonite (μm)	35270	62654	15072	22324	135320
L apparently liberated (μm)	33758	59522	14932	21300	129512
L% apparently liberated	95.7	95.0	99.1	95.4	95.7
L% in composite particles:					
Smithsonite + cerussite	3.2	5.0	0.6	3.7	4.3
Smithsonite + baryte	1.1		0.3	0.8	
TOTAL	100	100	100	100	100

Table 5.5: Baryte linear distribution data

a) -150 + 104 μm +2.96 SG

	Sample				
	A1	A2	B	C	Total
ΣL baryte (μm)	142694	39972	159158	255802	597626
L apparently liberated (μm)	142460	39766	158688	255316	596230
L% apparently liberated	99.8	99.5	99.4	99.8	99.8
L% in composite particles:					
Baryte + smithsonite	0.1	0.2	0.2	0.1	0.1
Baryte + galena	tr	0.1	tr	0	tr
Baryte + cerussite	0	0.2	0.2	0.1	0.1
Baryte + galena + cerussite	0.1	0	0	tr	tr
Baryte + sphalerite + smithsonite	0	0	tr	0	tr
Baryte + cerussite + smithsonite	0	0	tr	0	tr
TOTAL	100	100	100	100	100

b) -104 + 75 μm +2.96 SG

	A1	A2	B	C	Total
ΣL baryte (μm)	85040	26004	89090	45902	246036
L apparently liberated (μm)	84756	25882	88840	45890	245368
L% apparently liberated	99.7	99.5	99.7	100	99.7
L% in composite particles:					
Baryte + smithsonite	0.2	0.4	0.3	0	0.2
Baryte + galena	tr	0	0	0	tr
Baryte + cerussite	0.1	0.1	tr	tr	tr
Baryte + galena + cerussite	0	tr	tr	tr	tr
TOTAL	100	100	100	100	100

c) -75 + 53 μm +2.96 SG

	A1	A2	B	C	Total
ΣL baryte (μm)	102988	154868	119518	185160	562534
L apparently liberated	102592	153784	119252	184614	560242
L% apparently liberated	99.6	99.3	99.8	99.7	99.6
L% in composite particles:					
Baryte + smithsonite	0.3	0.7	0	0.1	0.4
Baryte + cerussite	0.1		0.1	0.1	
TOTAL	100	100	100	100	100

Figure 5.2 demonstrates the similarity seen in the linear intercept distributions of material of the same size from different samples. The distributions are skewed towards the finer sizes because of the fractured cockscomb form of the baryte mineralisation (section 4.3).

5.4.4 Discussion

The results of the linear analyses support the qualitative observations (section 4.3):

1. The dump material contains no unaltered galena.
2. All the galena grains are surrounded by an alteration product consisting of cerussite.
3. The proportion of alteration of the galena increases with decreasing particle size.
4. The proportion of alteration is very similar in all samples of a given size.
5. Virtually all of the sphalerite has altered to smithsonite.

Linear proportions are numerically equivalent to volume proportions (section 5.2). Therefore, the measured linear ratios of cerussite to galena provide the overall volumetric ratios of these two phases in the sections analysed (Table 5.6).

Table 5.6: Volumetric ratio of cerussite to galena as determined by linear image analysis

Particle size (μm)	Volumetric ratio of cerussite to galena in sample				
	A1	A2	B	C	Total
-150 + 104	2.6:1	3.1:1	2.4:1	2.8:1	2.6(8):1
-104 + 75	3.4:1	5.1:1	2.5:1	3.9:1	3.4(5):1
-75 + 53	5.2:1	4.6:1	4.4:1	4.2:1	4.7(3):1

These data show the overall state of alteration of galena to cerussite in each sample but a more important measure would be the volumetric grade (or alteration) distributions of the two-phase system. The stereological transformation of linear intercept data allows these parameters to be calculated under certain circumstances.

The observations that the cerussite replaces galena concentrically, and that the particles approach squares in section outline, are

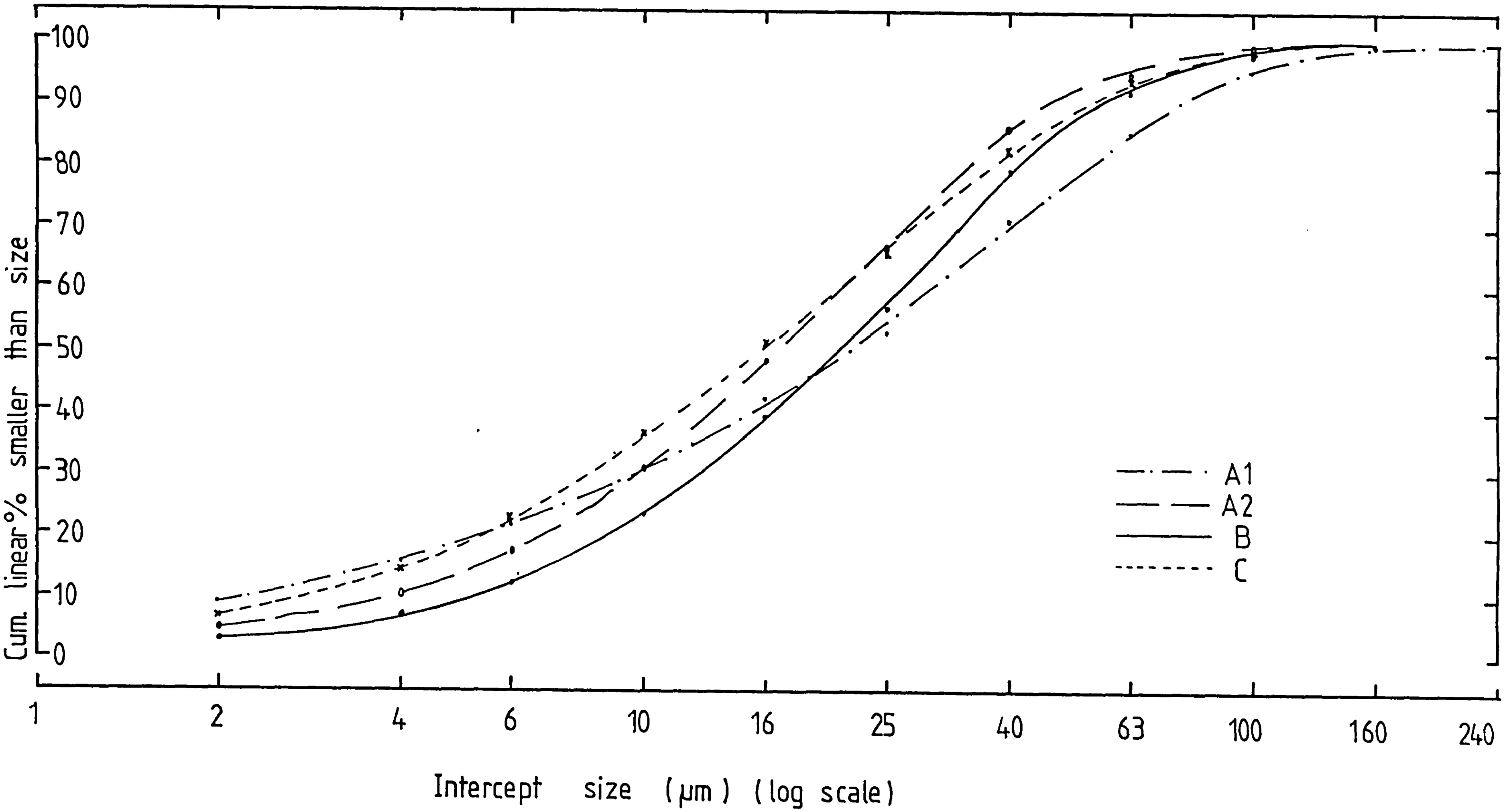

Figure 5.2 Baryte linear intercept distributions -150 + 104 µm, +2.96 SG material

important. For, such a particle system has been analysed theoretically by Horton (1978) and by Moore (1983). The system can be computer simulated by considering large numbers of (linear) random probes through concentric cubes having various volume proportions, or grades. Figure 5.3 shows the results of such simulations.

Comparison of linear intercept data with theoretical models

The linear alteration (or grade) distributions of the galena-cerussite particles are shown in Appendix 6. The total length of these particles in any given sample was too small for statistical reliability. Therefore, the results of the four samples at each given size were combined to provide a single result. This course of action appeared reasonable in view of the apparent similarity of the samples.

The combined alteration distributions are shown in Figure 5.4. Superimposed on this figure are selected results from Figure 5.3. The combined distributions are seen to differ from the ideal model. This could be due to several factors:

1. Not all the galena-cerussite particles within a sample are part of a concentric cubes particle system.
2. The cubic particles within a sample are not part of a unique concentric cubes system. This could be because the particles show a range of 'real' particle sizes and/or a range of alteration distributions within a sample.
3. Insufficient measurements were made for the statistical reliability of the data.

The galena-cerussite particles appeared to be square-shaped in polished sections. To check the quantitative integrity of this qualitative observation, the linear intercept data were reappraised to produce analyses showing the number, and the lengths, of the intercepts of cerussite and galena across every particle traversed. Composite particles of cerussite and galena that are part of a concentric cubes particle system can have only 3 intercepts - 2 of cerussite and 1 of galena. The results of the analyses are shown in Table 5.7.

Figure 5.3 Linear intercept distributions - concentric cubes model (program after Moore (1983))

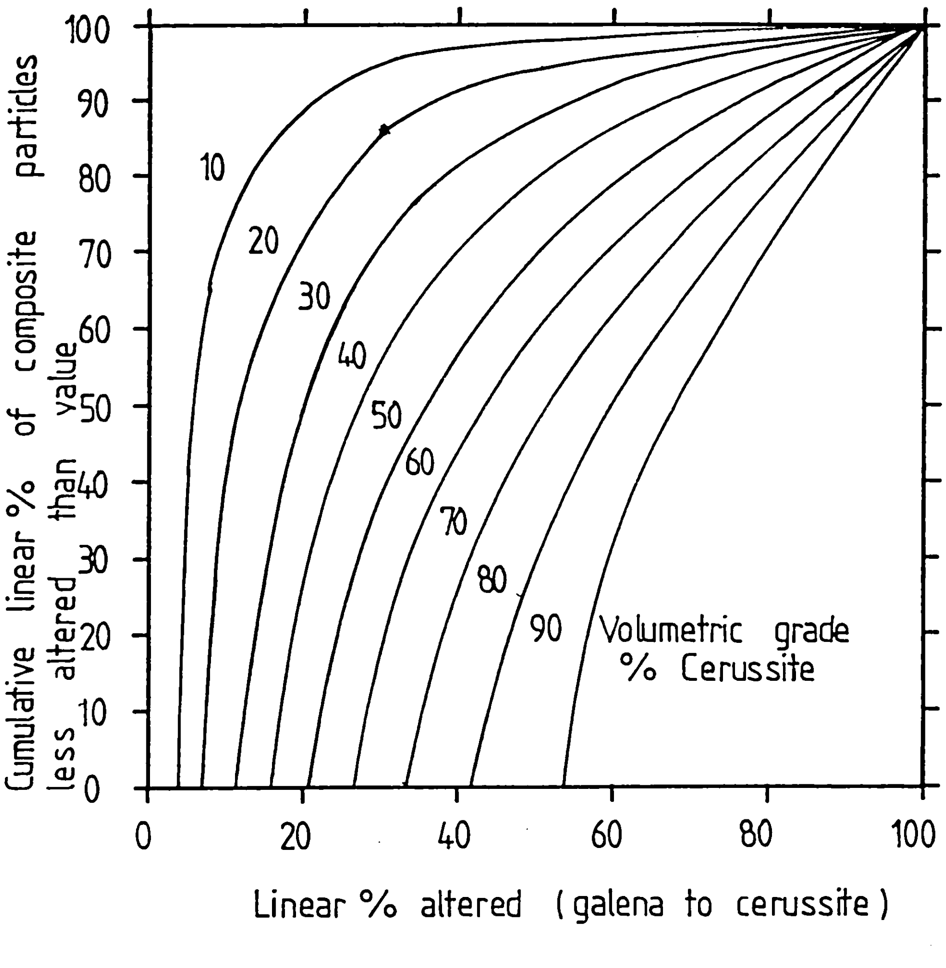

Figure 5.4 Combined alteration distributions with superimposed concentric cubes data

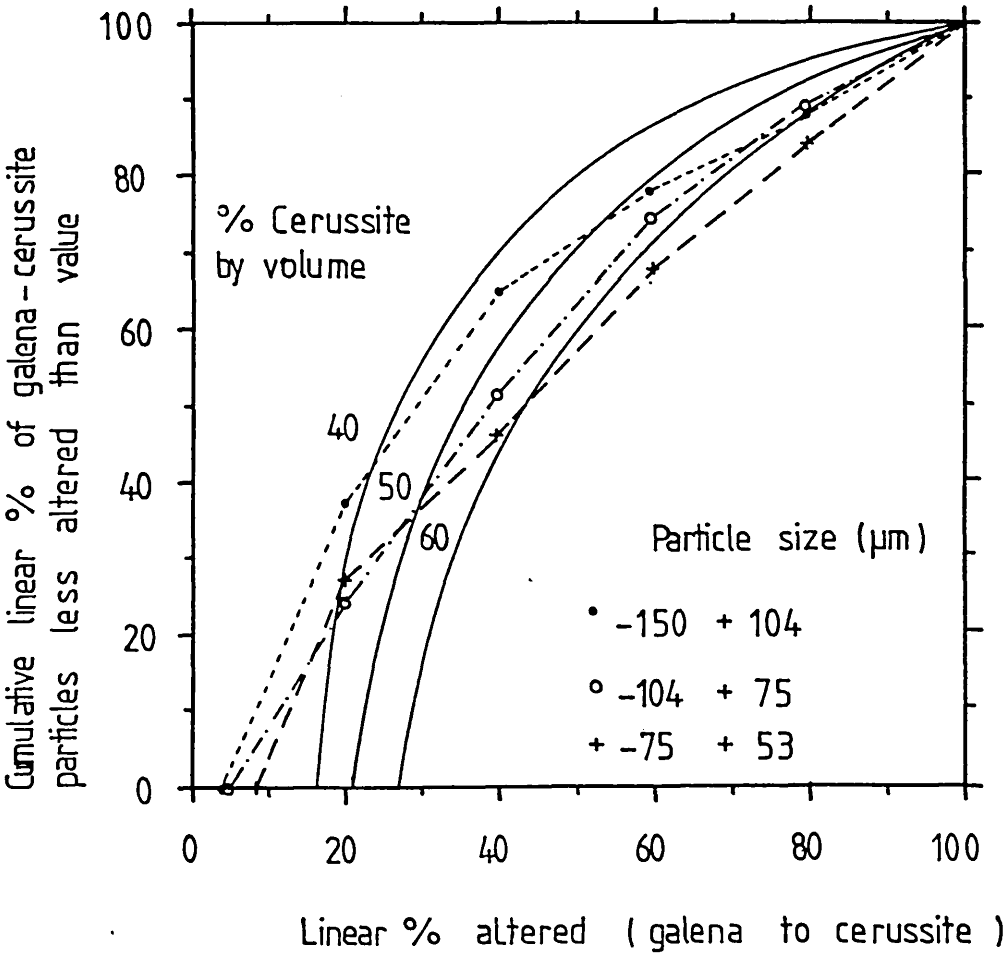

Table 5.7: Intercept distributions of galena and cerussite composite particles

	Linear % of particles occurring in each class											
		A1			A2			B			C	
No. of intercepts:	3	>3	2	3	>3	2	3	>3	2	3	>3	2
Particle size (μm)												
-150 + 104	43.6	55.6	0.8	61.1	38.9	0	63.2	30.9	5.9	56.1	36.0	7.9
-104 + 75	56.3	41.1	2.6	71.2	26.8	2.0	68.5	25.0	6.5	46.2	51.2	2.6
-75 + 53	65.9	31.4	2.7	74.3	24.7	1.0	42.4	50.9	6.7	61.4	28.0	10.6

Only about half of the total length of the cerussite-galena particles traversed were of the 3-intercept type. The 2-intercept particles were due mainly to cerussite-galena-smithsonite (or baryte) particles, whilst the particles with more than 3 intercepts are of the type shown in Figure 5.5.

Particles that have 3 intercepts are not necessarily part of a concentric cubes system - the presence of 3 intercepts merely implies a two-phase system where one phase surrounds the other. However, the alteration distributions of the 3 intercept particles can be compared with the concentric cubes model.

Only two of the 3 intercept distributions were found to approximate to concentric cube distributions, viz, A1 -150 + 104 μm and B -104 + 75 μm (Figure 5.6). However, the fit of the A1 data is of low reliability because it involves only 32 particles. The B sample data are more reliable since they consider 110 particles - a number which has been shown by computer simulation procedures (Moore (1983)) to provide distributions sufficiently close to the ideal for reasonable results.

Thus, it is seen that the measured data cannot be adequately modelled by the concentric cubes model. The model is inappropriate although it appeared, qualitatively, to be correct. The sensitivity to deviations in particle characteristics was greater than originally anticipated (Horton (1983)). The topographically similar concentric spheres model (Figure 5.7) did not provide better fits for either the total, or the 3 intercept distributions.

Therefore, the overall cerussite:galena linear (and, therefore, volumetric) ratios are the only linear data which can be used to describe the state of the galena alteration.

Figure 5.5 A typical galena-cerussite particle which would give rise to multiple linear intercepts

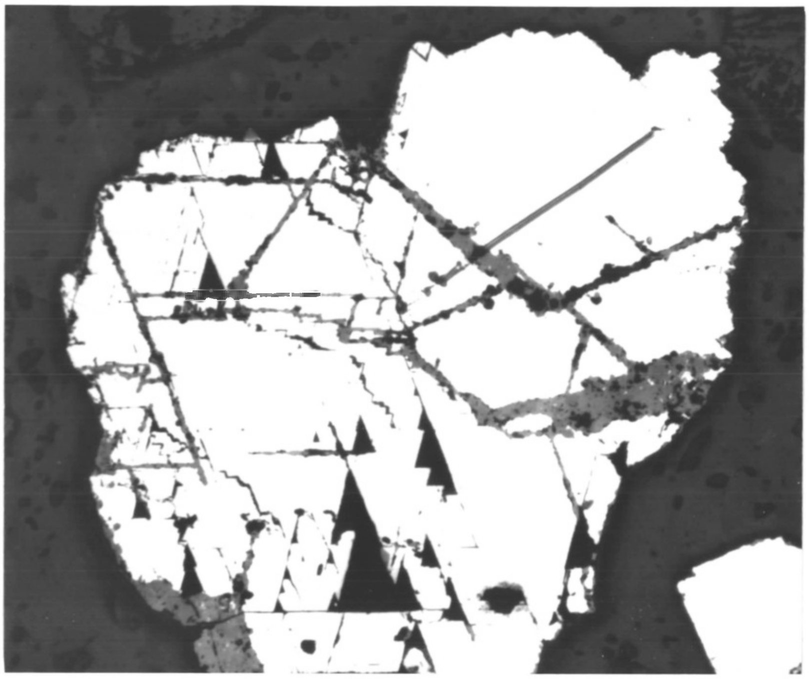

400 μm

Figure 5.6 3-intercept particle distributions showing concentric cube behaviour

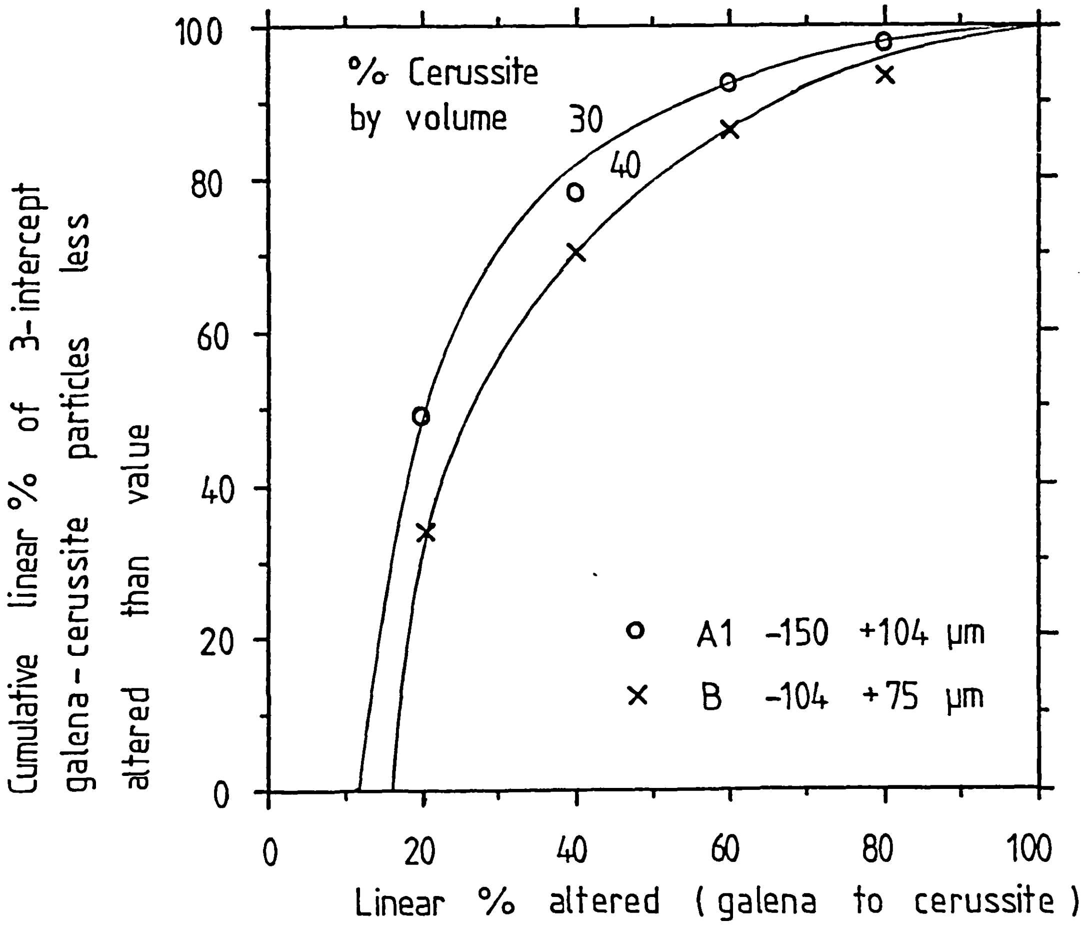

Figure 5.7 Linear intercept distributions - concentric spheres model

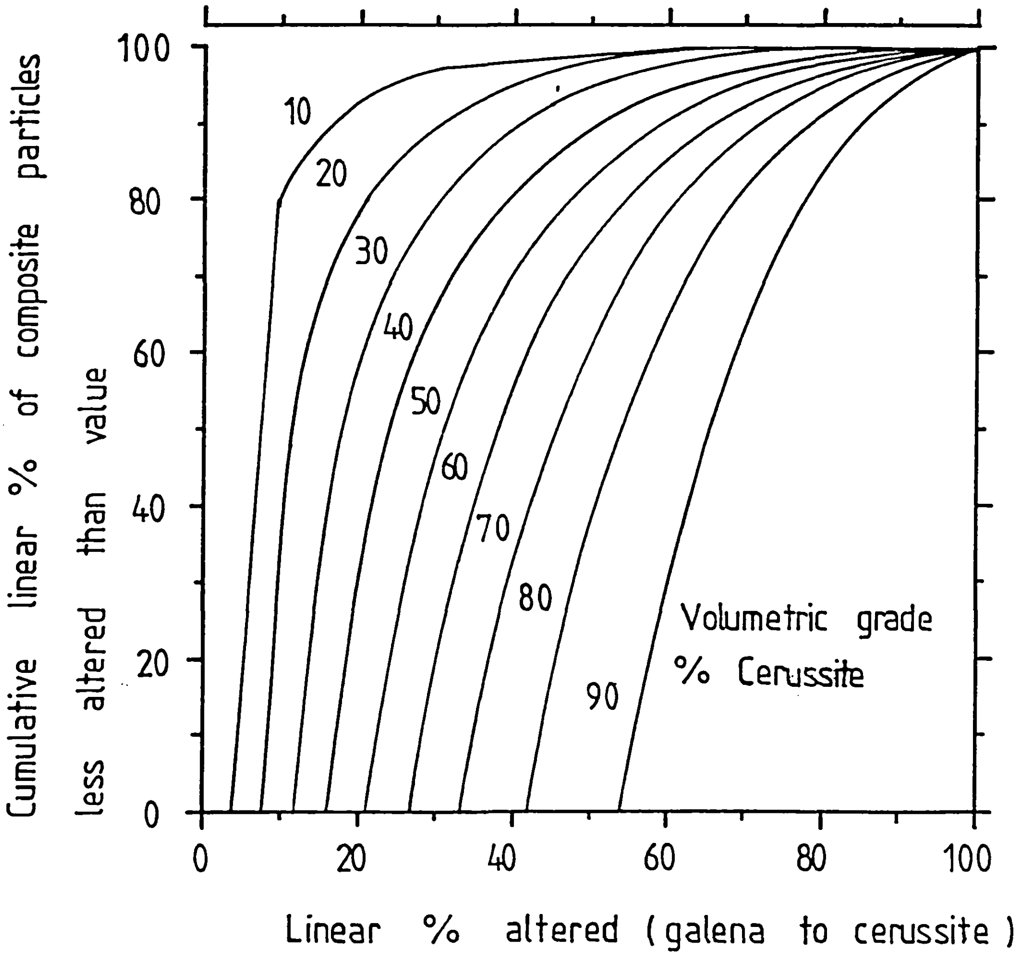

5.5 Chemical analysis

5.5.1 General

The selective dissolution of cerussite and anglesite from galena can be achieved by using an aqueous solution containing 15% ammonium ethanoate and 3% glacial ethanoic acid (Steger (1977)). The cerussite and anglesite are completely dissolved without significant loss of galena (Steger (1977)). The solution also dissolves the oxidation products of sphalerite and chalcocite (Steger (1977)).

5.5.2 Procedure

The attacking reagent was prepared by dissolving 150g of Analar ammonium ethanoate and 30 cm^3 of glacial Analar ethanoic acid in 400 cm^3 of distilled water and diluting to 1 dm^3.

Sub-samples of each of the density fractions produced in section 4.2 were ground to unit micrometre size in a laboratory mill. Sub-samples (0.35-0.45g) of each ground sample were placed in 75 cm^3 beakers and 25 cm^3 aliquots of the attacking reagent were added. The beakers were then covered with a watch glass and the contents were boiled for 5 minutes. Upon cooling, the contents were filtered and the filtrates were made up to 250 cm^3 in volumetric flasks.

The oxidised base-metal contents of the samples, i.e. those amounts soluble in the attacking reagent, were determined by inductively coupled plasma spectrometry (ICP). A Perkin Elmer model 5500 ICP unit was used for these analyses, with standard solutions prepared with similar ammonium ethanoate and ethanoic acid contents to the sample solutions.

The total, as opposed to the oxidised, base-metal contents of the density fractions were determined by dissolving 0.35-0.45g sub-samples of the ground material in nitric acid and analysing the solutes by ICP. The residues were analysed by XRF to check for the complete dissolution of the base-metal mineralisation.

5.5.3 Results

The results for lead, presented as mass % of lead occurring as oxidised species versus the arithmetic mid-point of screen fraction size, are shown in Figure 5.8. Only results for the +2.96 SG fractions are presented since very little lead occurred in the -2.96 SG fractions and that which did was found to be ostensibly totally oxidised. On the other hand, the points representing the -53 µm fractions refer to head values and not to +2.96 SG material.

Analytical errors, determined by replicate analyses, were about ±2% relative. This is typical for routine ICP analysis (Walsh (1982)). However, the variation in metal contents between sub-samples of the same material was found to be up to 10% relative. This sampling variation is represented by the confidence limits shown for the points on Figure 5.8.

The results for zinc showed that the small quantities of zinc in the -2.96 SG fractions were completely oxidised. Total oxidation, within the 10% sampling error, was also seen in the +2.96 SG fractions.

The results for copper showed that all the copper in the -2.96 SG material occurred in an oxidised form. The copper of the +2.96 SG material was seen to be 50 to 100% oxidised - the more oxidised contents occurring at finer sizes. The very low copper contents, together with a large sampling variation and the inability of the ethanoate solution to consistently dissolve copper-bearing secondary phases, make the finite alteration values for copper of low significance.

5.5.5 Discussion of chemical results

The chemical analyses show that the proportion of altered galena increases with decreasing particle size; this is expected. The results for each group of samples are very similar except sample A1. This difference must be due to variations in the original material since replicate analyses were within the acceptable error range.

The chemical results also show that galena particles smaller than about 25 µm have been completely oxidised to cerussite. This indicates an overall oxidation rate which is an order of magnitude lower than

Figure 5.8 Values of galena oxidation determined by chemical analysis

1. Sample A1

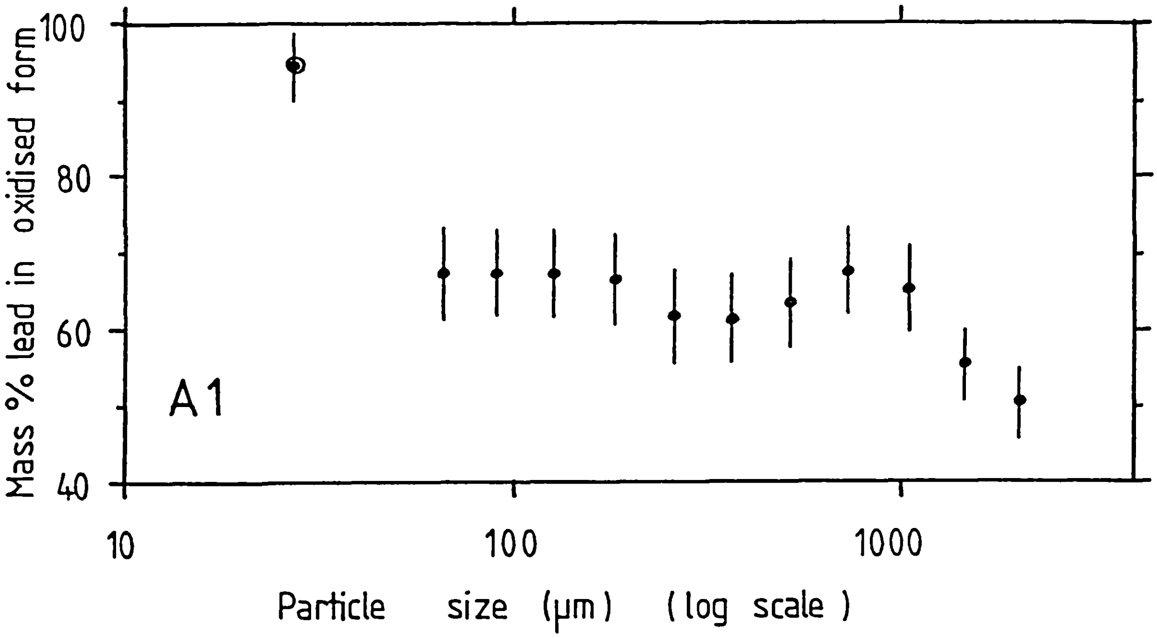

2. Sample A2

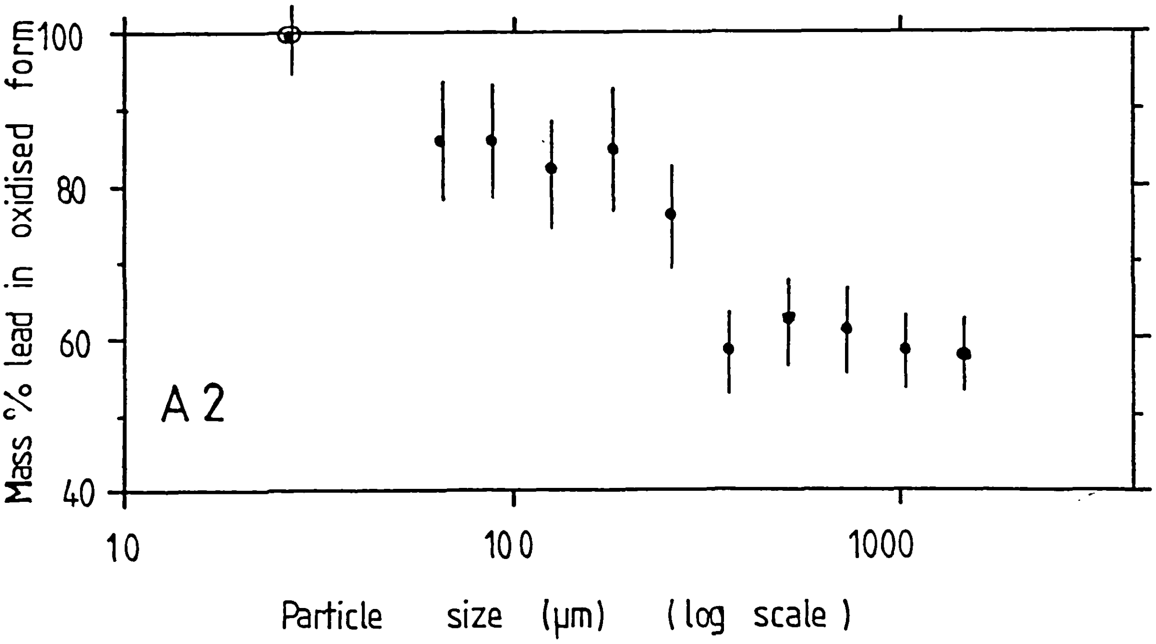

3. Sample B

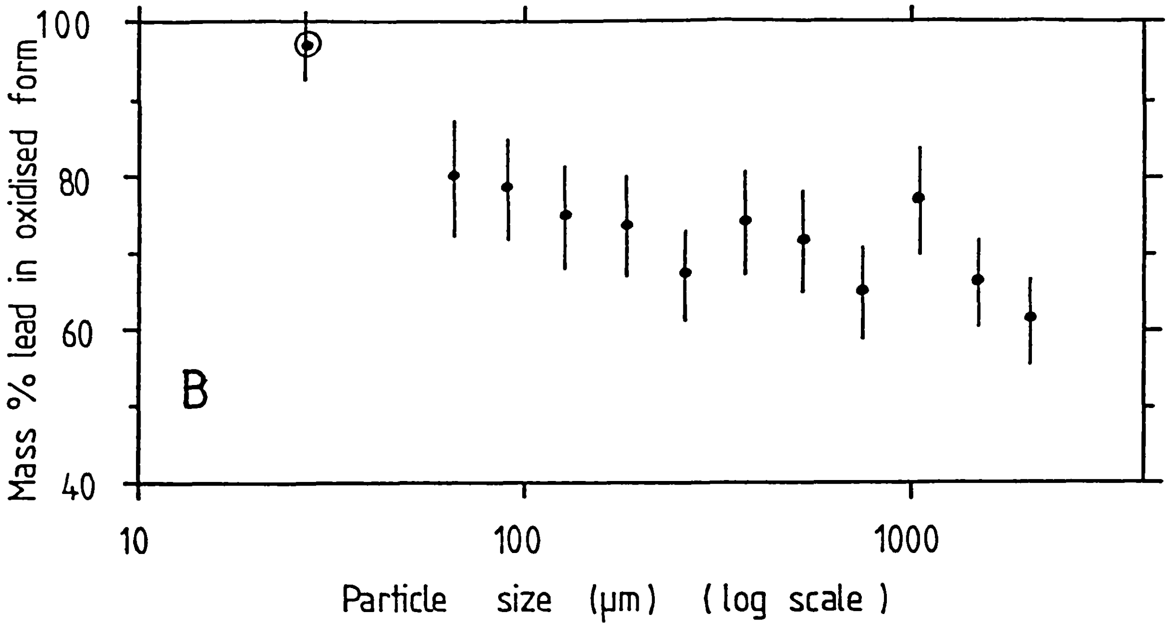

4. Sample C

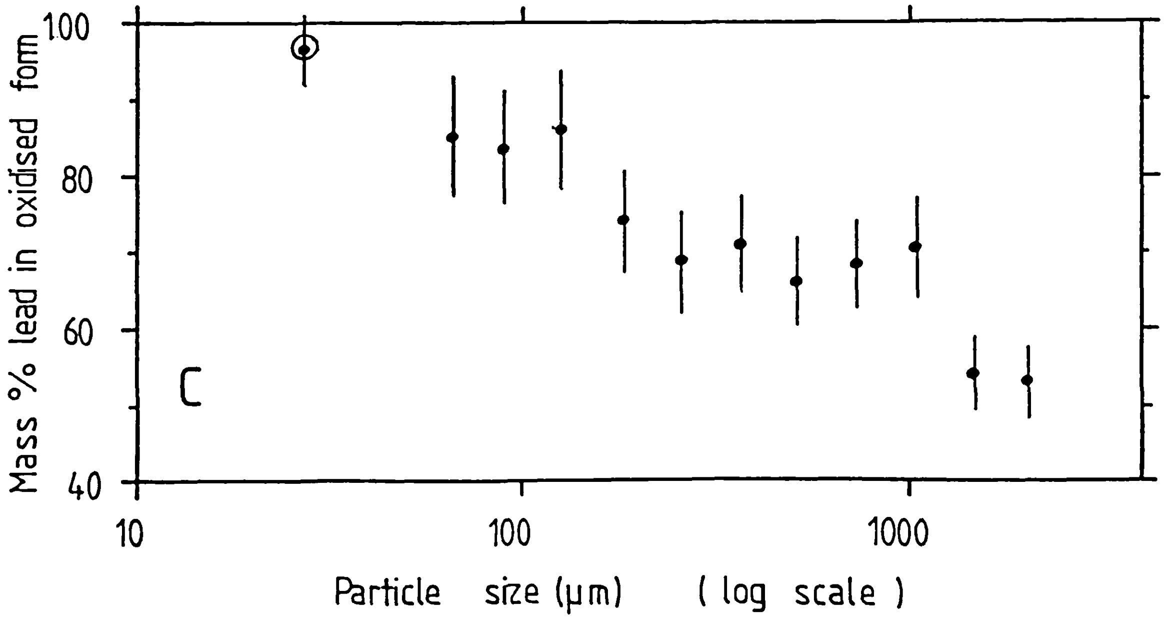

than measured by Eadington (1966) in systems where the surface oxidation products were not allowed to accumulate on the galena surface. Therefore, the effect of oxidation in a bicarbonate medium, where a cerussite coating reduces the rate of galena oxidation, is demonstrated.

Overall, the chemical analyses show that the relative degree of alteration of the base-metal sulphides is Zn > Cu ⩾ Pb. The Cu:Pb alteration ratio is uncertain because of the very low copper content of the samples (an order of magnitude lower than that of lead), and the apparent inability of the ethanoate solution to consistently dissolve all secondary copper-bearing minerals. However, the results are comparable with the chemical predictions of Mann and Deutscher (1980) who predicted the following orders of mobility in carbonate solutions:

pH	Mobility
6 - 8.3	Zn > Pb > Cu
8.3 - 9	Zn > Cu > Pb
9 - 10	Cu > Zn > Pb

Mobility equates with alteration since, for the metal to be mobile in solution, it must first have been produced by sulphide oxidation.

Comparison of linear and chemical data

The comparison of the results of linear and chemical analyses is shown in Table 5.8. The values for linear analysis were calculated with the assumption that the specific gravities of galena and cerussite are 7.5 and 6.55 respectively.

The results are seen to be very similar within the sampling error of the material. The comparisons are especially good when the validity of the assumptions of specific gravity is considered, together with the double sampling error involved in the chemical analysis.

Table 5.8: Comparison of linear and chemical measurements of galena alteration

	Mass % of lead occurring in an oxidised form							
	A1		A2		B		C	
Particle size (μm)	Lin.	Chem.	Lin.	Chem.	Lin.	Chem.	Lin.	Chem.
-150 + 104	67.0	66.9	70.8	82.2	65.3	74.6	68.7	85.9
-104 + 75	72.7	66.9	79.9	85.9	66.3	77.7	75.3	83.4
-75 + 53	80.3	67.0	78.3	85.8	77.5	79.7	76.7	85.1

5.6 Summary

The proportion of galena that has altered to cerussite has been quantified by automatic linear image analysis and by selective chemical dissolution. The two methods produced very similar results. Optical area image analysis was not suitable for measuring the alteration because of the difficulty of unequivocally discriminating all the cerussite.

The galena alteration was not adequately modelled by a concentric cubes particle model. The natural particles deviate from the ideal model both in complexity and in the range of alteration states. However, the overall linear cerussite:galena ratios provide good estimates of the oxidised lead content, assuming 'standard' galena and cerussite densities. The other linear data were seen to be rational and self-consistent.

The relative alteration of base-metal sulphides was found to be Zn > Cu $\gtrsim$ Pb which accords with published chemical predictions.

CHAPTER SIX

Studies of the galena-cerussite interface

6.1 Introduction

The alteration of galena to cerussite is generally assumed either to proceed via an intermediate anglesite phase, or to occur directly (section 3.4). An optical examination of the Dutchman dump material (section 4.3) suggested that the alteration proceeded directly and an analysis of the galena-cerussite interface should, therefore, provide information on the mechanism of cerussite formation.

During the linear image analysing procedures (section 5.4), two effects indicated that phases other than galena or cerussite were present in the interfacial region:

1. The cerussite showed a marked green cathodoluminescence under the electron beam. This effect often occurs when an electron beam strikes a phase that contains certain trace impurities, such as manganese or rare-earth elements, in an otherwise non-luminescent host (Long (1977)), and it is not uncommon in cerussite. However, when the cerussite-galena contacts were traversed, the cathodoluminescence stopped before the beam contacted the galena.

2. Secondary electron imagery revealed a narrow 'shadowy zone' of comparatively low mean atomic number surrounding galena and occurring between the unreacted galena core and the nearest cerussite.

These effects occurred in all the sections that contained galena (and not only in those used for the linear analyses). The effects were found in every sample and in each size fraction.

6.2 Microprobe studies of the galena-cerussite interface

6.2.1 Techniques

The Camebax-Micro (section 5.4.1) was used for both the automated quantitative and qualitative point analyses. Characteristic X-rays, secondary electrons, and back-scattered electrons (BSE) were used to produce selected area images.

6.2.2 Results

An interfacial zone was found between the galena and the cerussite in all sections in studies of the electron images of +2.96 SG material. This zone was always approximately 10 µm thick, irrespective of particle size, except where sectioning effects created exceptionally wide zones. Figure 6.1 shows BSE images of typical galena-cerussite interfaces.

Qualitative microprobe analyses of the interfacial zones showed the presence of major, but variable, amounts of lead, sulphur, and oxygen, minor amounts of carbon and calcium, together with trace amounts of iron, copper and zinc.

Typical qualitative variations in the lead and sulphur contents across galena-cerussite interfaces are shown in Figure 6.2. These results were reproducible in all galena-cerussite particles, irrespective of particle size. Figure 6.3 shows the variation in trace elements, as well as lead and sulphur, across a galena-cerussite interface. The interfacial zone, though heavily pitted, was one of the widest seen which was not obviously attributable to orientation and/or sectioning effects.

Figures 6.2 and 6.3 show a compositional trend which was supported by all the analyses obtained from the galena-cerussite interfaces. Where the narrow intermediate zone was only about 7 µm wide and where it was apparently continuous across the measured line (i.e. it did not intercept any large pores, pits, or cracks), the sulphur content decreased in an approximately linear fashion across the zone, from 13.4% in the galena to zero in the cerussite. The lead content first

Figure 6.1 Typical BSE images of the galena-cerussite interface

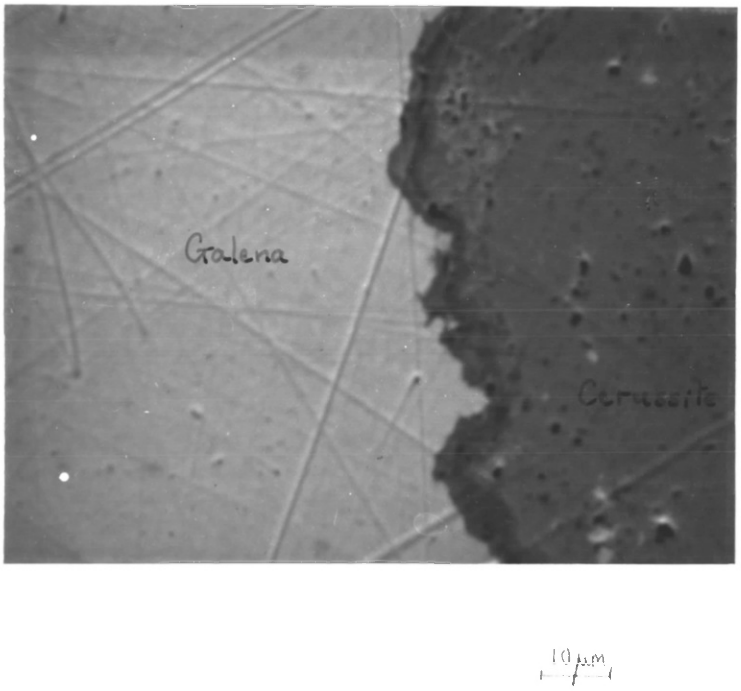
Galena
Cerussite
10μm

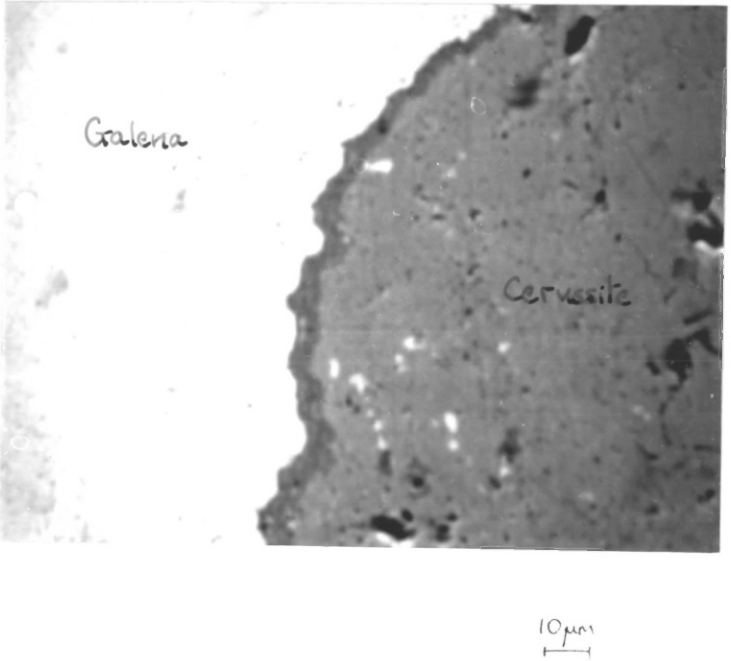
Galena
Cerussite
10μm

Figure 6.2 Typical variations in the lead and sulphur content across galena-cerussite interfaces

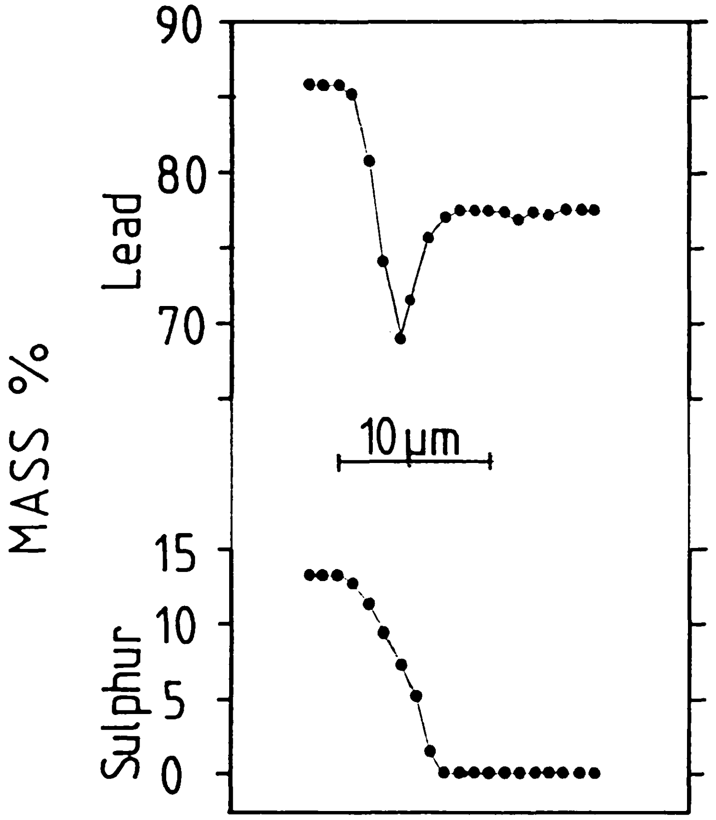

(i) B, -1.7 + 1.18mm, +2.96 SG

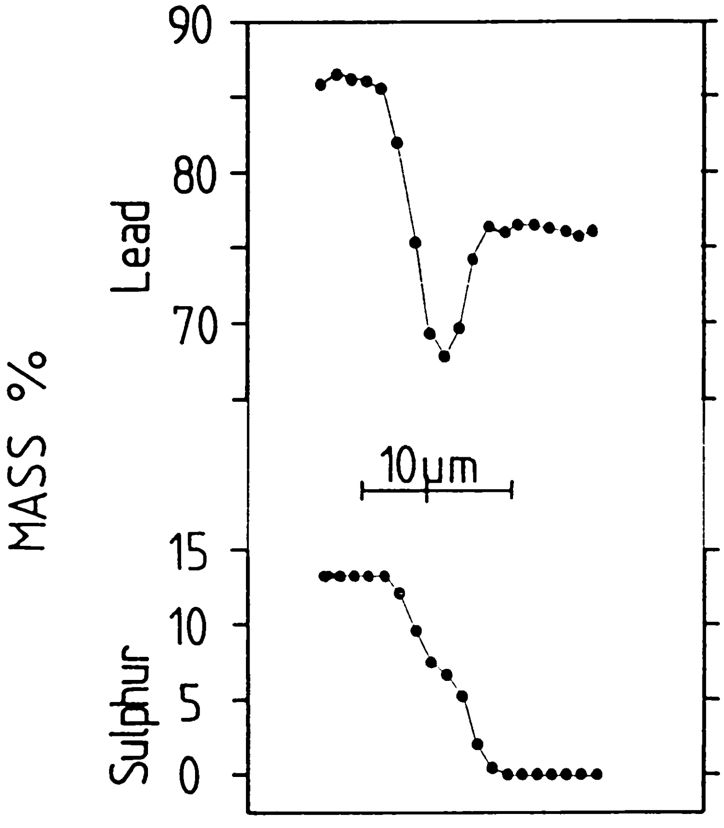

(ii) B, -1.7 + 1.18mm, + 2.96 SG

Figure 6.3 Typical variations in the lead, sulphur, and trace element contents across the galena-cerussite interface

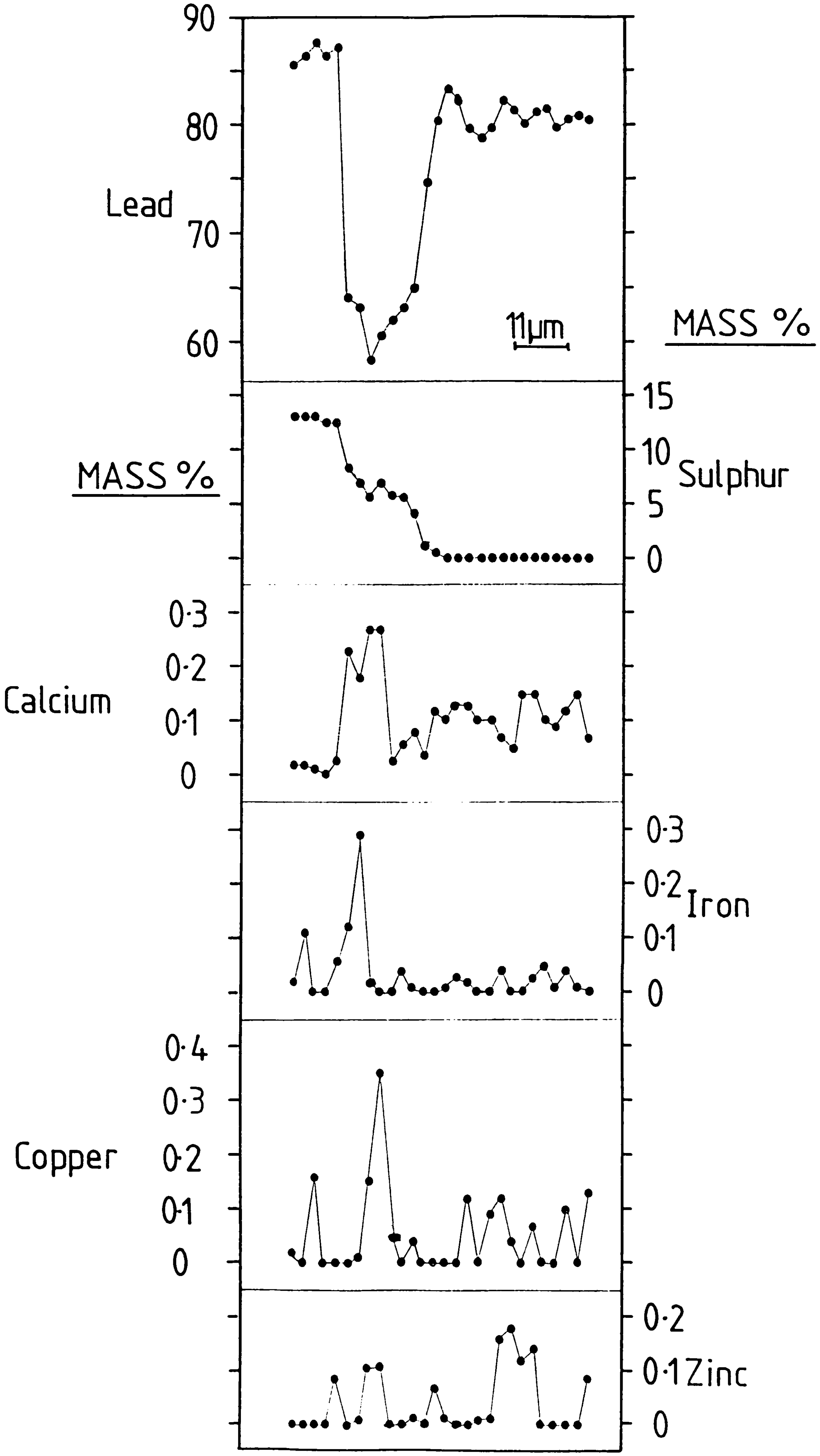

(A1, -600 + 420 µm, +2.96 SG)

decreased away from the galena 'surface' and then increased towards the cerussite phase. Where a slightly wider continuous zone existed (about 10 µm), there was a change in the sulphur profile slope corresponding with the minimum lead content (Figure 6.2(ii)). This inflection in the sulphur profile was more pronouned in the widest zones, and tended to a constant concentration. However, these wide zones tended to be quite heavily pitted in section.

Many of the analysed sections were re-polished and examined optically. It was then possible, in some cases (with the aid of the previously-taken BSE image photographs), to distinguish the galena-cerussite interfacial zone. The more-pitted zones were the most easily detected because of their negative polishing relief. However, optical differentiation was generally poor and, in most cases, the galena-cerussite contact appeared to be sharp.

6.2.3 Discussion

The results showed that an interfacial region, containing mainly lead and sulphur, existed between galena and its stable alteration product, cerussite. The zone was about 10 µm wide in all samples and at all particle sizes, and was thus independent of these variables.

It appears, therefore, that, under the conditions encountered in the dump, cerussite does not form 'directly' from galena but forms via the detected intermediate product(s). Quantitative microprobe analyses of the intermediate zone showed that it was not anglesite, $PbSO_4$, the commonly ~~s~~cited macroscopic intermediate product, nor any other simple stoichiometric lead-sulphur phase. Appendix 7 lists the major phases known, or proposed, to exist in the $Pb-S-CO_2$ system. The zoning within the intermediate region was also suggested by scanning electron microscope (SEM) examinations of mineral sections using a JEOL 35CF instrument. The material within the intermediate zone appeared to be more porous nearer the galena 'surface'. Typical SEM image photographs of a galena-cerussite interface are shown in Figure 6.4.

Figure 6.4 Typical SEM images of the galena-cerussite interface

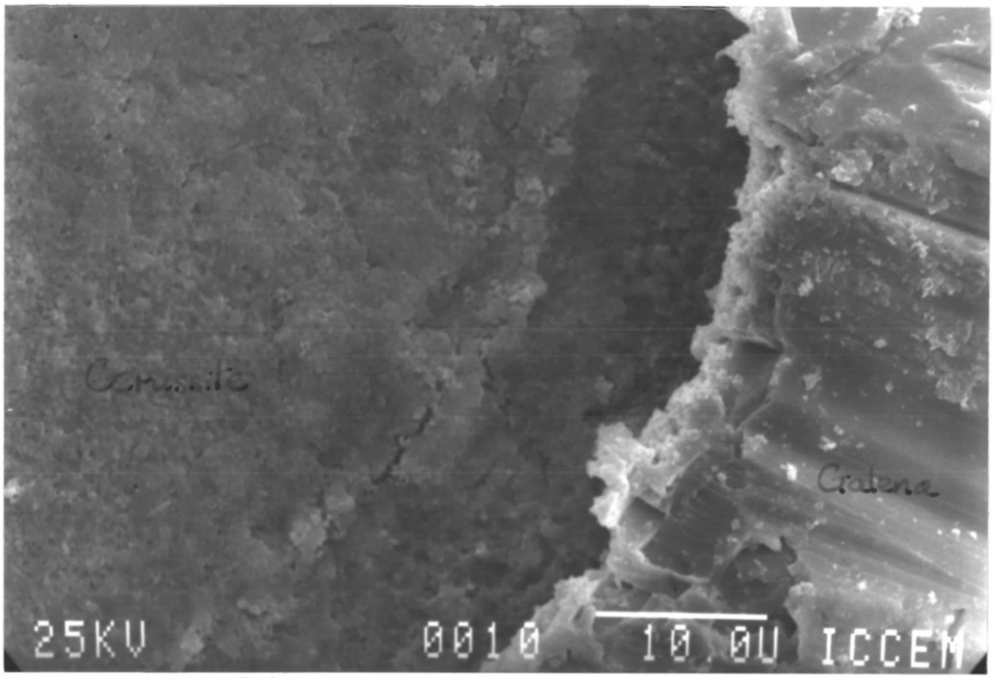
Cerussite
Galena
25KV
0010
10.0U
ICCEM
Intermediate Zone

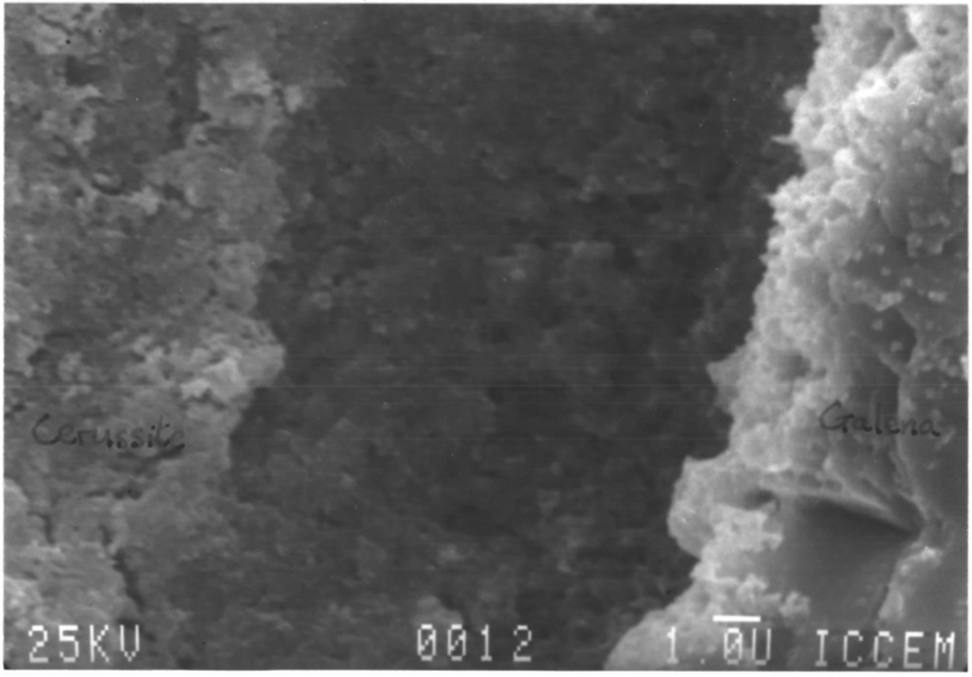
Intermediate Zone
Cerussite
Galena
25KV
0012
1.0U
ICCEM

6.3 Interpretation of microprobe results

6.3.1 General

The general form of the lead and sulphur elemental profiles across a galena-cerussite interface are shown in Figure 6.5, together with the (oxygen + carbon) profile. Three zones can be recognised in the interfacial material between the galena and cerussite:

Zone A - nearest to the galena 'surface', and showing a marked, near-linear decrease in both the lead and sulphur content away from the galena 'surface'. The combined (oxygen + carbon) profile shows a corresponding, near-linear increase.

Zone B - the central zone, in which the lead content is a minimum, the (oxygen + carbon) content is at a maximum, and the sulphur content is approximately constant.

Zone C - nearest the cerussite 'surface', and showing a rapid, near-linear increase in the lead content from its minimum in Zone B to the stoichiometric cerussite value at 'y'. The sulphur content shows a near-linear decrease from the plateau in Zone B to zero at the cerussite surface ('y'). The (oxygen + carbon) content shows a corresponding decrease to the stoichiometric cerussite value.

Thus, lead and sulphur species must be transferred from 'x' to 'y', and oxygen and carbon species must be introduced up to 'x', during the course of the alteration of galena to cerussite. It is assumed that the movement of lead and sulphur occurs via solution species because gaseous or solid phase reactions are unlikely under the ambient conditions. This assumption is supported by the presence of Ca, Fe, Zn and Cu in the intermediate zone (and also in the cerussite zone) which must have been introduced in solution. The galena-cerussite interfacial zone is constantly in contact with an aqueous solution since it is probable that each particle within the dump is surrounded by a film of stagnant water which is not part of the throughflow of water in the dump. This is a tenable assumption because the dump receives a large amount of direct precipitation year-round (Appendix 2) and, with the exception of the material on the surface of the dump, will be constantly damp. This coating of particles with thin films of water has been found even on dump material from arid areas (Prosser

Figure 6.5 Generalised galena-cerussite alteration profile

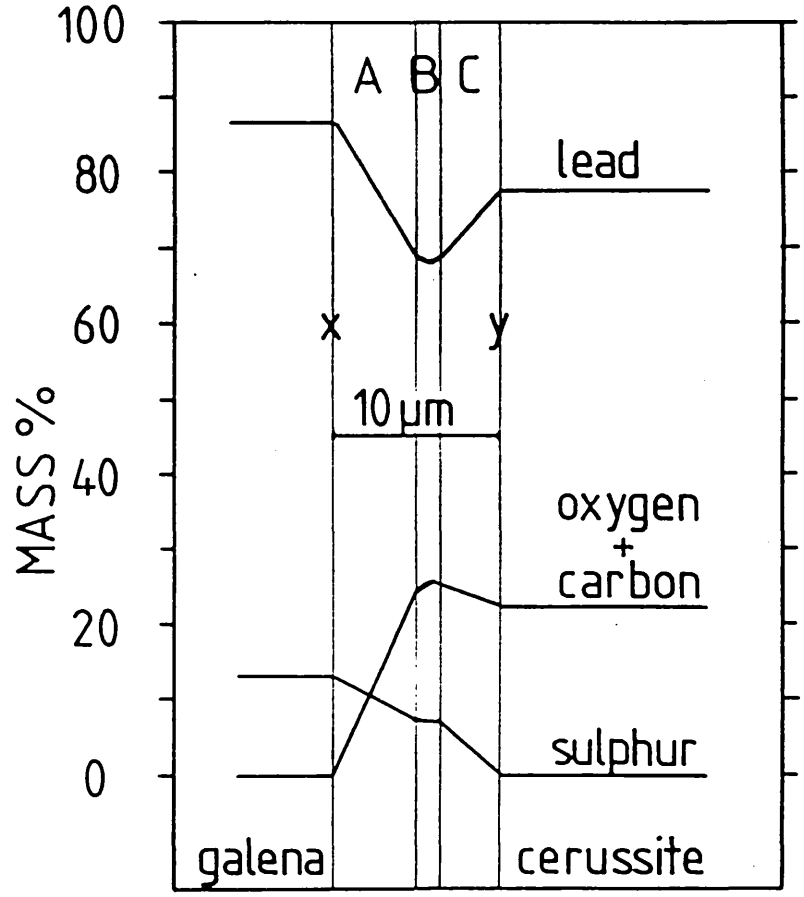

(1981)). Although the particles are in contact with a solution phase, the solubility of lead in bicarbonate solutions is exceedingly small (section 3.3.4). It is likely, therefore, that lead dissolved from galena is deposited around its parent particle, i.e. there will be little redistribution of lead between particles.

Therefore, given the above discussion, the sections examined represent static, dehydrated 'views' of dynamic, aqueous systems and thus require detailed chemical interpretation.

6.3.2 Lead and sulphur aqueous chemistry

The literature review of galena alteration (section 3.3) showed that the possible solid products derived from the alteration included various sulphates, thiosulphates, and carbonates, together with the hydroxide. The possible solution species are more numerous since both lead and sulphur are capable of forming many species, some of which are thermodynamically unstable.

The sulphate anion, SO_4^{2-}, is the thermodynamically stable aqueous sulphur species under the dump conditions (Figure 3.1). However, the literature review shows that thiosulphate, $S_2O_3^{2-}$, is probably the first sulphur solution species produced from galena, with possible later reaction to form a polythionate, $S_xO_6^{2-}$ (x = 2 to 6), such as tetrathionate, $S_4O_6^{2-}$, or to sulphate. The tendency for thiosulphate to oxidise to tetrathionate in commercial leaching processes has been noted by Flett et al (1984). Plante and Sutherland (1948), whilst noting that the oxidised sulphur species change with time, quoted the following polythionate stability ranges:

species	pH stability range
dithionate	3 to 12
trithionate	decomposes below 5.6, stable above 8.9
tetrathionate	decomposes below 8.9, stable to 11.4
pentathionate	stable below 2.5
hexathionate	stable below 0.3
(thiosulphate)	(decomposes below 5.0)

The literature review on galena (section 3.3) considered that the lead should normally exist in solution as the Pb^{2+} ion, with some plumbite, $HPbO_2^-$, at high pH values. Goleva et al (1970) considered that the $PbHCO_3^+$, $PbCO_3^\circ$ and $Pb(CO_3)_2^{2-}$ species predominate under bicarbonate conditions.

Additional data on the aqueous chemistry of lead are found in the extensive literature concerning the flotation of galena by thiol collectors. Burkin et al (1966) constructed an Eh-pH diagram for the $PbS-H_2O-O_2$ system (Figure 6.6) which shows that the simple lead oxide, PbO, is stable at the pH of the dump; decreasing sulphate concentrations move the $PbO-PbSO_4$ boundary to more acid pH values. These authors also considered that lead carbonates would replace the oxide in carbonate solutions (Figure 3.4).

Toperi and Tolun (1969) recalculated the potentials required for galena oxidation by assuming that, in practice, the sulphur oxidation proceeds no further than the metastable thiosulphate. They calculated the minimum potentials required for the oxidation from the following equations:

$$2PbS + 5H_2O = PbS_2O_3 + Pb(OH)_2 + 8H^+ + 8e^- \qquad (6.1a)$$

$$Eh = 0.505 - 0.059\ pH \qquad (6.1b)$$

$$2PbS + 7H_2O = 2Pb(OH)_2 + S_2O_3^{2-} + 10H^+ + 8e^- \qquad (6.2a)$$

$$Eh = 0.632 - 0.0737\ pH + 0.007\ \log\ [S_2O_3^{2-}] \qquad (6.2b)$$

$$2PbS + 7H_2O = 2HPbO_2^- + S_2O_3^{2-} + 12H^+ + 8e^- \qquad (6.3a)$$

$$Eh = 0.841 - 0.0885\ pH + 0.015\ \log[HPbO_2^-] + 0.007\ \log\ [S_2O_3^{2-}] \qquad (6.3b)$$

These results are summarised in Figure 6.7. At pH values between 7 and 10, reaction (6.2a) has the lowest potential.

Lead can also form a number of stable aqueous thiosulphate complexes. The stability constants are (Sillen (1964)):

$$PbS_2O_{3(s)} = Pb^{2+} + S_2O_3^{2-} \qquad K_{sp} = 10^{-6.5} \qquad (6.4)$$

$$Pb^{2+} + S_2O_3^{2-} = PbS_2O_3^\circ \qquad K = 10^{2.56} \qquad (6.5)$$

$$Pb^{2+} + 2S_2O_3^{2-} = Pb(S_2O_3)_2^{2-} \qquad \beta_2 = 10^{5.4} \qquad (6.6)$$

Figure 6.6 Part of the Eh-pH diagram for the galena-water system (from Burkin et al (1966))

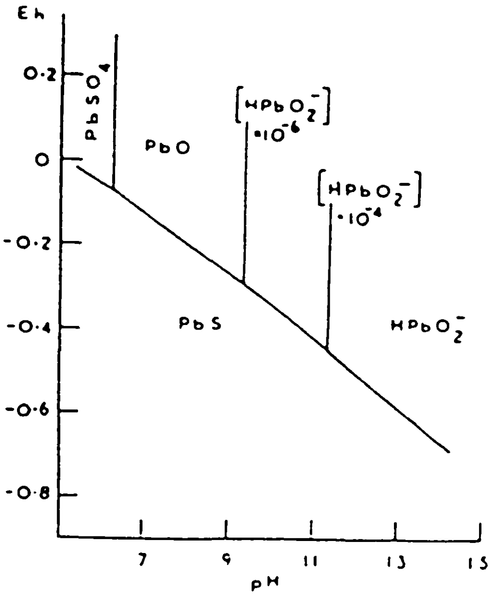

Figure 6.7 Part of the Eh-pH diagram for the galena-oxygen-water system (from Toperi and Tolun (1969))

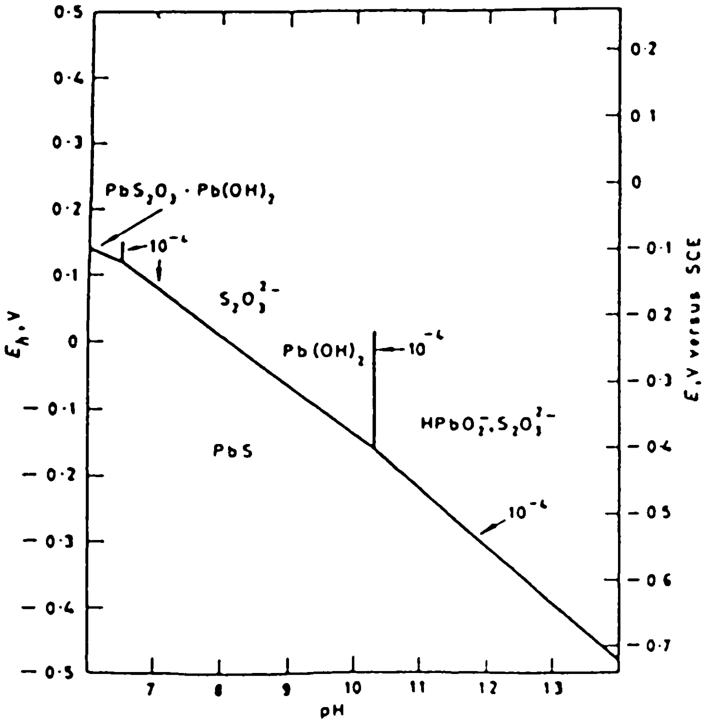

$$Pb^{2+} + 3S_2O_3^{2-} = Pb(S_2O_3)_3^{4-} \qquad \beta_3 = 10^{6.4} \qquad (6.7)$$

$$Pb^{2+} + 4S_2O_3^{2-} = Pb(S_2O_3)_4^{6-} \qquad \beta_4 = 10^{6} \qquad (6.8)$$

However, Maust et al (1976) state that, in alkaline solution, Pb(II) is present as plumbite, $HPbO_2^-$, and/or hydroxy complexes such as $PbOH^+$. These authors also consider that the introduction of carbonates to the system would result in the formation of lead-carbonate groups.

Gardner and Woods (1979) found, by cyclic voltammetry, that PbO was the stable solid product of galena oxidation at pH 6.8 to 11. They also considered thiosulphate to be the oxidised sulphur species that was formed. Similarly, the cyclic voltammetric investigations of Richardson and Maust (1976) showed Pb^{2+}, PbO or $HPbO_2^-$ to be the lead species formed with increasing pH.

There would, therefore, appear to be a consensus in the mineral literature that, in the absence of carbonate, the oxidised lead species are Pb^{2+}, PbO, or $HPbO_2^-$ depending on pH. However, Baes and Mesmer (1976), in their definitive text on cation hydrolysis, conclude their analysis of lead aqueous chemistry with a distribution diagram for the various lead species (Figure 6.8). From this diagram, it is seen that, in the absence of carbonates, the dominant species in the pH range 8 to 9.5 is $PbOH^+$.

In weakly alkaline carbonate solutions, Goleva et al (1970) consider lead to exist as $PbHCO_3^+$, $PbCO_3^\circ$, and $Pb(CO_3)_2^{2-}$ species, rather than the simple Pb^{2+}, $PbOH^+$ and $HPbO_2^-$ ions (Table 3.2). They used the carbonate equilibria shown in section 3.3.4, together with the following stability relationships to reach their conclusions:

$$PbCO_{3(s)} = Pb^{2+} + CO_3^{2-} \qquad K_{sp} = 3.3 \times 10^{-14} \qquad (6.9)$$

$$Pb^{2+} + CO_3^{2-} = PbCO_3^\circ \qquad K \simeq 10^{6} \qquad (6.10)$$

$$PbCO_3^\circ + CO_3^{2-} = Pb(CO_3)_2^{2-} \qquad K = 1.6 \times 10^{8} \qquad (6.11)$$

$$Pb^{2+} + HCO_3^- = PbHCO_3^+ \qquad K \simeq 10^{3} \qquad (6.12)$$

$$Pb(OH)_{2(s)} = Pb^{2+} + 2OH^- \qquad K_{sp} = 4.7 \times 10^{-16} \qquad (6.13)$$

Figure 6.8 Distribution diagram of Pb(II) hydrolysis products (after Baes and Mesmer (1976))

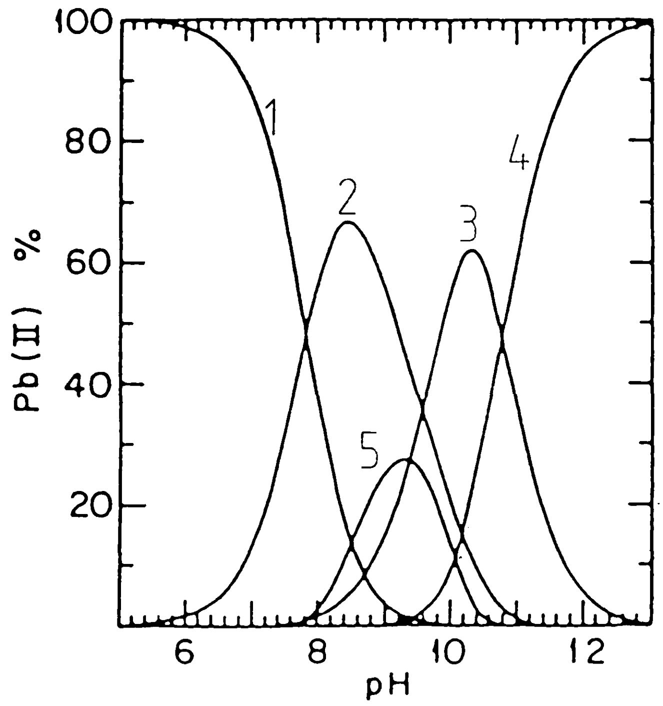

Pb(II) = 10^{-5} Mdm^{-3}

1. = Pb^{2+}

2. = $PbOH^{+}$

3. = $Pb(OH)_2^{\circ}$

4. = $HPbO_2^{-}$

5. = $Pb_3(OH)_4^{2+}$

$Pb^{2+} + 2OH^- = Pb(OH)_2{}^\circ \qquad K = 5 \times 10^9 \qquad (6.14)$

$Pb^{2+} + OH^- = PbOH^+ \qquad K = 1.7 \times 10^6 \qquad (6.15)$

Figure 6.9 shows the relationship of the Pb^{2+} and $PbCO_3{}^\circ$ contents with the pH of natural ground waters determined by Goleva et al (1970). However, as noted in section 3.3.4, the probable important role of the $PbHCO_3{}^+$ complex was not fully developed because of insufficient thermodynamic data on the species.

Thus, under the mildly alkaline, bicarbonate conditions of the Dutchman dump, lead could exist in solution as hydroxy, bicarbonate, carbonate, or thiosulphate complexes and the sulphur could exist as a variety of thiosulphate complexes, depending on local conditions.

6.3.3 Transport considerations

From the foregoing sections, it is evident that the reactions taking place in the intermediate zone between galena and cerussite do so in an aqueous phase. Further, it is evident that the active intermediate zone cannot be entirely aqueous but must contain some solid (or possibly colloidal) material. Precipitation and structural features will therefore complicate the chemical transport processes taking place in the intermediate zone.

It is often possible to consider the reactions of solids in aqueous systems in terms of Nernst solution behaviour. Nernst considered that the chemical processes occurring at a solid interface are always much faster than at least one of the transport processes, so that the reaction rate is transport-controlled. Therefore, in the simple case of a reaction between a single, aqueous reactant ion and a solid, the reaction is so fast that equilibrium is effectively attained instantaneously. Thus, the concentration of the reactant at the interface remains vanishingly small and the rate at which the reaction can occur is controlled by the rate at which the reactant reaches the interface. If the concentration of the reactant in the bulk solution approaches uniformity, then a linear concentration gradient would exist across a thin, stationary layer of liquid of thickness, δ. Thus, applying Fick's law of diffusion,

Figure 6.9 Variation of Pb^{2+} and $PbCO_3°$ content of ground waters with pH (from Goleva et al (1970))

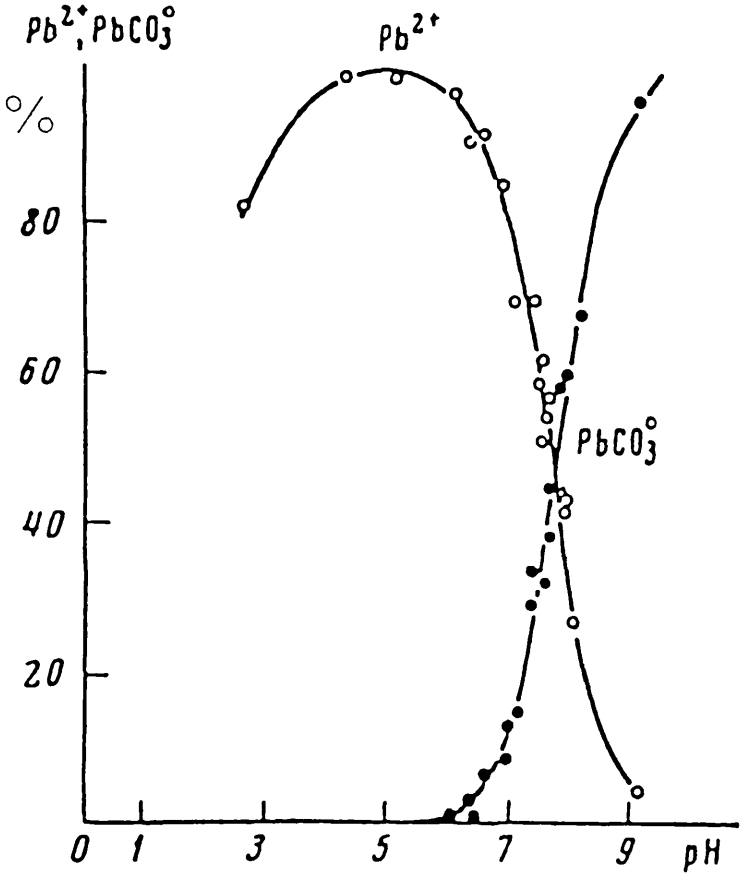

$$F = \frac{dn}{dt} = \frac{D\Delta c}{\Delta x} \tag{6.16}$$

where

F = flux of reactant, moles (n) per unit area (cm²) per unit time (s).

D = diffusion coefficient ($cm^2 s^{-1}$)

Δx = diffusion zone width (cm)

Δc = concentration difference.

For a number of reactions in water at 20°C, δ is about 3×10^{-3} cm (Burkin (1966), and the value of D for the Pb^{2+} ion is about $10^{-5} cm^2 s^{-1}$ (Sohn and Wadsworth (1978)). In addition to the reactant concentration gradient, there would also be a concentration gradient of product species established at the interface. Figure 6.10 shows these effects and also the errors introduced by the oversimplifications of the Nernst theory.

The principles of reaction and diffusion can be developed to encompass the case of a porous product layer formed around the reacting solid. Shrinking-core type models can be formulated by considering the system as comprising three phases - aqueous boundary diffusion, diffusion through porous products, and surface reaction. However, except in simple cases, these models are mathematically complex (Sohn and Wadsworth (1978)).

Whilst a diffusion system could be described mathematically, shrinking-core type models do not appear to be immediately applicable to the galena-cerussite system. For, as noted above, the lead- and sulphur-rich intermediate zone must contain solid (or colloidal) material. Therefore, the equilibria and reactivities of the solid material need to be considered in addition to diffusion properties.

6.3.4 Reaction considerations

It should be possible to describe the processes taking place in the intermediate zone in terms of sequence of simple reactions. Several assumptions need to be made in this connection.

Figure 6.10 Steady-state diffusion boundary at the solid-liquid interface (from Sohn and Wadsworth (1978))

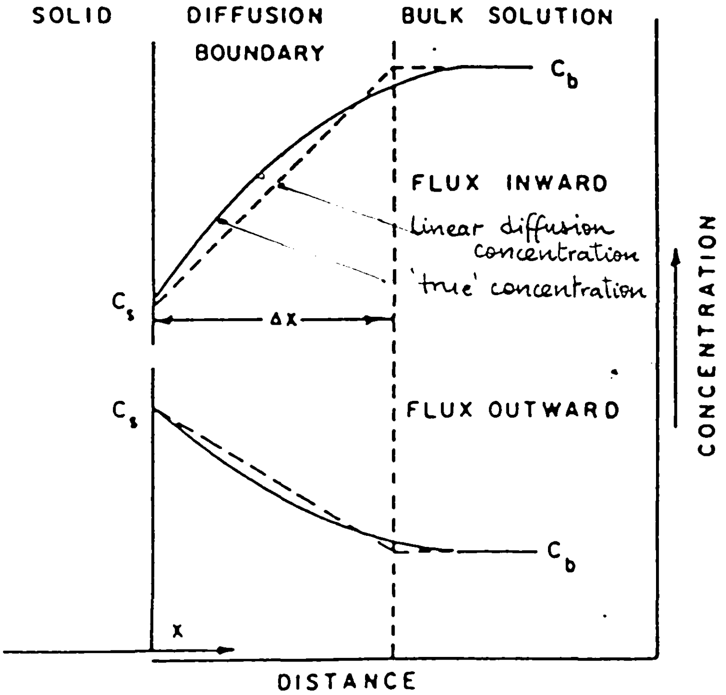
SOLID
DIFFUSION BOUNDARY
BULK SOLUTION
C_b
FLUX INWARD
Linear diffusion concentration
'true' concentration
C_s
Δx
C_s
FLUX OUTWARD
C_b
x
DISTANCE
CONCENTRATION

Firstly, the 'surface' oxidation of galena is considered to proceed broadly via the mechanism proposed by Eadington and Prosser (1969) (section 3.3.5), with the following 'surface' reactions:

$$2PbS = 2Pb^{2+} + 2S^{\circ}_{(sulphur)} + 4e^{-} \qquad (3.17a)$$

$$O_{2(aq)} + 2H_2O + 4e^{-} = 4OH^{-} \qquad (3.17b)$$

However, the authors proposed that, during the initial steady rate period, the lead hydroxide, precipitated at the galena 'surface' from Pb^{2+} and OH^{-}, reacts with the 'surface' sulphur, according to

$$4Pb^{2+} + 8OH^{-} + 4S^{\circ} = 2PbS + PbO.PbS_2O_3.nH_2O + (4-n)H_2O \qquad (3.18)$$

This reaction is identical to that proposed by Reuter and Stein (1957).

Eadington and Prosser (1969) qualitatively tested reaction (3.18) by mixing lead hydroxide and a colloidal suspension of sulphur 'with, and without oxygen'. In both cases the mixture turned orange-brown within three hours, and sulphide and thiosulphate were detected. (Sulphate was detected after twenty four hours). However, this result is insufficient to prove that the reaction takes place since it is difficult to exclude oxygen from such a system - even if only a fraction of a monolayer of oxygen were adsorbed, equation (3.18) would be inapplicable. Moreover, reaction (3.18) would appear to be unlikely because of the reformation of lead sulphide: having oxidised the sulphide, it is not apparent where the energy necessary to reform the sulphide would come from. Therefore, whilst equation (3.18) presents an elegant view of the thiosulphate formation in that it provides a balanced chemical equation, the present author doubts if such a reaction takes place. From the experimental results of Eadington (1966), it is possible that the formation of the basic thiosulphate involves additional oxygen. Consider an alternative reaction,

$$2Pb^{2+} + 4OH^{-} + 2S^{\circ} + O_{2(aq)} = PbO.PbS_2O_3 + 2H_2O \qquad (6.17a)$$

or

$$2Pb^{2+} + 4OH^{-} + 2S^{\circ} + O_{2(aq)} = PbO.PbS_2O_3.nH_2O + (2-n)H_2O \qquad (6.17b)$$

This reaction has reactants in the same ratio as (3.18) but it includes molecular oxygen. The standard free energy change, ΔG°_{r}, for reaction (6.17a) is

$$\Delta G^{o}_{r(6.17a)} = -195 + 2(-56.69) - [2(-5.81) + 4(-37.59) - 2(0) + 0]$$
$$= -146.4 \text{ Kcal mole}^{-1}$$

(Data from Weast (1981) and Eadington (1966)).

The corresponding value for reaction (3.18) is

$$\Delta G^{o}_{r(3.18)} = -195 + 2(-22.15) + 4(-56.69) - [4(-5.81) + 8(-37.59) + 4(0)]$$
$$= -142.10 \text{ Kcal mole}^{-1}$$

Therefore, it is seen that reaction (6.17a) is thermodynamically more favourable by 4.3 Kcal mole^{-1}, or 18 kJ mole^{-1}. Whilst it is not possible, or necessarily correct, to describe mechanistic reactions in terms of balanced chemical equations, reaction (6.17a) appears to be a more correct view of the formation of the thiosulphate.

For the subsequent reactions of the basic thiosulphate, Eadington and Prosser (1969) proposed that lead sulphate is formed by disproportionation,

$$PbO.PbS_2O_3.nH_2O = PbS + PbSO_4 + nH_2O \qquad (3.6)$$

The presence of sulphate in solution after twenty four hours of reaction between lead hydroxide and sulphur was cited as being 'presumably' the result of (3.6). However, the presence of aqueous sulphate does not prove that the reaction occurs. Reuter and Stein (1957) found reaction (3.6) to proceed at 100°C. Lead thiosulphate (PbS_2O_3) decomposes to lead sulphate at the same temperature (Leja et al (1963)). Also, the formation of lead sulphide again appears unlikely. Therefore, the reactions of the basic thiosulphate are probably more complex, especially under a bicarbonate/carbonate regime.

With reference to the generalised alteration profile, Figure 6.5, it must be assumed that the basic thiosulphate is formed close to the galena 'surface'. The Pb:S ratio in the thiosulphate is 6.5:1 (as it is in galena). This was the observed Pb:S ratio immediately next to the galena 'surface'. Figure 6.11 shows typical Pb:S ratios across the intermediate zone. The ratio is seen to increase away from the galena 'surface'. Thus, the basic thiosulphate reacts and loses sulphur faster than it loses lead. This could be due to:

$$PbO.PbS_2O_3.nH_2O = 2PbOH^{+} + S_2O_3^{2-} + (n-1)H_2O \qquad (6.18a)$$

and

$$PbOH^{+} + HCO_3^{-} = PbCO_{3(s)} + H_2O \qquad (6.18b)$$

Figure 6.11 Typical lead:sulphur mass ratios across the galena-cerussite interface

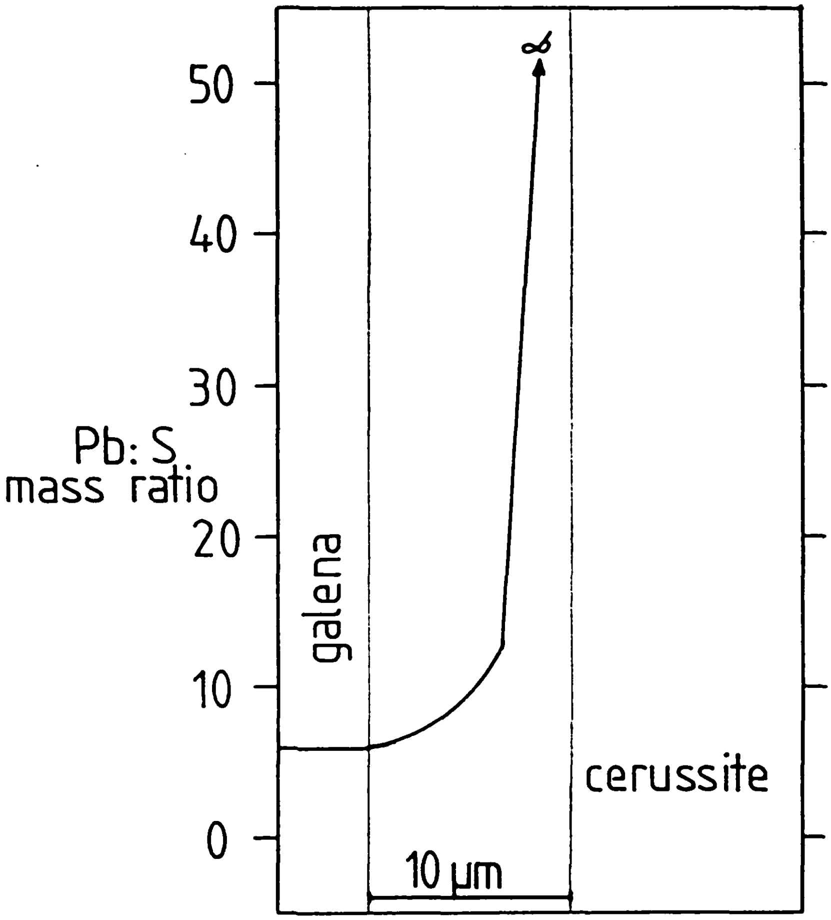

These reactions are possible if the bicarbonate concentration at the thiosulphate solution site is very small, so that the $PbOH^+$ lead species predominates. This would occur, according to the Nernst solution theory, if the influx of bicarbonate ions which react with the $PbOH^+$ ions (equation 6.18b) is effectively consumed further away (nearer to the cerussite 'surface'). This would result in a gradual increase in lead carbonate content away from the solution zone up to the cerussite 'surface' and a corresponding decrease in basic thiosulphate content. At the same time, the thiosulphate ions released would be free to diffuse away from the solution zone and out of the particle.

6.4 Mechanism for the natural alteration of galena to cerussite

The following mechanism is proposed for the natural alteration of galena to cerussite under mildly alkaline, bicarbonate conditions. Such conditions are found in systems where calcite is in equilibrium in aqueous solutions that are open to the atmosphere.

The initial alteration of galena is thought to proceed in the manner proposed by Eadington and Prosser (1969), described in section 3.3.5:

1. Chemisorbed oxygen initiates 'surface' oxidation,

$$PbS + O_{surface} + H_2O = Pb^{2+} + S^{\circ}_{surface} + 2OH^- \qquad (3.16)$$

2. The rate of oxidation accelerates according to

$$2PbS = 2Pb^{2+} + S^{\circ}_{surface} + 4e^- \qquad (3.17a)$$

$$O_{2(aq)} + 2H_2O + 4e^- = 4OH^- \qquad (3.17b)$$

3. A 'steady rate' period is established when the Pb^{2+} and OH^- ions react with the 'surface' sulphur to form a basic thiosulphate. Eadington and Prosser (1969) proposed the following equation to describe this process,

$$4Pb^{2+} + 8OH^- + 4S^{\circ} = 2PbS + PbO.PbS_2O_3.nH_2O + (4-n)H_2O \qquad (3.18)$$

However, as discussed in section 6.3.4, the present author proposes the alternative equation,

$$2Pb^{2+} + 4OH^- + 2S^{\circ} + O_{2(aq)} = PbO.PbS_2O_3.nH_2O + (2-n)H_2O \qquad (6.17b)$$

Equations (3.16), (3.17) and (6.17b) constitute the initial stage of the natural alteration of galena - a stage which should be complete in a matter of hours after the exposure of the galena surface to the atmosphere.

The final stage of the process involves the breakdown of the basic thiosulphate and the formation of cerussite; this is accounted for by

$$PbO.PbS_2O_3.nH_2O = 2PbOH^+ + S_2O_3^{2-} + (n-1)H_2O \qquad (6.18a)$$

and

$$PbOH^+ + HCO_3^- = PbCO_{3(s)} + H_2O \qquad (6.18b)$$

The $PbO.PbS_2O_3.nH_2O$ forms a porous structure at the 'surface' of the galena. The porous zone dissolves according to equation (6.18a) forming $PbOH^+$ and $S_2O_3^{2-}$ ions which diffuse towards the bulk solution. The lead species, $PbOH^+$, encounters HCO_3^- ions and precipitates out as lead carbonate (equation (6.18b)).

Eadington and Prosser (1969) considered that the chemical reduction of oxygen is the rate controlling step during the initial stage. The rate of oxygen reduction (3.17b) and sulphide oxidation (3.17a) must be similar to the rate of formation of the basic thiosulphate (6.17b): Eadington (1966) found that the sulphur content was almost constant during this initial alteration.

The rate of formation of $PbO.PbS_2O_3.nH_2O$ is faster than its rate of decomposition and subsequent formation of cerussite (equation (6.18)). An intermediate product ($PbO.PbS_2O_3.nH_2O$) has been detected, rather than a distinct PbS-$PbCO_3$ interface, so that the rate of reaction (6.17b) must be greater than that of reaction (6.18).

The features of the general alteration profile, Figure 6.5, can be explained on the basis of the above discussion. Thus:

Zone A is a porous product composed largely of basic lead thiosulphate and some lead carbonate. The decrease in the sulphur content is due to the dissolution of $PbO.PbS_2O_3.nH_2O$ to give $S_2O_3^{2-}$ ions.

Zone B is the zone in which $PbCO_3$ predominates over $PbO.PbS_2O_3.nH_2O$. In this zone, the aqueous thiosulphate concentration is lower than in Zone A due to diffusion (see section 6.3.3), and, therefore, carbonate precipitation is increased. Also, the bicarbonate concentration is increased, thus creating conditions favourable for $PbCO_3$ precipitation. However, bicarbonate is consumed by this reaction and stabilises the remaining solid $PbO.PbS_2O_3.nH_2O$. This may account for the apparent plateau in the sulphur profile. Furthermore, it is the consumption of bicarbonate ions in this zone which allows the aqueous lead in Zone A to exist as $PbOH^+$, rather than a lead-bicarbonate complex.

In Zone C, the bicarbonate concentration is further increased, whereas the thiosulphate concentration is decreased. Thus, the $PbO.PbS_2O_3.nH_2O$ is totally converted to cerussite. In this zone it is unlikely that aqueous lead would exist as $PbOH^+$ because of the high bicarbonate concentration. Therefore, the general equation for carbonate formation in this zone is:

$$PbO.PbS_2O_3.nH_2O + 2HCO_3^- = 2PbCO_3 + S_2O_3^{2-} + (n+1)H_2O \qquad (6.19)$$

Thus, the reaction interface advances concentrically into the galena and ultimately forms cerussite. The measured rate of interfacial advance in the Dutchman dump galena was an order of magnitude lower than that determined by Eadington's (1966) work, where surface oxidation products were not allowed to accumulate (section 5.5.5): viz, $n.10^{-11}$ m $hour^{-1}$ as opposed to 10^{-10} m $hour^{-1}$. Therefore, it is likely that the rate of galena oxidation is transport-limited, most probably by the diffusion of oxygen from the bulk solution to the reaction interface. The oxidation of both n- and p-type galena would occur at about the same rate, for, Eadington (1973), subsequent to his initial study, found that for all practical purposes, the rates of oxidation are equal for both the n- and the p-types.

6.5 Summary

The measured chemical variations in the interfacial zone(s) between galena and cerussite have been explained in terms of a new alteration model. This model assumes that, initially, the galena oxidation occurs broadly via the mechanism proposed by Eadington and Prosser (1969) - chemisorbed oxygen initiates the 'surface' galena oxidation which results in the formation of basic lead thiosulphate. The model then describes how the solution of the thiosulphate results in aqueous lead species which react with bicarbonate ions to produce lead carbonate, whilst thiosulphate ions diffuse away to the bulk solution.

CHAPTER SEVEN

Alteration features of sphalerite, chalcopyrite, and pyrite

7.1 General

Optical examination has shown that chalcopyrite, sphalerite, and pyrite alter to their stable oxidate mineral phases, i.e. geothite plus malachite; smithsonite; and goethite, respectively (section 4.3). These changes are in accord with the chemical principles discussed in Chapter Three. However, in view of the discovery of an intermediate product zone between galena and cerussite, detailed microprobe analyses were carried out on the other sulphides.

7.2 Microprobe studies

7.2.1 Zinc minerals

No sphalerite was seen in the Dutchman dump samples. Sphalerite specimens from other dumps on Ecton Hill showed either a very thin smithsonite coating or no coating at all. Where such a coating existed, the contact was seen to be very sharp. The complete loss of sphalerite from the Dutchman dump samples is understandable in view of the discussion presented in section 3.6. The high solubility of zinc carbonate in bicarbonate solutions explains the general lack of smithsonite coatings on the original sulphide grains.

7.2.2 Chalcopyrite

Optical examination (section 4.3) showed that the alteration of chalcopyrite to goethite and malachite produced sharp interfaces. Typical alteration textures are shown in Figure 4.2. The microprobe analyses confirmed the presence of sharp mineral interfaces; Figure 7.1 shows typical elemental variations across an altered chalcopyrite grain. The figure shows that the chalcopyrite-goethite and goethite-malachite phase changes occur over a distance of about 2 µm, i.e. the resolution limit of the microprobe. The chalcopyrite-goethite interface tended to be serrated (Figure 7.2) with, apparently, an enhanced reaction rate along specific crystallographic planes. The goethite product was unstable under the electron beam and dehydrated

Figure 7.1 Element concentration profiles across a chalcopyrite-goethite-malachite particle

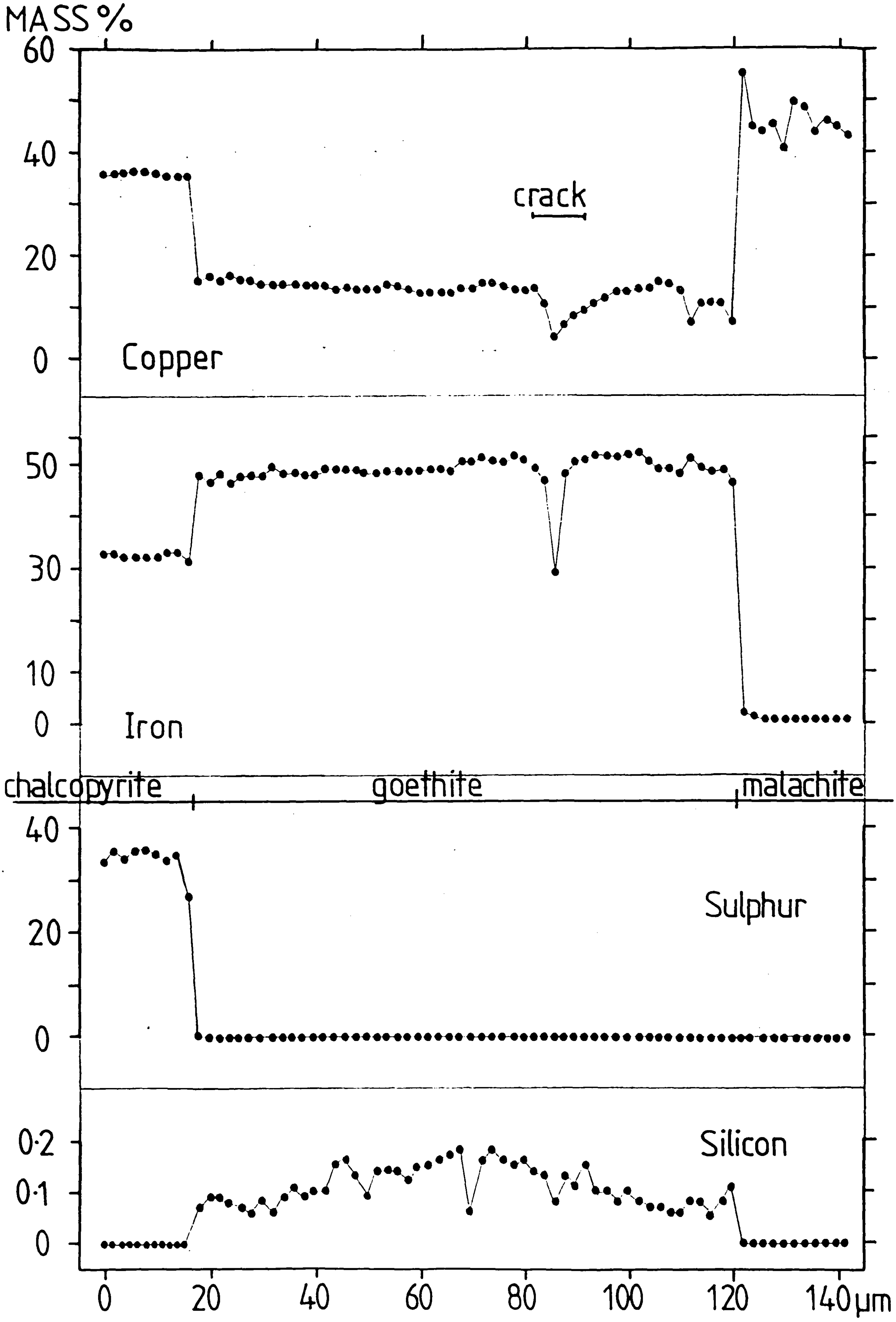

Figure 7.2 BSE image of an altered chalcopyrite grain

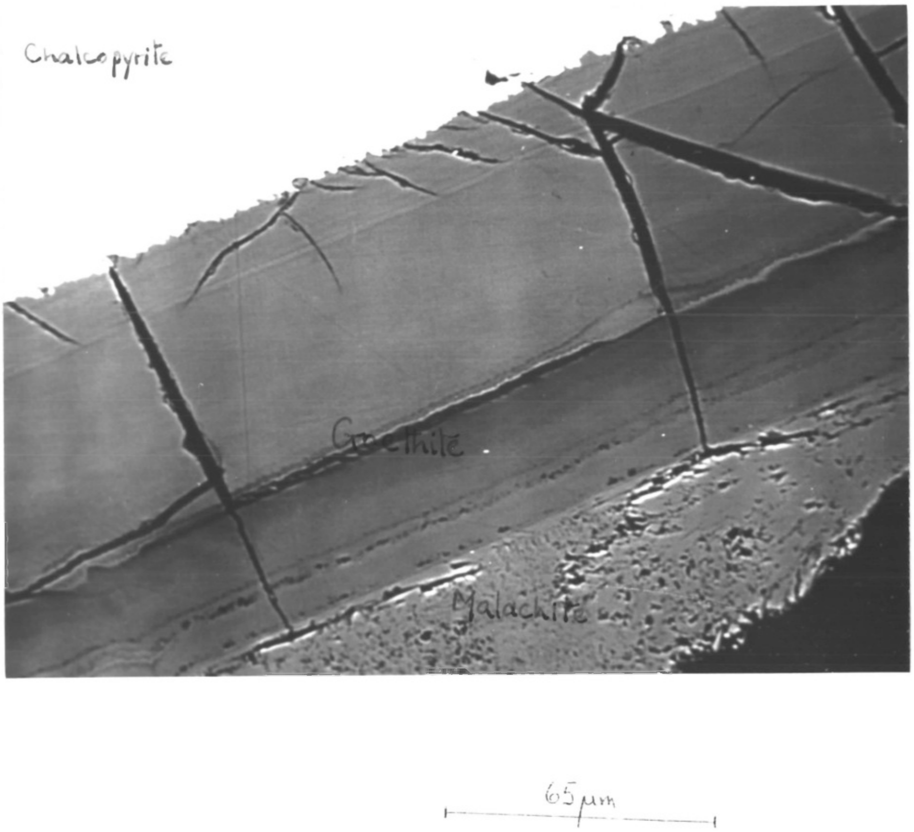
Chalcopyrite
Goethite
Malachite
65 µm

very rapidly. This goethite zone was seen to contain a large amount of copper. The slow outward diffusion of copper away from the chalcopyrite reaction interface was expected - the goethite provides favourable sites for the copper ions (section 3.5.5). This slow loss of copper contrasts with the rapid loss observed under commercial leaching conditions (Figure 3.16). The goethite zone also contained approximately 0.15% silicon. This was not unexpected since goethite has a tendency to 'absorb' silicon. The efflorescent malachite contained little extraneous material, except for traces of calcium.

Chalcopyrite from other dumps on Ecton Hill showed the same pattern of alteration as that described above, except that up to 15% silicon was contained within the goethitic product zones. This difference in silicon contents probably reflects the differing aqueous silicon contents available in the various dumps.

7.2.3 Pyrite

Optical examination (section 4.3) showed that pyrite altered to goethite in accordance with the chemical principles presented in section 3.5.4. Figure 7.3 shows a typical altered pyrite grain enclosed in baryte. Analyses of the pyrite-goethite interfaces showed sharp contacts similar to those seen in Figure 7.1 between chalcopyrite and goethite. Pyrite-derived goethite, however, in general had a higher silicon content than the chalcopyrite-derived goethite. This suggests that the malachite at the surface of chalcopyrite grains limits the transfer of silicon from bulk solution to the goethite.

7.3 Summary

The alteration of chalcopyrite, pyrite, and sphalerite under mildly alkaline, bicarbonate conditions results in the formation of goethite, malachite, and smithsonite. These alterations were predicted from chemical principles. The alteration of sphalerite was seen to be complete, so that no interfacial studies could be carried out. The alteration of both chalcopyrite and pyrite to goethite occurs at a very sharp (less than 2 μm wide) interface.

Figure 7.3 BSE and characteristic X-ray density images of an altered pyrite grain in baryte

BSE

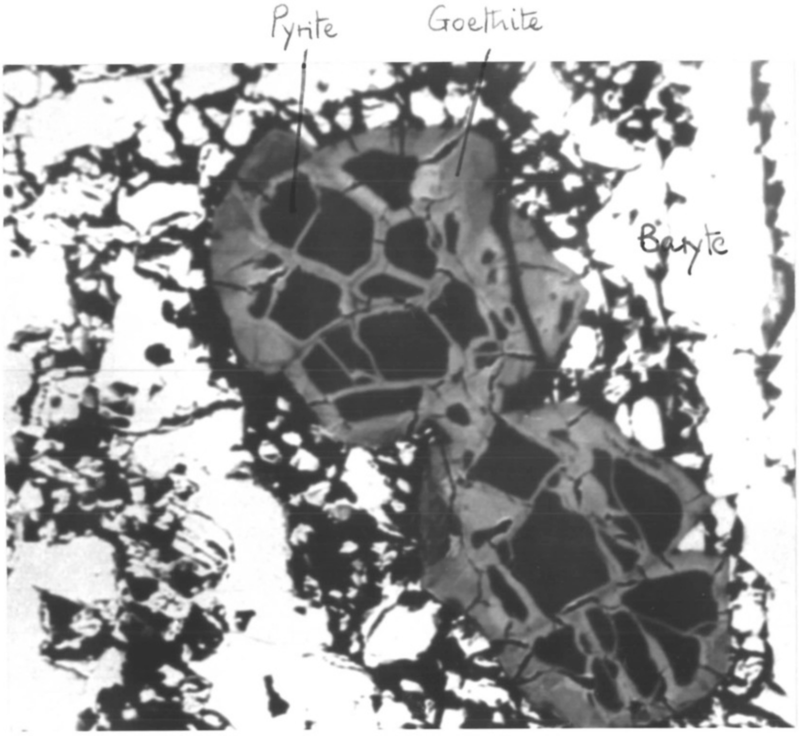
Pyrite
Goethite
Baryte

Fe

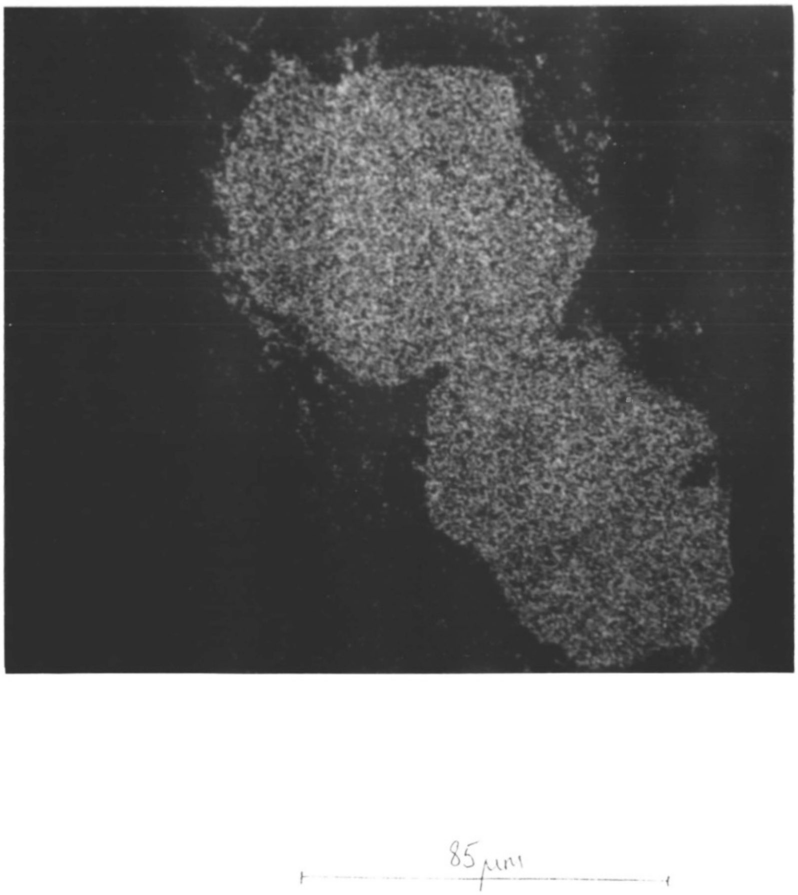

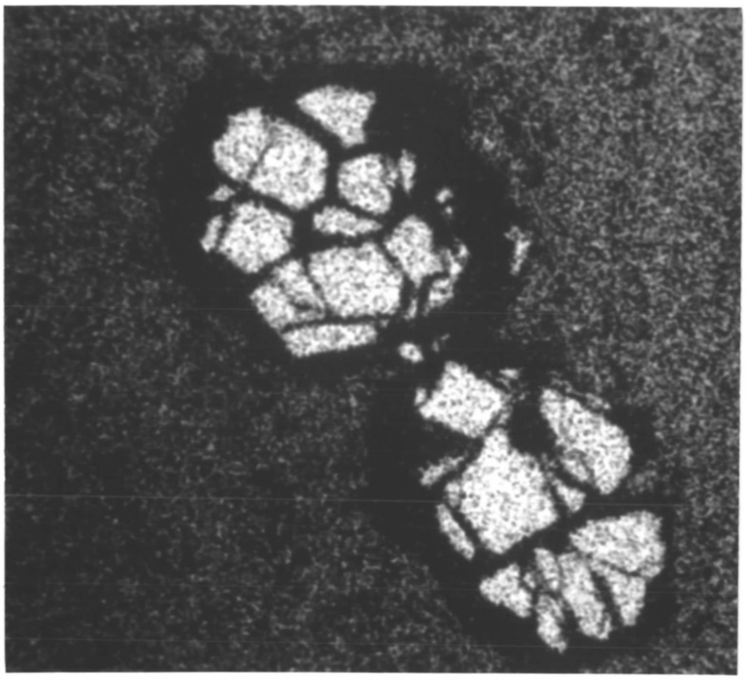

S

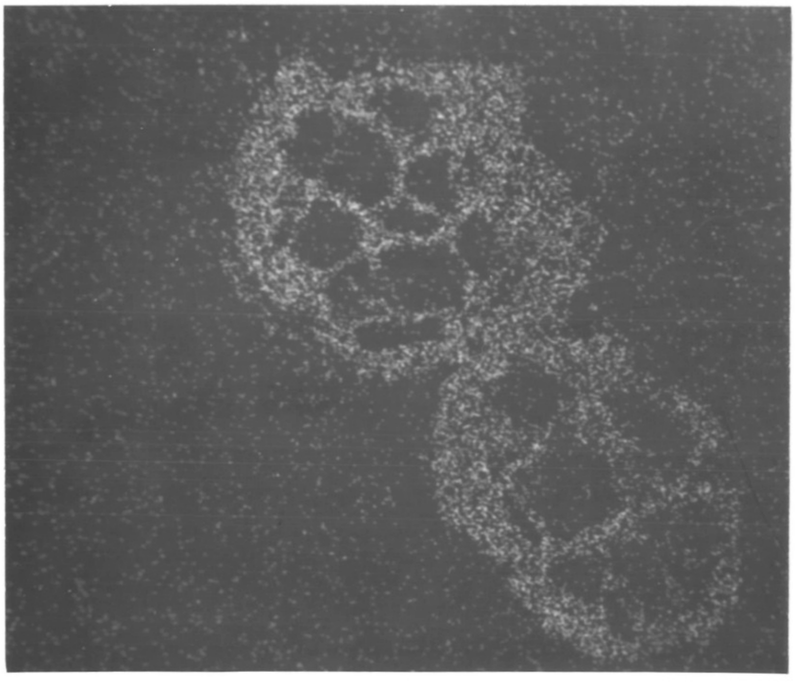

Si

85 μm

CHAPTER EIGHT

Conclusions

The Dutchman mine dump originally contained galena, chalcopyrite, and sphalerite, together with baryte and fluorite, in a limestone matrix. Some 300 years after its formation, all the sphalerite has altered to smithsonite, the chalcopyrite has partly altered to goethite plus malachite, and the galena has partly altered to cerussite. These changes produce the mineral assemblage that is expected in such an environment; the relative rates of alteration were also expected.

The alteration of galena to cerussite proceeds concentrically inward from the original surfaces, consequently the proportion of alteration increases with decreasing particle size. This proportion can be measured by electron probe linear image analysis: optical image analysis was found to be unsuitable for this work because of the difficulty of discriminating the cerussite from similar minerals in the absence of contiguous grains of galena. Linear ratios of cerussite:galena (and, therefore, the volumetric ratios) matched the value~~d~~s deduced from chemical analyses. The linear ratios did, however, underestimate the degree of alteration. The galena-cerussite linear grade distributions did not fit those obtained from the ideal concentric cubes model because the particles showed a range of shapes and varying amounts of alteration.

An interfacial zone, 10 μm wide, always exists between the galena and the cerussite. This zone contains variable, but major, amounts of lead, sulphur, and oxygen, with minor amounts of carbon and calcium, and trace amounts of iron, copper, and zinc. This zone is not normally visible using optical methods. A textural variation within the interfacial zone was revealed by SEM. This corresponds with chemical variations determined by microprobe.

A new model of the alteration of galena to cerussite has been developed to explain the chemical and the structural features of the interfacial region. The oxidation of galena proceeds initially to the formation of a basic lead thiosulphate. The thiosulphate dissolves and releases lead and thiosulphate species. The lead precipitates as lead carbonate on encountering bicarbonate ions, and the thiosulphate diffuses into the bulk solution. The presence of an intermediate zone shows that the rate of formation of the basic lead thiosulphate is greater than the overall rate of formation of the carbonate. The constant width of the intermediate zone (about 10 µm) is either a function of the available time for the alteration, or it is an 'equilibrium' width which is initially established and then advances 'en masse' into the galena grain. The rate of advancement of the oxidation front into the galena was an order of magnitude lower than that measured in systems where the surface oxidation product was not allowed to accumulate. Therefore, it appears that the surface oxidation product exerts some control over the oxidation rate - probably over the transfer of oxygen from bulk solution to the reaction interface.

The presence of the sulphur-bearing intermediate region between the galena and the cerussite was the reason that the linear analyses underestimated the degree of alteration determined from chemical analyses, since the phase discrimination capabilities of the system was based on the presence or the absence of sulphur.

The alteration of chalcopyrite to produce goethite and malachite occurs over a distance of less than 2 µm, and no intermediate phases were detected.

The silver contents of the galena samples from the Dutchman dump were so small that they did not allow the silver distribution to be established. Similarly, no consistent individual oxygen and carbon determinations could be made across the interface because of machine limitations. Future work on the alteration zone between galena and cerussite should include studies of the distribution of the trace elements (e.g. silver), found in the galena.

References

Abdul-Samad, F et al, Mode of formation of some rare copper(II) and lead(II) minerals from aqueous solution, with particular reference to deposits at Tiger, Arizona. Transition Met. Chem. 7, 1982, 32-7

Anderson, A L, The incipient oxidation of galena. Econ. Geol. 25, 1930, 582-42

Anderson, J E et al, Kinetics of oxidation of galena in NaOH solutions under oxygen pressure. Trans. Amer. Inst. Min. Engrs. 197, 1953, 554-8

Artiola, J and Fuller, W H, Limestone liner for landfill leachates containing beryllium, cadmium, iron, nickel and zinc. Soil Sci. 129, 1980, 167-79

Bateman, A M, Economic mineral deposits, 2nd edition (London; John Wiley and Sons, 1965)

Bauer, J P et al, Initial stage sulphuric acid leaching kinetics of chalcopyrite using radiochemical techniques. Metall. Soc, Amer. Inst. Min. Engrs, Pamphlet 72-8-96, 1972

Bertenshaw, M P, Temporal and spatial controls on the geochemistry of groundwaters in the south eastern part of the Derbyshire Dome. Ph.D thesis, University of Nottingham, 1979

Blain, C F and Andrew, R L, Sulphide weathering and the evaluation of gossans in mineral exploration. Mineral Sci. Engng. 9, 1977, 119-50

Blanchard, R and Boswell, P F, Notes on the oxidation products derived from chalcopyrite. Econ. Geol. 20, 1925, 613-38

Blanchard, R and Boswell, P F, Additional limonite types of galena and sphalerite derivation. Econ. Geol. 29, 1934, 671-90

Bloem, J and Kruger, F A, The p-T-x phase diagram of the lead sulphur system. Z. Physik. Chem. 7, 1956, 1-14

Brown, J B, Jarosite-goethite stabilities at 25°C, 1 atm. Mineral Deposita 6, 1971, 245-52

Burkin, A R, The chemistry of hydrometallurgical processes (London; Spon Ltd, 1966)

Burken, A R et al, Adsorption and reaction of xanthates at galena-liquid interfaces. Proc. 7th Intern. Mineral Proc. Congr, New York, 1964, Part 7, 337-45

Collins, B I, The concentration control of soluble copper in a mine tailings stream. Geochim. Cosmochim. Acta, 37, 1973, 69-75

Cotton, F A and Wilkinson, G, Advanced inorganic chemistry (London; Interscience, 1962)

Cox, G, Private communication, 1981

Dave, S R et al, Bio-oxidation studies with Thiobacillus ferroxidans in the presence of copper and zinc. Trans. Instn. Min. Metall. 88, 1977, C234-7

De Grys, A, Seasonal variations in copper content in some Andean streams of Central Chile. Econ. Geol. 57, 1962, 1031-44

Derbyshire Records Office, Item 158M/E43

Dreybrodt, W, Deposition of calcite from thin films of natural calcareous solutions and the growth of speleothems. Chem. Geol. 29, 1980, 89-105

Eadington, P, The oxidation of lead sulphide in aqueous suspension. Ph.D thesis, Univ. of London, 1966

Eadington, P, Leaching of illuminated lead sulphide with nitric as a function of the solid-state electronic properties. Trans. Instn. Min. Metall. 82, 1973, C158-61

Eadington, P, Study of oxidation layers on surfaces of chalcopyrite by use of Auger electron spectroscopy. Trans. Instn. Min. Metall. 86, 1977, C186-9

Eadington, P and Prosser, A P, Contribution to discussion. Trans. Instn. Min. Metall. 74, 1965, 398-480

Eadington, P and Prosser, A P, Oxidation of lead sulphide in aqueous suspensions. Trans. Instn. Min. Metall. 78, 1969, C74-82

Fisher, C and Cole, M, The Metals Research image analysing computer. Microscope 16, 1968, 81-94

Flett, D S et al, Chemical study of thiosulphate leaching of silver sulphide. Trans. Instn. Min. Metall. 92, 1984, C216-22

Forbes, C L, private communication, 1982

Ford, T D (ed), Limestones and caves of the Peak District (Norwich; GeoAbstracts Ltd, 1977)

Ford, T D and King, R J, Layered epigenetic galena-barite deposits in the Golconda Mine, Brassington, Derbyshire, England. Econ. Geol. 60, 1965, 1686-1701

Forward, F A et al, Unpublished work referred to Eadington (1966)

Forward, F A and Peters, E, Advances in hydrometallurgical research. Proc. 8th Comm. Min. Metall. Congr, Melbourne, 1965, 6, 631-42. J T Woodcock et al (eds) (Melbourne; Aust. IMM, 1969)

Freund, H (ed), Applied ore microscopy, theory and technique (London; Macmillan, 1966)

Gardner, J R and Woods, R, A study of the surface oxidation of galena using cyclic voltammetry. J. Electroanal. Chem. 100, 1979, 447-60

Garrels, R M, Mineral species as functions of pH and oxidation-reduction potentials, with special reference to the zone of oxidation and secondary enrichment. Geochim. Cosmochim. Acta 5, 1954, 153-68

Garrels, R M and Christ, C L, Solutions, minerals, and equilibria (New York; Harper and Row, 1965)

Giblin, A M, Experiments to demonstrate mobility of metals in waters near base-metal sulphides. Chem. Geol. 23, 1978, 215-23

Goleva, G A et al, Distribution and migration of lead in groundwaters. Geochem. Int., 7, 1970, 256-68

Gorlich, E and Gorlich, Z, Adsorption series of some cations on pure calcium carbonate and on natural limestone and dolomite. Chem. Abst. 59:7717b, 1958

Govett, G J S et al, Experimental aqueous dispersion of elements around sulphides. Econ. Geol. 71, 1976, 925-40

Greenler, R G, An infra-red investigation of xanthate adsorption on lead sulphide. J. Phys. Chem. 60, 1962, 879-83

Griffin, R A and Shimp, N F, Attenuation of pollutants in municipal landfill leachate by clay minerals. US Envir. Prot. Agency Report EPA-600/2-78-157 (MERL), 1978

Habashi, F, Chalcopyrite - its chemistry and metallurgy (New York; McGraw Hill, 1978)

Hagihara, H, Surface oxidation of galena in relation to its flotation as revealed by electron diffraction. J. Phys. Chem. 56, 1952, 610-15

Haskett, P R et al, Hydrometallurgical process for copper recovery from sulphide ores. US Patent Applic. 559, 942 (1975). Chem. Abst. 84, 63143d

Hem, J D, Chemistry and occurrence of cadmium and zinc in surface water and groundwater. Water Resour. Res. 8, 1972, 661-79

Hiskey, J B and Wadsworth, M E, Galvanic conversion of chalcopyrite. Metall. Trans. 6B, 1975, 183-90

Horton, R, Determination of the volumetric composition of idealised mineral particles by random intercepts. Ph.D thesis, Univ. of London, 1978

Horton, R, private communication, 1983

Ichikuni, M, Sur la Dissolution des Minerais Sulfurés en Divers Milieux. II Dissolution de la Pyrite et de la Chalcopyrite. Bull. Chem. Soc. Japan 33, 1960, 1052-7

Ineson, P R and Al-Kufaishi, F A M, The mineralogy and paragenetic sequence of Long Rake Vein at Raper Mine, Derbyshire. Mercian Geol. 3, 1970, 337-51

James, R O and MacNaughton, M G, The adsorption of aqueous heavy metals on inorganic materials. Geochim. Cosmochim. Acta 41, 1977, 1549-55

Jellinek, F, Sulfides. In: G. Nickless (ed) Inorganic sulfur chemistry. (Amsterdam; Elsevier, 1968)

Jenne, E A, Controls on Mn, Fe, Co, Ni, Cu and Zn concentrations in soils and water: The significant role of hydrous Mn and Fe oxides. In: R A Baker (ed), Trace inorganics in water, Adv. Chem. Ser. No. 73

Jones, M P, Designing an X-ray image analyser for measuring mineralogical data. Proc. 14th Intern. Mineral Proc. Congr., Toronto, 1982 (in press)

Jones, M P, Application of electron probe microanalysis in the mineral industry. In: Sampling and analysis for the minerals industry (London; IMM, 1982)

Jones, M P and Gavrilovic, J, Automatic quantitative mineralogy in mineral technology. Rudy, 5, 1970, 189-97

Kirkham, N and Ford, T D, The Ecton copper mines. Peak Dist. Mines Hist. Soc, Sp. Pub. 1, 2nd ed, 1967

Kolthoff, I M and Belcher, R, Volumetric Analysis 3. (New York; Interscience, 1957)

Krauskopf, K B, Factors controlling the concentration of 13 rare metals in sea water. Geochim. Cosmochim. Acta 9, 1956, 1-32

Leja, J, Surface chemistry of froth flotation (New York; Plenum Press, 1982)

Leja, J et al, Xanthate adsorption studies using infra-red spectroscopy. Trans. Instn. Min. Metall. 72, 1963, 407-23

Long, J V, Electron probe microanalysis. In: J. Zussman (ed), Physical methods in determinative mineralogy, 2nd edition (London; Academic Press, 1978)

Majima, H, How oxidation affects selective flotation of complex sulphide ores. Can. Metall. Quart. 8, 1969, 269-73

Mallio, W J et al, Parameters and petrographic interpretation of in situ copper leaching. In: D M Hausen (ed) Process Mineralogy (New York; AIME, 1981)

Mann, A W and Deutscher, R L, Solution geochemistry of copper in water containing carbonate, sulphate, and chloride ions. Chem. Geol. 19, 1977, 253-65

Mann, A W and Deutscher, R L, Hydrogeochemistry of a calcrete-containing aquifer near Lake Way, Western Australia. J. Hydrol. 38, 1978, 357-77

Mann, A W and Deutscher, R L, Solution geochemistry of lead and zinc in water containing carbonate, sulphate, and chloride ions. Chem. Geol. 29, 1980, 293-311

Mason, B and Berry, L G, Elements of mineralogy (San Fransisco; W H Freeman and Co, 1968)

Maust, E E Jr et al, A conceptual model for the role of oxygen in xanthate adsorption on galena. US Bureau of Mines, Report 8143, Washington, 1976

Mitrofanov, S I and Buzanova, N M, Adsorption of cupric ion by sphalerite. Mine Quarry Engng. 25, 1959, 225-6

Moore, S W, private communication, 1983

Nickel, E H, The mineralogy and geochemistry of the Whim Creek Gossan. Proc. Aust. Inst. Min. Metall, No 282, 1982, 33-45

Orgel, L E, An introduction to Transition Metal Chemistry Ligand - Field Theory (London; John Wiley and Sons, 1966)

Park, C F and Macdiarmid, R A, Ore deposits, 3rd edition (San Fransisco; W H Freeman and Co, 1975)

Pauling, L, Crystallography and chemical bonding of sulfide minerals. Mineral Soc. Amer., Sp. Paper 3, 1970, 125-31

Pawlek, F E, Research in pressure leaching. J. S. Afr. Inst. Min. Metall. 69, 1969, 632-54

Pearse, M J, Chemical study of oxidation of sulphide concentrates. Trans. Instn. Min. Metall. 89, 1980, C26-36

Peters, E, Direct leaching of sulphides: chemistry and applications. Metall. Trans. 7B, 1976, 505-17

Plante, E C and Sutherland, K L, Effects of oxidation of sulphide minerals on their flotation properties. Trans. Amer. Inst. Min. Engrs. 183, 1949, 160-88

Plot, R, Natural history of Staffordshire, 1686

Posnjak, E and Merwin, H E, The hydrated ferric oxides. Amer. J. Sci. 47, 1919, 311-17

Posnjak, E and Merwin, H E, The system Fe_2O_3-SO_3-H_2O. J. Amer. Chem. Soc. 44, 1922, 1965-71

Prater, J D et al, The sulphation of copper-iron sulphides with concentrated sulphuric acid. J. Metals 22, no. 12, 1970, 23-7

Prosser, A P, private communication, 1981

Reuter, B and Stein, R, Die oxydation von Bleisulfid bei niederen temperaturen. Z. Elektrochem. 61, 1957, 440-54

Richardson, P E and Maust, E E Jr, Surface stoichiometry of galena in aqueous electrolytes and its effect on xanthate interactions. In: M C Fuerstenau (ed) Flotation - A M Gaudin Memorial Volume (New York; AIME, 1976)

Rickard, D T, The chemistry of copper in natural aqueous solutions. Stockholm Contrib. Geol. 23, 1971, 1-64

Riley, G A, Limnological studies in Connecticut. I. General limnological survey. II. The copper cycle. Ecol. Monogr. 9, 1939, 66-94

Robey, J A and Porter, L, The copper and lead mines of Ecton Hill, Staffordshire (Buxton; Moorland Pub. Co., 1972)

Roman, R J and Benner, B R, The dissolution of copper concentrates. Minerals Sci. Engng. 5, 1973, 3-24

Sarjeant, W A S, The mineralogy of Ecton Hill. J. Univ. Sheffield Geol. Soc. 2, No. 3, 1956, 87-92

Sato, M, Half-cell potentials of semiconductive simple binary sulphides in aqueous solution. Electrochim. Acta, 11, 1966, 361-73

Scott, T R and Dyson, N F, The catalyzed oxidation of zinc sulphide under acid pressure leaching conditions. Trans. Amer. Inst. Min. Engrs. 242, 1968, 1815-21

Seraphim, P S and Samis, C S, Kinetics of the oxidation of galena in ammonium acetate solutions under oxygen pressure. Trans. Amer. Inst. Min. Engrs, 206, 1950, 1096-99

Shuey, R T, Semiconducting ore minerals. Developments in Economic Geology No. 4 (Amsterdam; Elsevier, 1975)

Sillen, L G, Stability constants of metal-ion complexes (London; The Chem. Soc, 1964)

Sohn, H Y and Wadsworth, M E (eds), Rate processes of extractive metallurgy (London; Plenum Press, 1979)

Steger, H F, Oxidation of sulphide minerals. II. Determination of metal in the oxidation products of galena, sphalerite and chalcocite. Talanta 24, 1977, 268-70

Steger, H F and Desjardins, L E, Oxidation of sulfide minerals. IV. Pyrite, chalcopyrite, and pyrrhotite. Chem. Geol. 23, 1978, 225-37

Steger, H F and Desjardins, L E, Oxidation of sulfide minerals. V. Galena, sphalerite, and chalcocite. Can. Mineral. 18, 1980, 365-72

Takahashi, T, Supergene alteration of zinc and lead deposits in limestone. Econ. Geol. 55, 1083-115

Taylor, et al, Action of alkali xanthates on galena. Trans. Amer. Inst. Min. Engrs. 112, 1934, 382-97

Thornber, M R and Wildman, J E, Supergene alteration of sulphides. IV. Laboratory study of the weathering of nickel ores. Chem. Geol. 24, 1979, 97-110

Toperi, D and Tolun, R, Electrochemical study and thermodynamic equilibria of the galena-oxygen-xanthate flotation system. Trans. Instn. Min. Metall. 78, 1969, C191-7

Vaughan, D J and Craig, J R, Mineral chemistry of metal sulfides (Cambridge; Camb. Univ. Press, 1978)

Vizsolyi, A et al, Aqueous oxidation of galena under pressure in ammonia solutions. Proc. Amer. Inst. Min. Engrs. Intern. Symp. on Unit Processes in Hydrometall, Dallas, 1963, 24-28

Vizsolyi, A et al, Copper and elemental sulfur from chalcopyrite by pressure leaching. J. Metals 19, 1967, 52-9

Vukotic, S, Solubility of galena, sphalerite and chalcopyrite in water and in the presence of H_2S. Bull. Bur. Rech. Geol. Minieres, No. 3, 1961, 11-27

Wadsworth, M E, Advances in the leaching of sulphide minerals. Minerals Sci. Engng. 4, 1972, 36-47

Walsh, J N, Whole rock analysis by inductively coupled plasma spectrometry. In: Sampling and analysis for the minerals industry. (London; IMM, 1982)

Wang, Y T, The formation of the oxidised ores of zinc from the sulphide. Trans. Amer. Inst. Min. Engrs. 52, 1915, 657-710

Warren, I H, The generation of sulphuric acid from pyrite by pressure leaching. Aust. J. Appl. Sci. 7, 1956, 346-58

Weast, R C (ed), Handbook of chemistry and physics, 61st edition (Boca Raton, Florida; CRC Press, 1981)

Woodcock, J T, Some aspects of the oxidation of sulphide minerals in aqueous suspension. Proc. Aust. Inst. Min. Metall. No 198, 1961, 47-84

Woodward, J, An attempt towards a Natural History of the fossils of England. (Second Additional English Native fossils), London, 1729

APPENDIX 1

Description of Woodward's (1729) Ecton samples

Specimen u.5 (A.30.25 of present arrangement)

> 'Blue Lead-Ore, very clean: but glossy, and appearing to be of difficult Fusion'.
> This is a large piece of cuboid galena which is slightly tarnished but not otherwise altered.

Specimen u.29 (B.1.14)

> 'Another Mass, compos'd of Lead-Ore, with spar, and a stoney Copper Ore, with veins of Marcasite'.
> This specimen shows slightly tarnished galena with baryte. The 'marcasite' has altered to a goethite material and the 'copper ore' has altered to malachite.

Specimen t.6 (A.24.36)

> 'A piece of Copper-Ore, appearing to be pretty good. 'Tis of a dusky Copper-Colour, with Veins of green and blue. 'Tis pretty thick set with small Caverns, cross'd by Fibres of a talky spar, of a bright green Colour. To one Side of it adheres a Mass of blue Lead-Ore.'
> The 'copper ore' has altered to a vitreous, goethitic material covered by layered malachite. Some azurite staining is visible. The galena is slightly tarnished.

Specimen u.28 (A.30.33)

> 'A mass of Lead Ore. 'Tis compos'd partly of blue Lead Ore, and partly of Copper Ore. The latter appears in some parts, like the piped Waxen-Vein, and is yellow and shining: in others 'tis vein'd with green, and with a Blue, very bright, and not inferior to that of the Lapis Lazuli. On one part is a Mass of a pale brown Spar, somewhat like Lapis Calaminaris: and, in Texture, cavernous, fibrous, and much resembling some Sea-Coralline Masses. There seems to be Calamine upon it; and that too very good, and fine.'
> This specimen shows tarnished, unaltered galena with a goethite-malachite mass which was the Teredo-like 'piped waxen vein'. There is abundant azurite staining and some smithsonite.

APPENDIX 2

Climatic data

The daily weather reports of the Buxton meteorological station (the nearest, topographically similar station to Ecton) for the period 1908 to 1958 were examined at the National Meteorological Archive, Bracknell. The mean daily temperature for this period was calculated as being 9°C and precipitation averaged 1.24 m^3/m^2 land/year; the distributions of temperature and rainfall are shown in Figures A.2.1 and A.2.2. Ford (1977) gives a figure for 'effective' precipitation, i.e. that volume available for infiltration, of 0.75 m^3/m^2 land/year for the area. Freeze/thaw weathering was especially evident on the dump during February 1982. No other form of physical weathering appears to have had much effect on the dump surface.

No rainfall samples were analysed but those analysed by Bertenshaw (1979) in the area gave the results shown in Table A2.1. These analyses show that the precipitation is of a fairly neutral character and should have no unusual effects on the dump.

Table A2.1 Chemical analyses of rainfall from the Ecton area (from Bertenshaw (1979))

		Concentration (ppm)	
Species	Mean	Max	Min
F	0.15	0.27	0.07
Cl	5	15	3
SO_4	12	21	7
HPO_4	0.38	1.0	0.06
NO_3	1.6	2.3	1.0
Ca	2.3	3.8	1.8
Mg	0.44	1.2	0.24
Sr	0	0.02	0
Zn	0.06	0.09	0.04
K	0.48	0.8	0.25
Na	2.3	8.0	0.85
pH	5.6	6.7	4.2

(7 samples)

Figure A.2.1 Mean monthly rainfall at Buxton, 1908-58

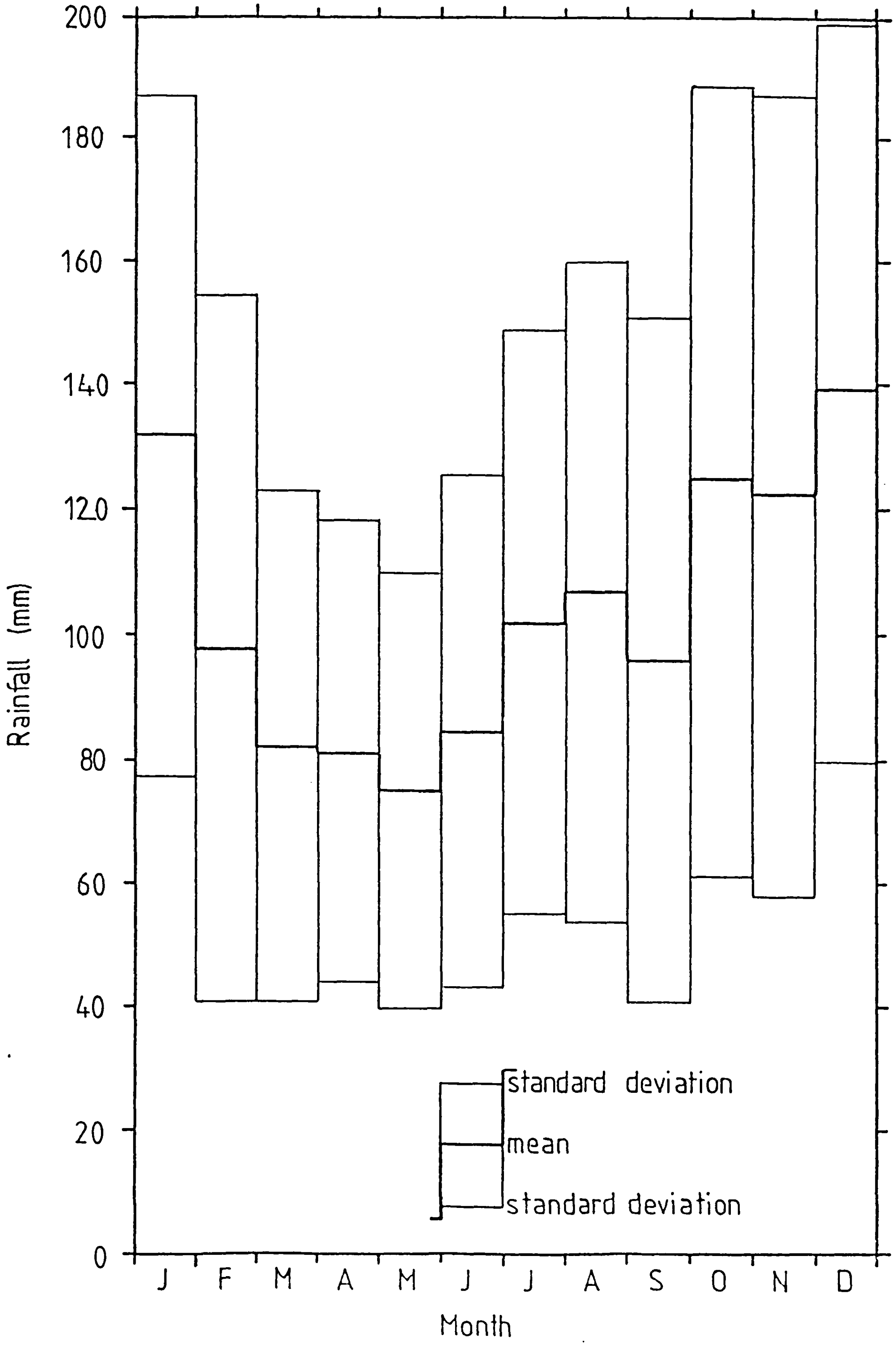

Figure A.2.2 Mean monthly daytime temperature at Buxton, 1908-58

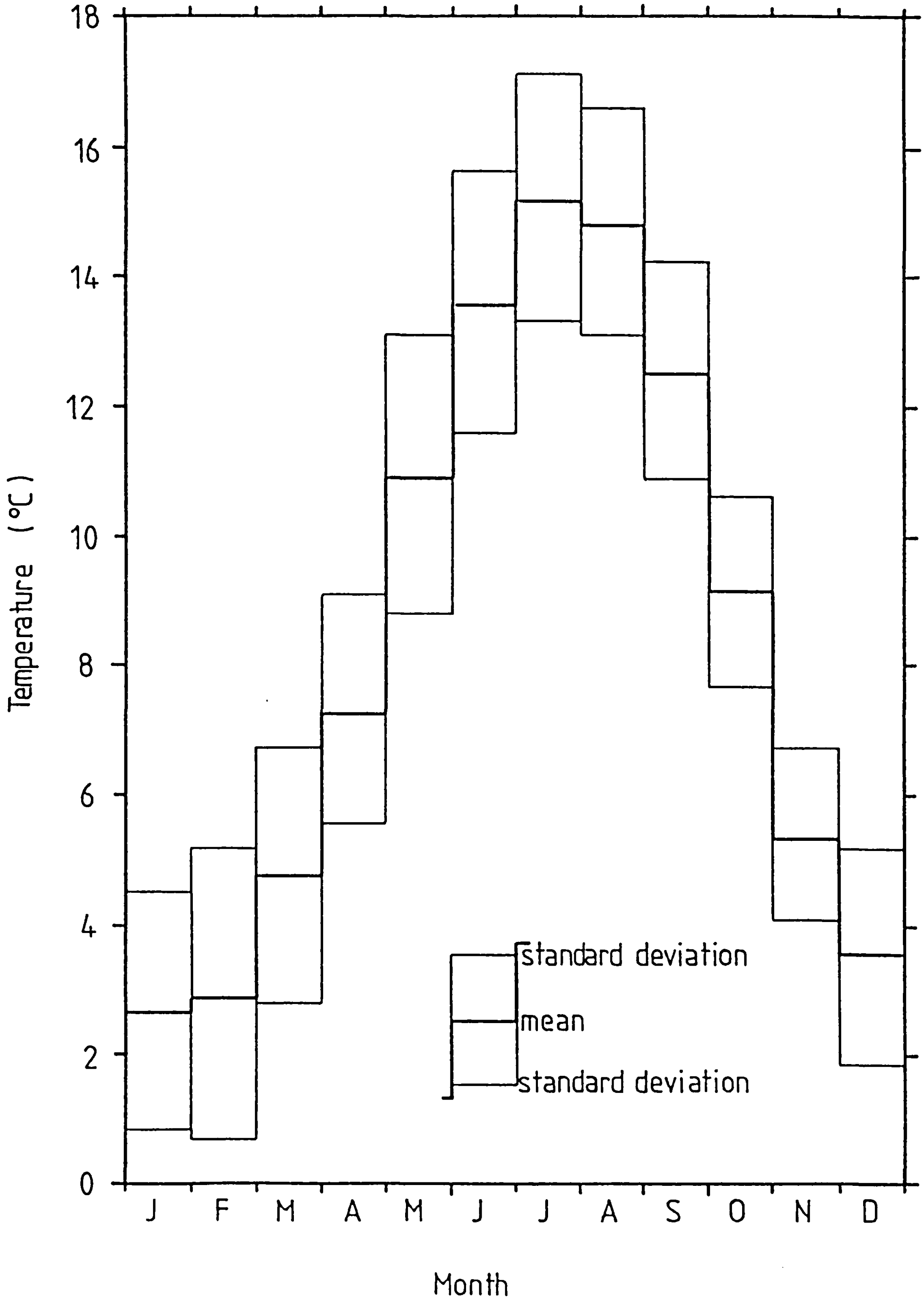

APPENDIX 3

Size distributions of the Dutchman dump samples

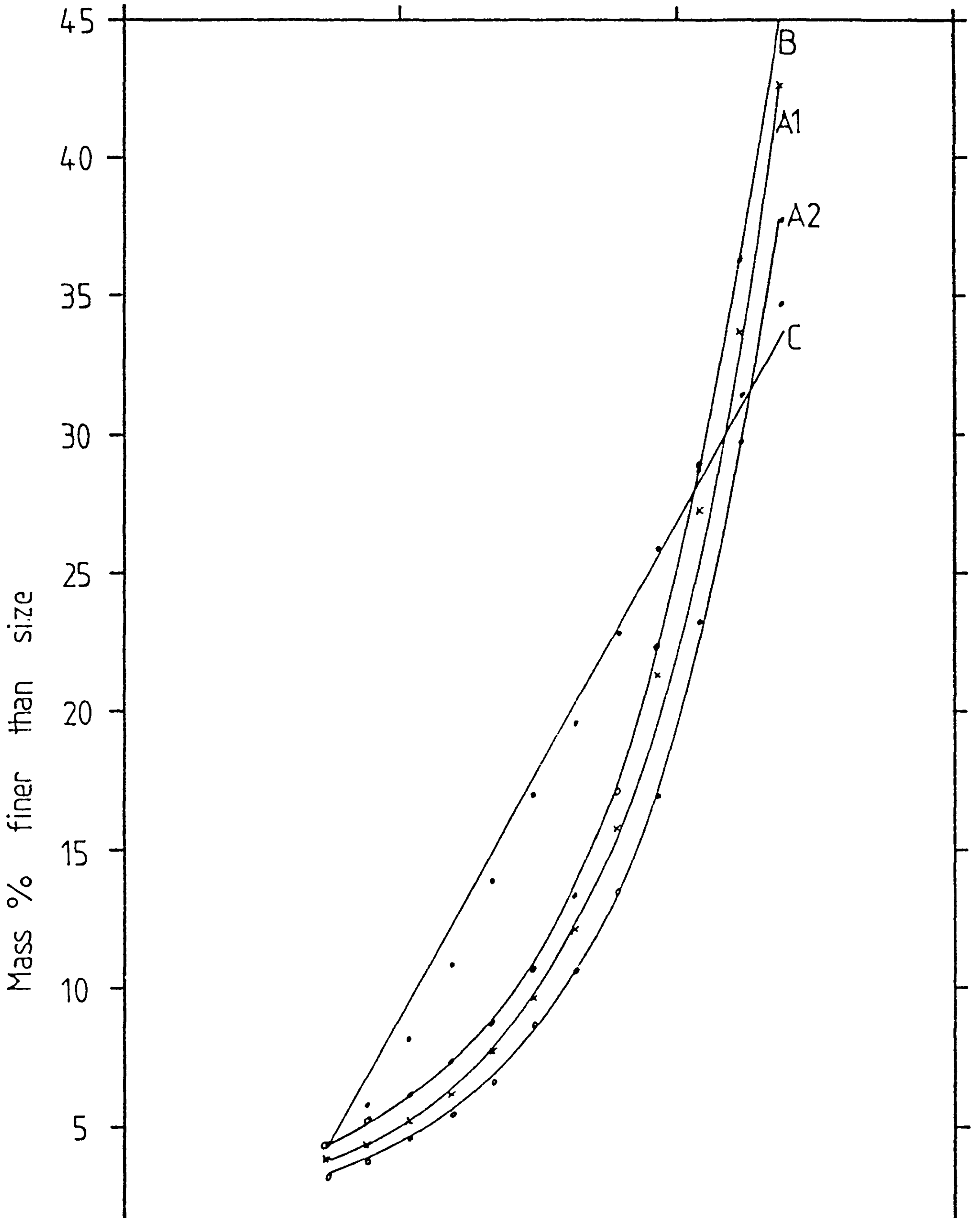

APPENDIX 4

Summary of size and chemical data for the Dutchman dump samples

Table A.4.a Sample A1

		Mass % metal in size fraction						Mass % soluble in	
Size (μm)	Mass %	Cu	Pb	Zn	Fe	Ca	Mg	HCl(dil)	HNO_3(conc)
-2300+1700	20.9	0.05	1.10	1.72	0.95	13.9	7.8	57	87
-1700+1180	15.0	0.09	0.96	2.28	0.88	13.7	8.6	72	83
-1180+ 850	14.1	0.08	1.31	2.17	0.88	13.6	7.7	78	85
-850+ 600	12.8	0.09	0.71	2.12	1.00	14.5	4.8	76	85
-600+ 420	8.7	0.08	0.76	2.12	1.10	15.2	7.8	68	85
-420+ 300	5.9	0.08	0.93	1.84	1.12	15.0	6.6	60	77
-300+ 210	4.4	0.08	1.03	1.99	1.08	12.2	7.7	60	77
-210+ 150	3.5	0.08	1.14	2.12	1.02	12.9	5.5	57	72
-150+ 104	2.4	0.10	1.27	1.81	1.22	10.4	4.6	60	73
-104+ 75	1.9	0.09	1.45	2.37	1.07	10.3	7.0	51	90
-75+ 53	1.5	0.11	2.13	2.66	1.39	10.6	7.1	62	74
-53	8.9	0.12	2.69	2.36	2.33	6.8	4.2	53	71

Analytical error: better than 3% relative

Water content of bulk sample: 3%
Mass % bulk sample finer than 2.3mm: 42.6%

HCl (dil) residue XRF analysis: > 5%: Ca, Ba
(Si ⟶ U) 5 - 0.5%: Si, S, Fe, Pb
0.5 - 0.05%: K, Zn, Sr
< 0.05%: Cl, Mn, Ni, Cu

XRD analysis: baryte and fluorite dominant

HNO_3(conc) residue XRF analysis: > 5%: Ba, S
(Si ⟶ U) 5 - 0.5%: Si
0.5 - 0.05%: Sr, K, Fe, Cl, Ca
< 0.05%: Zn, (Br)

XRD analysis: baryte dominant

Table A.4.b Sample A2

		Mass % metal in size fraction						Mass % soluble in	
Size (μm)	Mass %	Cu	Pb	Zn	Fe	Ca	Mg	HCl(dil)	HNO_3(conc)
-2300+1700	21.4	0.06	1.21	2.39	1.00	19.6	6.0	80	75
-1700+1180	17.2	0.06	1.73	2.52	1.03	18.5	6.0	74	79
-1180+ 850	16.8	0.06	1.43	2.21	1.08	22.9	5.7	67	74
-850+ 600	9.0	0.06	0.94	2.46	1.07	18.7	5.5	65	74
-600+ 420	7.7	0.06	1.19	2.47	1.21	18.4	5.0	67	70
-420+ 300	5.1	0.06	1.38	2.09	1.25	17.2	4.1	63	71
-300+ 210	5.5	0.08	1.71	2.27	1.39	14.7	3.9	59	77
-210+ 150	3.0	0.08	1.60	2.68	1.60	14.5	4.2	63	71
-150+ 104	2.7	0.09	4.41	3.27	1.65	13.0	3.5	59	68
-104+ 75	2.0	0.10	3.87	3.94	1.97	12.3	3.4	66	65
-75+ 53	1.5	0.12	6.35	4.71	2.05	12.0	3.1	63	64
-53	8.1	0.17	7.44	4.41	3.54	8.6	1.8	59	63

Analytical error: better than 3% relative

Water content of bulk sample: 5%

Mass bulk of bulk sample finer than 2.3mm: 37.7%

HCl (dil) residue XRF analysis: > 5%: Ca, Ba
(Si→U) 5 - 0.5%: Si, S, Fe, Pb
0.5 - 0.05%: Cl, K, Zn, Sr
< 0.05%: Mn, Ni, Cu

XRD analysis: baryte and fluorite dominant

HNO_3(conc) residue XRF analysis: > 5%: S, Ba
(Si→U) 5 - 0.5%: Si
0.5 - 0.05%: Sr, Fe, K
< 0.05%: Cl, Ca, Zn, (Br)

XRD analysis: baryte dominant

Table A.4.c Sample B

		Mass % metal in size fraction						Mass % soluble in	
Size (μm)	Mass %	Cu	Pb	Zn	Fe	Ca	Mg	HCl(dil)	HNO_3(conc)
-2300+1700	20.5	0.06	1.63	1.97	0.97	22.0	5.4	75	72
-1700+1180	16.3	0.08	1.23	1.68	0.95	21.2	5.8	75	79
-1180+ 850	14.4	0.09	1.89	1.93	1.03	26.8	7.7	70	74
-850+ 600	11.6	0.08	1.86	2.21	1.11	20.0	7.2	65	74
-600+ 420	8.0	0.09	2.21	2.03	1.22	17.3	6.4	62	70
-420+ 300	5.7	0.11	2.37	1.85	1.19	18.3	6.0	59	71
-300+ 210	4.5	0.11	2.56	1.80	1.34	19.3	6.0	60	77
-210+ 150	2.8	0.11	2.09	1.64	1.37	25.8	6.5	59	71
-150+ 104	2.7	0.10	2.72	1.57	1.32	17.1	6.0	54	68
-104+ 75	2.0	0.10	3.46	1.32	1.25	15.9	5.8	56	65
-75+ 53	2.0	0.10	5.23	1.23	1.44	18.7	6.2	58	64
-53	9.5	0.15	3.71	1.45	2.93	13.3	5.1	50	63

Analytical error: better than 3% relative

Water content of bulk sample: 6%
Mass % of bulk sample finer than 2.3mm: 45.6%

HCl(dil) residue XRF analysis: > 5%: Ca, Ba
(Si → U) 5 - 0.5%: Si, S, Fe, Pb
0.5 - 0.05%: K, Cu, Zn, Sr
< 0.05%: Cl, Mn, Ni

XRD analysis: baryte and fluorite dominant

HNO_3(conc) residue XRF analysis: > 5%: S, Ba, Si
(Si → U) 5 - 0.5%: -
0.5 - 0.05%: Sr, Cl, K, Fe
< 0.05%: Ca, Zn, (Br)

XRD analysis: baryte dominant

Table A.4.d Sample C

		Mass % metal in size fraction						Mass % soluble in	
Size (µm)	Mass %	Cu	Pb	Zn	Fe	Ca	Mg	HCl(dil)	HNO_3(conc)
-2300+1700	9.9	0.04	1.68	1.62	0.94	17.2	7.3	75	77
-1700+1180	7.6	0.06	2.58	1.55	1.25	16.4	6.4	67	72
-1180+ 850	8.1	0.05	2.04	1.26	1.32	17.9	6.9	69	74
-850+ 600	8.9	0.08	2.79	1.23	1.36	15.2	5.5	56	66
-600+ 420	9.4	0.07	3.35	1.15	1.12	15.7	5.4	53	66
-420+ 300	7.1	0.07	3.30	1.17	1.26	16.9	5.1	52	65
-300+ 210	9.0	0.06	3.70	1.08	1.37	15.4	4.7	50	68
-210+ 150	8.6	0.06	3.02	1.12	1.78	16.3	5.5	54	67
-150+ 104	8.0	0.06	4.11	1.08	1.77	14.2	4.8	50	63
-104+ 75	6.4	0.07	5.32	1.11	1.77	12.9	4.8	51	60
-75 + 53	4.5	0.07	8.27	1.41	1.84	9.8	5.0	52	61
-53	12.5	0.13	5.17	1.75	4.20	9.7	4.5	52	63

Analytical error: better than 3% relative

Water content of bulk sample: 7%
Mass % of bulk sample finer than 2.3mm: 34.7%

HCl (dil) residue XRF analysis: > 5%: Ca, Ba
(Si → U) 5 - 0.5%: Si, S, Fe, Pb
0.5 - 0.05%: K, Zn, Sr
< 0.05%: Cl, Mn, Ni, Cu

XRD analysis: baryte and fluorite dominant

HNO_3(conc) residue XRF analysis: > 5%: S, Ba
(Si → U) 5 - 0.5%: Si
0.5 - 0.05%: Sr, K, Fe, Cl
< 0.05%: Ca, Zn, (Br)

XRD analysis: baryte dominant

APPENDIX 5

A linear analysis results print-out

```
                  HIGH  SPEED  LINEAR  SCAN
                   X-RAY  DATA  REDUCTION


     ************************************
     *                                  *
     *                                  *
     *      SAMPLE  IDENTIFICATION      *
     *                                  *
     *                                  *
     *    JDS   ECTON   A2   -150+104 UM   *
     *                                  *
     *                                  *
     *  TIME 14:49:43     DATE 13-JAN-83  *
     *                                  *
     *                                  *
     ************************************



              TRAVERSE DETAILS AND COUNT TIME

                  POSITION Y-START =    2000.
                   POSITION Y-STOP =   17000.
                       Y-STEP (UM) =       2.
                  POSITION X-START =    2000.
                   POSITION X-STOP =   17000.
                       X-STEP (UM) =     150.
               LENGTH OF SCAN (UM) = 1500000.
                COUNTING TIME (MS) =      20.


                    SPECTROMETER SETTINGS


   SPECTROMETER                             ELEMENT  EMISSION THRESHOLD
 NUMBER   CRYSTAL      LAMBDA    POSITION    SYMBOL    LINE     LEVEL


    2       PET       5.28600    0.60405     /PB       MA1        20
    3       PET       5.37216    0.61419      S        KA1        20
    4       TAP      12.25400    0.47698      ZN       LA1        20
```

```
                  LINEAR  INTERCEPT  SIZE  DISTRIBUTIONS

                 PERCENT  LENGTH  OF  INTERCEPTS  WITHIN  SIZE  RANGE

   SIZE RANGE      1111          S           ZN          PB          PB S
    (MICRONS)
      <    2        0.28        4.42        0.63        2.68        1.20
      2-   4        0.15        5.94        1.65        3.07        1.44
      4-   6        0.10        6.89        1.85        2.99        2.16
      6-  10        0.11       13.49        2.90        4.68        1.20
     10-  16        0.10       17.76        6.11        7.36        3.36
     16-  25        0.07       17.80       10.42       12.96        9.83
     25-  40        0.11       19.62       17.22       10.51       15.11
     40-  63        0.17        8.99       19.07       17.10       24.46
     63- 100        0.41        4.56       24.19       34.51       28.78
    100- 160        0.66        0.53       14.68        4.14       12.47
    160- 250        1.31        0.00        1.29        0.00        0.00
    250- 400        3.41        0.00        0.00        0.00        0.00
    400- 630        6.37        0.00        0.00        0.00        0.00
    630-1000       10.57        0.00        0.00        0.00        0.00
   1000-1600       19.15        0.00        0.00        0.00        0.00
   1600-2500       17.74        0.00        0.00        0.00        0.00
   2500-4000       22.44        0.00        0.00        0.00        0.00
      > 4000       16.88        0.00        0.00        0.00        0.00

    SIGMA-N        4454        3756         533         143          30
    SIGMA-L     1442018.     39972.      14568.       2608.        834.
    MEAN -L         323.76       10.64       27.33       18.24       27.80


                              MODAL  ANALYSIS

 PHASE     NUMBER OF    TOTAL LENGTH    -------- PERCENT COMPOSITION -------
  NAME     INTERCEPTS   OF INTERCEPTS   NUMBER    LENGTH    NUMBER    LENGTH

 1111         4454        1442018.       49.96     96.13
 S            3756          39972.       42.13      2.66     84.18     68.94
 ZN            533          14568.        5.98      0.97     11.95     25.13
 PB            143           2608.        1.60      0.17      3.20      4.50
 PB S           30            834.        0.34      0.06      0.67      1.44

  TOTAL       8916        1500000.      100.00    100.00    100.00    100.00
```

```
                      LIBERATION ANALYSIS

            LINEAR INTERCEPT SIZE DISTRIBUTIONS OF
                "APPARENTLY" LIBERATED PARTICLES


          PERCENT LENGTH OF PARTICLES WITHIN SIZE RANGE

SIZE RANGE       S          ZN          PB
 (MICRONS)
  <    2        4.42        0.62        2.65
  2-   4        5.89        1.62        2.65
  4-   6        6.88        1.74        1.44
  6-  10       13.52        2.79        3.85
 10-  16       17.81        6.21        3.97
 16-  25       17.68       10.14       11.91
 25-  40       19.65       16.44        9.15
 40-  63        9.03       19.70       18.05
 63- 100        4.58       24.99       39.83
100- 160        0.53       14.42        6.50
160- 250        0.00        1.33        0.00
250- 400        0.00        0.00        0.00
400- 630        0.00        0.00        0.00
630-1000        0.00        0.00        0.00
  > 1000        0.00        0.00        0.00

 SIGMA-N      3731        509          79
 SIGMA-L     39766.     14104.       1662.
 MEAN -L        10.66       27.71       21.04


            LINEAR INTERCEPT SIZE DISTRIBUTIONS OF
                      COMPOSITE PARTICLES


          PERCENT LENGTH OF PARTICLES WITHIN SIZE RANGE

                 PB          PB          ZN          PB          S
SIZE RANGE       PB S        S           S           ZN          PB S
 (MICRONS)
  <    2        0.00        0.00        0.00        0.00        0.00
  2-   4        0.00        0.00        0.00        0.00        0.00
  4-   6        0.00        0.00        0.00        0.00        0.00
  6-  10        0.00       15.00        2.30        0.00        0.00
 10-  16        0.00       23.33        0.00        6.93        0.00
 16-  25        0.00       38.33        6.90        4.46        0.00
 25-  40        6.13       23.33       18.39        0.00        0.00
 40-  63       16.56        0.00       72.41       21.29      100.00
 63- 100       31.94        0.00        0.00       41.09        0.00
100- 160       45.37        0.00        0.00       26.24        0.00
160- 250        0.00        0.00        0.00        0.00        0.00
250- 400        0.00        0.00        0.00        0.00        0.00
400- 630        0.00        0.00        0.00        0.00        0.00
630-1000        0.00        0.00        0.00        0.00        0.00
  > 1000        0.00        0.00        0.00        0.00        0.00

 SIGMA-N        20           7           9           8           1
 SIGMA-L      1534.        120.        348.        404.         44.
 MEAN -L        76.70       17.14       38.67       50.50       44.00
```

DISTRIBUTION OF PHASES BY LENGTH IN THE COMPOSITES

```
                              COMPOSITE TYPE

         PB         PB         ZN         PB         S
PHASE    PB S       S          S          ZN         PB S       TOTAL

S          0.00      37.86      41.75       0.00      20.39     100.00
         ( 0.00)    (65.00)    (24.71)    ( 0.00)    (95.45)

ZN         0.00       0.00      56.47      43.53       0.00     100.00
         ( 0.00)    ( 0.00)    (75.29)    (50.00)    ( 0.00)

PB        74.21       4.44       0.00      21.35       0.00     100.00
         (45.76)    (35.00)    ( 0.00)    (50.00)    ( 0.00)

PB S      99.76       0.00       0.00       0.00       0.24     100.00
         (54.24)    ( 0.00)    ( 0.00)    ( 0.00)    ( 4.55)

(TOTAL) (100.00)   (100.00)   (100.00)   (100.00)   (100.00)
```

LINEAR GRADE ASSESSMENT

PHASE PB

INVARIANT RANDOM

		PERCENT NUMBER OF PARTICLES IN		PERCENT NUMBER OVER ALL PARTICLES
LINEAR GRADE	NUMBER OF PARTICLES	COMPOSITE FORM	ALL FORMS	
OTHERS	4250			97.39
0 - 10	3	8.57	2.63	0.07
10 - 20	8	22.86	7.02	0.18
20 - 30	2	5.71	1.75	0.05
30 - 40	3	8.57	2.63	0.07
40 - 50	3	8.57	2.63	0.07
50 - 60	4	11.43	3.51	0.09
60 - 70	2	5.71	1.75	0.05
70 - 80	2	5.71	1.75	0.05
80 - 90	4	11.43	3.51	0.09
90 -100	4	11.43	3.51	0.09
APP LIB	79		69.30	1.81
TOTAL	4364	100.00	100.00	100.00

LENGTH WEIGHTED RANDOM

		PERCENT LENGTH OF PARTICLES IN		PERCENT LENGTH OVER ALL PARTICLES	LENGTH OF PHASE WITHIN PARTICLES	PERCENT LENGTH OF PHASE IN ALL FORMS
LINEAR GRADE	LENGTH OF PARTICLES	COMPOSITE FORM	ALL FORMS			
OTHERS	54262.			93.58		
0 - 10	224.	10.88	6.02	0.39	12.	0.46
10 - 20	602.	29.25	16.18	1.04	94.	3.60
20 - 30	110.	5.34	2.96	0.19	24.	0.92
30 - 40	106.	5.15	2.85	0.18	38.	1.46
40 - 50	152.	7.39	4.09	0.26	64.	2.45
50 - 60	126.	6.12	3.39	0.22	68.	2.61
60 - 70	94.	4.57	2.53	0.16	64.	2.45
70 - 80	32.	1.55	0.86	0.06	24.	0.92
80 - 90	244.	11.86	6.56	0.42	210.	8.05
90 -100	368.	17.88	9.89	0.63	348.	13.34
APP LIB	1662.		44.68	2.87	1662.	63.73
TOTAL	57982.	100.00	100.00	100.00	2608.	100.00

LINEAR GRADE ASSESSMENT

PHASE PB S

INVARIANT RANDOM

LINEAR GRADE	NUMBER OF PARTICLES	PERCENT NUMBER OF PARTICLES IN		PERCENT NUMBER OVER ALL PARTICLES
		COMPOSITE FORM	ALL FORMS	
OTHERS	4343			99.52
0 - 10	4	19.05	19.05	0.09
10 - 20	3	14.29	14.29	0.07
20 - 30	0	0.00	0.00	0.00
30 - 40	2	9.52	9.52	0.05
40 - 50	2	9.52	9.52	0.05
50 - 60	1	4.76	4.76	0.02
60 - 70	2	9.52	9.52	0.05
70 - 80	1	4.76	4.76	0.02
80 - 90	5	23.81	23.81	0.11
90 -100	1	4.76	4.76	0.02
APP LIB	0		0.00	0.00
TOTAL	4364	100.00	100.00	100.00

LENGTH WEIGHTED RANDOM

LINEAR GRADE	LENGTH OF PARTICLES	PERCENT LENGTH OF PARTICLES IN		PERCENT LENGTH OVER ALL PARTICLES	LENGTH OF PHASE WITHIN PARTICLES	PERCENT LENGTH OF PHASE IN ALL FORMS
		COMPOSITE FORM	ALL FORMS			
OTHERS	56404.			97.28		
0 - 10	342.	21.67	21.67	0.59	20.	2.40
10 - 20	148.	9.38	9.38	0.26	24.	2.88
20 - 30	0.	0.00	0.00	0.00	0.	0.00
30 - 40	94.	5.96	5.96	0.16	30.	3.60
40 - 50	96.	6.08	6.08	0.17	44.	5.28
50 - 60	98.	6.21	6.21	0.17	58.	6.95
60 - 70	94.	5.96	5.96	0.16	60.	7.19
70 - 80	92.	5.83	5.83	0.16	72.	8.63
80 - 90	524.	33.21	33.21	0.90	444.	53.24
90 -100	90.	5.70	5.70	0.16	82.	9.83
APP LIB	0.		0.00	0.00	0.	0.00
TOTAL	57982.	100.00	100.00	100.00	834.	100.00

LINEAR GRADE ASSESSMENT

PHASE ZN

INVARIANT RANDOM

LINEAR GRADE	NUMBER OF PARTICLES	PERCENT NUMBER OF PARTICLES IN COMPOSITE FORM	PERCENT NUMBER OF PARTICLES IN ALL FORMS	PERCENT NUMBER OVER ALL PARTICLES
OTHERS	3838			87.95
0 - 10	1	5.88	0.19	0.02
10 - 20	2	11.76	0.38	0.05
20 - 30	1	5.88	0.19	0.02
30 - 40	0	0.00	0.00	0.00
40 - 50	0	0.00	0.00	0.00
50 - 60	1	5.88	0.19	0.02
60 - 70	1	5.88	0.19	0.02
70 - 80	3	17.65	0.57	0.07
80 - 90	5	29.41	0.95	0.11
90 -100	3	17.65	0.57	0.07
APP LIB	509		96.77	11.66
TOTAL	4364	100.00	100.00	100.00

LENGTH WEIGHTED RANDOM

LINEAR GRADE	LENGTH OF PARTICLES	PERCENT LENGTH OF PARTICLES IN COMPOSITE FORM	PERCENT LENGTH OF PARTICLES IN ALL FORMS	PERCENT LENGTH OVER ALL PARTICLES	LENGTH OF PHASE WITHIN PARTICLES	PERCENT LENGTH OF PHASE I ALL FORM
OTHERS	43126.			74.38		
0 - 10	70.	9.31	0.47	0.12	2.	0.01
10 - 20	132.	17.55	0.89	0.23	14.	0.10
20 - 30	16.	2.13	0.11	0.03	4.	0.03
30 - 40	0.	0.00	0.00	0.00	0.	0.00
40 - 50	0.	0.00	0.00	0.00	0.	0.00
50 - 60	44.	5.85	0.30	0.08	24.	0.16
60 - 70	42.	5.59	0.28	0.07	26.	0.18
70 - 80	88.	11.70	0.59	0.15	68.	0.47
80 - 90	170.	22.61	1.14	0.29	144.	0.99
90 -100	190.	25.27	1.28	0.33	182.	1.25
APP LIB	14104.		94.94	24.32	14104.	96.81
TOTAL	57982.	100.00	100.00	100.00	14568.	100.00

LINEAR GRADE ASSESSMENT

PHASE S

INVARIANT RANDOM

LINEAR GRADE	NUMBER OF PARTICLES	PERCENT NUMBER OF PARTICLES IN COMPOSITE FORM	PERCENT NUMBER OF PARTICLES IN ALL FORMS	PERCENT NUMBER OVER ALL PARTICLES
OTHERS	616			14.12
0 - 10	2	11.76	0.05	0.05
10 - 20	3	17.65	0.08	0.07
20 - 30	3	17.65	0.08	0.07
30 - 40	1	5.88	0.03	0.02
40 - 50	1	5.88	0.03	0.02
50 - 60	1	5.88	0.03	0.02
60 - 70	2	11.76	0.05	0.05
70 - 80	0	0.00	0.00	0.00
80 - 90	2	11.76	0.05	0.05
90 -100	2	11.76	0.05	0.05
APP LIB	3731		99.55	85.49
TOTAL	4364	100.00	100.00	100.00

LENGTH WEIGHTED RANDOM

LINEAR GRADE	LENGTH OF PARTICLES	PERCENT LENGTH OF PARTICLES IN COMPOSITE FORM	PERCENT LENGTH OF PARTICLES IN ALL FORMS	PERCENT LENGTH OVER ALL PARTICLES	LENGTH OF PHASE WITHIN PARTICLES	PERCENT LENGTH OF PHASE IN ALL FORMS
OTHERS	17704.			30.53		
0 - 10	84.	16.41	0.21	0.14	6.	0.02
10 - 20	116.	22.66	0.29	0.20	16.	0.04
20 - 30	86.	16.80	0.21	0.15	20.	0.05
30 - 40	42.	8.20	0.10	0.07	16.	0.04
40 - 50	22.	4.30	0.05	0.04	10.	0.03
50 - 60	8.	1.56	0.02	0.01	4.	0.01
60 - 70	22.	4.30	0.05	0.04	14.	0.04
70 - 80	0.	0.00	0.00	0.00	0.	0.00
80 - 90	60.	11.72	0.15	0.10	52.	0.13
90 -100	72.	14.06	0.18	0.12	68.	0.17
APP LIB	39766.		98.73	68.58	39766.	99.48
TOTAL	57982.	100.00	100.00	100.00	39972.	100.00

APPENDIX 6

Linear intercept data

Table A.6.1a Modal analyses
-150 + 104 µm +2.96 SG material

Sample	Phase	ΣL (µm) intercepts	No. of intercepts	% composition by length	
A1	Cerussite	12590	583	0.84	5.89
	Galena	4880	157	0.33	2.28
	Smithsonite	53608	1401	3.57	25.08
	Baryte	142694	14880	9.51	66.75
	(Matrix)	(1286228)	(16691)	(85.75)	-
	TOTAL	1500000	33712	100	100
A2	Cerussite	2608	143	0.17	4.50
	Galena	834	30	0.06	1.44
	Smithsonite	14568	533	0.97	25.13
	Baryte	39972	3756	2.66	68.94
	(Matrix)	(1442018)	(4454)	(96.13)	-
	TOTAL	1500000	8916	100	100
B	Cerussite	14704	633	0.98	7.09
	Galena	6128	159	0.41	2.95
	Smithsonite	27116	876	1.81	13.07
	Baryte	159158	12291	10.61	76.74
	(Matrix)	(1292606)	(13611)	(86.17)	-
	TOTAL	1500000	27570	100	100
C	Cerussite	37292	1665	2.49	11.52
	Galena	13228	435	0.88	4.09
	Smithsonite	17416	644	1.16	5.36
	Baryte	255802	28045	17.05	79.02
	(Matrix)	(1176262)	(29906)	(78.42)	-
	TOTAL	1500000	60695	100	100

Table A.6.1b Modal analyses
-104 + 75 μm +2.96 SG material

Sample	Phase	ΣL (μm) intercepts	No. of intercepts	% composition by length	
A1	Cerussite	10308	580	0.69	7.99
	Galena	3078	132	0.21	2.38
	Smithsonite	30664	1237	2.04	23.75
	Baryte	85040	9813	5.67	65.88
	(Matrix)	(1370910)	(11478)	(91.39)	-
	TOTAL	1500000	23240	100	100
A2	Cerussite	13048	785	0.87	18.45
	Galena	2540	149	0.17	3.59
	Smithsonite	29118	1409	1.94	41.18
	Baryte	26004	4729	1.73	36.78
	(Matrix)	(1429290)	(6782)	(95.29)	-
	TOTAL	1500000	13854	100	100
B	Cerussite	15188	851	1.01	11.55
	Galena	6002	209	0.40	4.57
	Smithsonite	21174	795	1.41	16.11
	Baryte	89090	17480	5.94	67.77
	(Matrix)	(1368546)	(18924)	(91.24)	-
	TOTAL	1500000	38259	100	100
C	Cerussite	14716	1082	0.98	16.80
	Galena	3798	212	0.25	4.34
	Smithsonite	23176	876	1.55	26.46
	Baryte	45902	9058	3.06	52.40
	(Matrix)	(1412408)	(10882)	(94.16)	-
	TOTAL	1500000	22110	100	100

Table A.6.1c Modal analyses
-75 + 53 μm +2.96 SG material

Sample	Phase	ΣL (μm) intercepts	No. of intercepts	% composition by length	
A1	Cerussite	14026	843	0.62	9.05
	Galena	2708	165	0.12	1.75
	Smithsonite	35270	1554	1.57	22.76
	Baryte	102988	9643	4.58	66.45
	(Matrix)	(2095008)	(11876)	(93.11)	-
	TOTAL	2250000	24081	100	100
A2	Cerussite	19912	871	0.88	8.24
	Galena	4294	183	0.19	1.78
	Smithsonite	62654	2107	2.78	25.92
	Baryte	154868	12873	6.88	64.07
	(Matrix)	(2008272)	(15595)	(89.26)	-
	TOTAL	2250000	31629	100	100
B	Cerussite	27558	2226	1.22	16.37
	Galena	6230	425	0.28	3.70
	Smithsonite	15072	708	0.67	8.95
	Baryte	119518	8932	5.31	70.95
	(Matrix)	(2081622)	(11559)	(92.52)	-
	TOTAL	2250000	23850	100	100
C	Cerussite	55812	Incomplete	2.48	20.16
	Galena	13440		0.60	4.88
	Smithsonite	22359		0.99	8.05
	Baryte	185195		8.23	66.91
	(Matrix)	(1973188)		(87.70)	-
	TOTAL	2249994		100	100

Table A.6.2a Cerussite and galena particle grade distribution
-150 + 104 μm +2.96 SG material

Sample	Linear Grade % Cerussite	Intercepts (μm)			Length % distrib.			No. of Particles
		Total	Gal.	Cer.	Total	Gal.	Cer.	
A1	0	2	2	0	tr	tr	0	1
	0-20	2766	2430	336	16.9	52.9	2.9	25
	20-40	2244	1592	652	13.7	34.6	5.6	25
	40-60	620	304	316	3.8	6.6	2.7	7
	60-80	668	196	472	4.1	4.3	4.0	9
	80-100	536	74	462	3.3	1.6	3.9	9
	100	9506	0	9506	58.2	0	80.9	316
A2	0	0	0	0	0	0	0	0
	0-20	614	526	88	19.2	63.2	3.7	6
	20-40	186	132	54	5.8	15.9	2.3	3
	40-60	194	102	92	6.1	12.3	3.9	3
	60-80	94	30	64	2.9	3.6	2.7	2
	80-100	446	42	404	14.0	5.1	17.1	6
	100	1662	0	1662	52.0	0	70.3	79
B	0	118	118	0	0.6	1.9	0	3
	0-20	3960	3530	430	20.2	57.7	3.2	42
	20-40	2538	1784	754	12.9	29.2	5.6	34
	40-60	814	430	384	4.2	7.0	2.8	13
	60-80	690	212	478	3.5	3.5	3.5	12
	80-100	788	46	742	4.0	0.8	5.5	14
	100	10730	0	10730	54.6	0	79.4	311
C	0	96	96	0	0.2	0.8	0	5
	0-20	6646	5926	720	13.9	47.6	2.0	72
	20-40	5334	3800	1534	11.2	30.5	4.3	71
	40-60	3280	1646	1634	6.9	13.2	4.6	47
	60-80	2468	744	1724	5.2	6.0	4.9	48
	80-100	2820	244	2576	5.9	2.0	7.3	45
	100	27212	0	27212	56.9	0	76.9	920
Overall	0	216	216	0	0.3	0.9	0	9
	0-20	13986	12412	1574	16.1	51.8	2.5	145
	20-40	10302	7308	2994	11.8	30.4	4.8	133
	40-60	4908	2482	2426	5.6	10.3	3.9	70
	60-80	3920	1182	2738	4.5	4.9	4.3	71
	80-100	4590	406	4184	5.3	1.7	6.6	74
	100	49110	0	49110	56.4	0	77.9	1626

Table A.6.2b Cerussite and galena particle grade distribution
-104 + 75 µm +2.96 SG material

	Linear Grade	Intercepts (µm)			Length % distrib.			No. of
Sample	% Cerussite	Total	Gal.	Cer.	Total	Gal.	Cer.	Particles
A1	0	0	0	0	0	0	0	0
	0-20	1300	1110	190	10.6	36.7	2.1	17
	20-40	1686	1196	490	13.8	39.5	5.3	27
	40-60	764	382	382	6.2	12.6	4.1	13
	60-80	772	252	520	6.3	8.3	5.6	15
	80-100	960	86	874	7.8	2.8	9.5	18
	100	6762	0	6762	55.2	0	73.4	296
A2	0	0	0	0	0	0	0	0
	0-20	266	236	30	1.8	9.4	0.2	5
	20-40	1176	808	368	7.9	32.3	3.0	22
	40-60	1978	990	988	13.3	39.6	8.0	37
	60-80	1306	394	912	8.8	15.8	7.4	32
	80-100	788	74	714	5.3	3.0	5.8	17
	100	9396	0	9396	63.0	0	75.7	474
B	0	0	0	0	0	0	0	0
	0-20	3036	2696	340	15.0	45.3	2.4	43
	20-40	2756	1972	784	13.6	33.1	5.5	49
	40-60	1708	868	840	8.4	14.6	5.9	29
	60-80	1042	332	710	5.1	5.6	5.0	19
	80-100	650	84	566	3.2	1.4	4.0	13
	100	11100	0	11100	54.7	0	77.4	446
C	0	0	0	0	0	0	0	0
	0-20	1684	1432	252	9.3	39.3	1.7	29
	20-40	1604	1138	466	8.8	31.2	3.2	29
	40-60	1594	814	780	8.8	22.3	5.4	30
	60-80	668	214	454	3.7	5.9	3.1	17
	80-100	534	48	486	2.9	1.3	3.4	16
	100	12082	0	12082	66.5	0	83.2	742
Overall	0	0	0	0	0	0	0	0
	0-20	6286	5474	812	9.6	36.2	1.6	94
	20-40	7222	5114	2108	11.0	33.8	4.2	127
	40-60	6044	3054	2990	9.2	20.2	5.9	109
	60-80	3788	1192	2596	5.8	7.9	5.1	83
	80-100	2932	292	2640	4.5	1.9	5.2	64
	100	39340	0	39340	60.0	0	78.0	1958

Table A.6.2c Cerussite and galena particle grade distribution
-75 + 53 μm +2.96 SG material

Sample	Linear Grade % Cerussite	Intercepts (μm) Total	Gal.	Cer.	Length % distrib. Total	Gal.	Cer.	No. of Particles
A1	0	0	0	0	0	0	0	0
	0-20	650	562	88	4.1	20.8	0.7	13
	20-40	1400	948	452	8.9	35.0	3.5	27
	40-60	1412	720	692	8.9	26.6	5.3	35
	60-80	1188	380	808	7.5	14.0	6.2	27
	80-100	972	98	874	6.2	3.6	6.7	23
	100	10176	0	10176	64.4	0	77.7	488
A2	0	0	0	0	0	0	0	0
	0-20	978	844	134	4.4	19.8	0.7	12
	20-40	2628	1 2842	786	11.7	43.2	4.3	37
	40-60	1818	938	880	8.1	22.0	4.9	37
	60-80	1580	516	1064	7.1	12.1	5.9	31
	80-100	1078	126	952	4.8	3.0	5.2	20
	100	14338	0	14338	64.0	0	78.8	480
B	0	0	0	0	0	0	0	0
	0-20	2512	2216	296	7.6	37.3	1.1	35
	20-40	2966	2058	908	9.0	34.6	3.4	48
	40-60	1730	890	840	5.2	15.0	3.1	33
	60-80	1572	510	1062	4.8	8.6	3.9	31
	80-100	2582	270	2312	7.8	4.5	8.6	57
	100	21626	0	21626	65.6	0	80.0	1594
C	0	0	0	0	0	0	0	0
	0-20	4164	3666	498	6.2	28.1	0.9	80
	20-40	7042	4996	2046	10.4	38.4	3.8	156
	40-60	5564	2832	2732	8.2	21.8	5.0	133
	60-80	3768	1176	2592	5.6	9.0	4.8	109
	80-100	3090	336	2754	4.6	2.6	5.1	76
	100	43816	0	43816	64.9	0	80.5	2329
Overall	0	0	0	0	0	0	0	0
	0-20	8304	7288	1016	6.0	28.1	0.9	140
	20-40	14036	9844	4192	10.1	38.0	3.7	268
	40-60	10524	5380	5144	7.6	20.8	4.6	238
	60-80	8108	2582	5526	5.8	10.0	4.9	198
	80-100	7722	830	6892	5.6	3.2	6.1	176
	100	89956	0	89956	64.9	0	79.8	4891

APPENDIX 7

Solid phases in the Pb-S-CO_3 system

Phase	Mass %		
	S	Pb	O+C
PbS_5O_6	34.5	44.8	20.7
PbS_4O_6	29.6	48.2	22.2
PbS_3O_6	24.0	52.0	24.0
PbS_2O_3	20.0	65.0	15.0
PbS_2O_4	19.5	61.9	19.5
PbS_2O_5	18.2	59.1	22.7
$PbS_2O_6.4H_2O$	14.5	47.3	38.2
$PbS_2O_8.3H_2O$	14.1	45.8	40.1
PbS (galena)	13.4	86.7	0
$PbO.PbS_2O_3$	11.8	76.4	11.8
$PbO.PbS_2O_3.H_2O$ $Pb(OH)_2.PbS_2O_3$	11.4	74.0	14.6
PbS_2O_3	11.1	72.2	16.7
$PbO.PbS_2O_3.2H_2O$	11.0	71.7	17.3
$PbO.PbS_2O_3.3H_2O$	10.7	69.6	19.7
$PbO.PbS_2O_3.4H_2O$	10.4	67.5	22.1
$PbSO_4$ (anglesite)	10.5	68.4	21.1
$PbO.PbSO_4$ (lanarkite)	6.0	78.8	15.2
$Pb_2SO_4(OH)_2$ (linarite, Cu→0)	5.9	72.2	17.9
$2PbO.PbSO_4$	4.2	83.0	12.8
$Pb_4SO_4(CO_3)_2(OH)_2$ (leadhillite)	3.0	76.8	20.2
$4PbO.PbSO_4$	2.6	86.7	10.7
PbO	0	92.9	7.1
$Pb(OH)_2$	0	86.0	14.0
$PbCO_3.Pb(OH)_2$	0	81.5	18.5
$Pb_3(CO_3)_2(OH)_2$ (hydrocerussite)	0	80.2	19.8
$PbCO_3$ (cerussite)	0	77.6	22.4